

**NONLINEAR DYNAMICS AND SYSTEMS THEORY**

An International Journal of Research and Surveys

Volume 23                      Number 3                      2023

**CONTENTS**

Weights Optimization Using Firefly Algorithm for Dengue Fever Optimal Control Model by Vaccination, Treatment, and Abataseae.....237  
*A. Y. Asih, B. Gunawan, N. Hidayati, T. Herlambang, D. Rahmalia and K. Oktafianto*

Inverse Problem of a Semilinear Parabolic Equation with an Integral Overdetermination Condition.....249  
*Amal Benguesmia, Iqbal M. Batiha, Taki-Eddine Oussaeif, Adel Ouannas and Waseem G. Alshanti*

Some Generalized Nonlinear Volterra-Fredholm Type Integral Inequalities with Delay of Several Variables and Applications .....261  
*Ammar Boudeliou*

An Adaptive Step Size for Chaotic Local Search Algorithm.....273  
*Aziza Filali and Tayeb Hamaizia*

On the Dynamics and FSHP Synchronization of a New Chaotic 3-D System with Three Nonlinearities .....283  
*Fareh Hannachi and Rami Amira*

Numerical Solution of the Black-Scholes Partial Differential Equation for the Option Pricing Model Using the ADM-Kamal Method.....295  
*M. D. Johansyah, I. Sumiati, E. Rusyaman, Sukono, M. Muslikh, M. A. Mohamed and A. Sambah*

A Novel Adaptive Method Based on New Minorant-Majorant Functions without Line Search for Semidefinite Optimization .....310  
*S. Leulmi and A. Leulmi*

Electronic Nose for Classifying Civet Coffee and Non-Civet Coffee.....323  
*D. B. Magfira, R. Sarno, F. A. Susanto, T. Herlambang, K. Oktafianto, W. Hartawan and I. W. Farid*

Global Existence for the 3-D Generalized Micropolar Fluid System in Critical Fourier-Besov Spaces with Variable Exponent.....338  
*F. Ouidirne, H. Srhiri, C. Allalou and M. Oukessou*

The Regularization Method for Solving Sub-Riemannian Geodesic Problems .....348  
*R. Safdine and N. Bensalem*

NONLINEAR DYNAMICS & SYSTEMS THEORY

Volume 23, No. 3, 2023

# Nonlinear Dynamics and Systems Theory

**An International Journal of Research and Surveys**

**EDITOR-IN-CHIEF A.A.MARTYNYUK**

*S.P.Timoshenko Institute of Mechanics  
National Academy of Sciences of Ukraine, Kiev, Ukraine*

**MANAGING EDITOR I.P.STAVROULAKIS**

*Department of Mathematics, University of Ioannina, Greece*

**REGIONAL EDITORS**

P.BORNE, Lille, France  
 A.OKNIŃSKI, Kielce, Poland  
*Europe*

M.BOHNER, Rolla, USA  
 HAO WANG, Edmonton, Canada  
*USA and Canada*

T.A.BURTON, Port Angeles, USA  
 C.CRUZ-HERNANDEZ, Ensenada, Mexico  
*USA and Latin America*

M.ALQURAN, Irbid, Jordan  
*Jordan and Middle East*

T.HERLAMBANG, Surabaya, Indonesia  
*Indonesia and New Zealand*

Nonlinear Dynamics and Systems Theory  
An International Journal of Research and Surveys

**EDITOR-IN-CHIEF A.A.MARTYNYUK**

The S.P.Timoshenko Institute of Mechanics, National Academy of Sciences of Ukraine,  
Nesterov Str. 3, 03680 MSP, Kiev-57, UKRAINE / e-mail: journalndst@gmail.com

**MANAGING EDITOR I.P.STAVROULAKIS**

Department of Mathematics, University of Ioannina  
451 10 Ioannina, HELLAS (GREECE) / e-mail: ipstav@cc.uoi.gr

**ADVISORY EDITOR A.G.MAZKO,**

Institute of Mathematics of NAS of Ukraine, Kiev (Ukraine)  
e-mail: mazko@imath.kiev.ua

**REGIONAL EDITORS**

M.ALQURAN (Jordan), e-mail: marwan04@just.edu.jo  
P.BORNE (France), e-mail: Pierre.Borne@ec-lille.fr  
M.Bohner (USA), e-mail: bohner@mst.edu  
T.A.BURTON (USA), e-mail: taburton@olypen.com  
C.CRUZ-HERNANDEZ (Mexico), e-mail: ccruz@cicese.mx  
T.HERLAMBANG (Indonesia), e-mail: teguh@unusa.ac.id  
A.OKNINSKI (Poland), e-mail: fizao@tu.kielce.pl  
HAO WANG (Canada), e-mail: hao8@ualberta.ca

**EDITORIAL BOARD**

Adzkiya, D. (Indonesia)	Kloedon, P. (Germany)
Artstein, Z. (Israel)	Kokologiannaki, C. (Greece)
Awrejcewicz, J. (Poland)	Kouzou, A. (Algeria)
Braiek, N.B. (Tunisia)	Krishnan, E.V. (Oman)
Chen Ye-Hwa (USA)	Limarchenko, O.S. (Ukraine)
De Angelis, M. (Italy)	Lopez Gutierrez R.M. (Mexico)
Denton, Z. (USA)	Peterson, A. (USA)
Djemai, M. (France)	Radziszewski, B. (Poland)
Dshalalow, J.H. (USA)	Shi Yan (Japan)
Gajic Z. (USA)	Sivasundaram, S. (USA)
Georgiev, S.G. (France)	Sree Hari Rao, V. (India)
Georgiou, G. (Cyprus)	Staicu V. (Portugal)
Honglei Xu (Australia)	Vatsala, A. (USA)
Jafari, H. (South African Republic)	Zuyev, A.L. (Germany)
Khusainov, D.Ya. (Ukraine)	

**ADVISORY COMPUTER SCIENCE EDITORS**

A.N.CHERNIENKO and A.S.KHOROSHUN, Kiev, Ukraine

**ADVISORY LINGUISTIC EDITOR**

S.N.RASSHYVALOVA, Kiev, Ukraine

© 2023, InforMath Publishing Group, ISSN 1562-8353 print, ISSN 1813-7385 online, Printed in Ukraine  
No part of this Journal may be reproduced or transmitted in any form or by any means without  
permission from InforMath Publishing Group.

**INSTRUCTIONS FOR CONTRIBUTORS**

**(1) General.** Nonlinear Dynamics and Systems Theory (ND&ST) is an international journal devoted to publishing peer-refereed, high quality, original papers, brief notes and review articles focusing on nonlinear dynamics and systems theory and their practical applications in engineering, physical and life sciences. Submission of a manuscript is a representation that the submission has been approved by all of the authors and by the institution where the work was carried out. It also represents that the manuscript has not been previously published, has not been copyrighted, is not being submitted for publication elsewhere, and that the authors have agreed that the copyright in the article shall be assigned exclusively to InforMath Publishing Group by signing a transfer of copyright form. Before submission, the authors should visit the website:

<http://www.e-ndst.kiev.ua>

for information on the preparation of accepted manuscripts. Please download the archive Sample\_NDST.zip containing example of article file (you can edit only the file Samplefilename.tex).

**(2) Manuscript and Correspondence.** Manuscripts should be in English and must meet common standards of usage and grammar. To submit a paper, send by e-mail a file in PDF format directly to

*Professor A.A. Martynyuk, Institute of Mechanics,  
Nesterov str.3, 03057, MSP 680, Kiev-57, Ukraine  
e-mail: journalndst@gmail.com*

or to one of the Regional Editors or to a member of the Editorial Board. Final version of the manuscript must typeset using LaTeX program which is prepared in accordance with the style file of the Journal. Manuscript texts should contain the title of the article, name(s) of the author(s) and complete affiliations. Each article requires an abstract not exceeding 150 words. Formulas and citations should not be included in the abstract. AMS subject classifications and key words must be included in all accepted papers. Each article requires a running head (abbreviated form of the title) of no more than 30 characters. The sizes for regular papers, survey articles, brief notes, letters to editors and book reviews are: (i) 10-14 pages for regular papers, (ii) up to 24 pages for survey articles, and (iii) 2-3 pages for brief notes, letters to the editor and book reviews.

**(3) Tables, Graphs and Illustrations.** Each figure must be of a quality suitable for direct reproduction and must include a caption. Drawings should include all relevant details and should be drawn professionally in black ink on plain white drawing paper. In addition to a hard copy of the artwork, it is necessary to attach the electronic file of the artwork (preferably in PCX format).

**(4) References.** Each entry must be cited in the text by author(s) and number or by number alone. All references should be listed in their alphabetic order. Use please the following style:

Journal: [1] H. Poincare, Title of the article. *Title of the Journal* **volume**  
(issue) (year) pages. [Language]

Book: [2] A.M. Lyapunov, *Title of the Book*. Name of the Publishers, Town, year.

Proceeding: [3] R. Bellman, Title of the article. In: *Title of the Book*. (Eds.).  
Name of the Publishers, Town, year, pages. [Language]

**(5) Proofs and Sample Copy.** Proofs sent to authors should be returned to the Editorial Office with corrections within three days after receipt. The corresponding author will receive a sample copy of the issue of the Journal for which his/her paper is published.

**(6) Editorial Policy.** Every submission will undergo a stringent peer review process. An editor will be assigned to handle the review process of the paper. He/she will secure at least two reviewers' reports. The decision on acceptance, rejection or acceptance subject to revision will be made based on these reviewers' reports and the editor's own reading of the paper.

# NONLINEAR DYNAMICS AND SYSTEMS THEORY

An International Journal of Research and Surveys  
Published by InforMath Publishing Group since 2001

Volume 23

Number 3

2023

## CONTENTS

Weights Optimization Using Firefly Algorithm for Dengue Fever Optimal Control Model by Vaccination, Treatment, and Abateseae .....	237
<i>A. Y. Asih, B. Gunawan, N. Hidayati, T. Herlambang, D. Rahmalia and K. Oktafianto</i>	
Inverse Problem of a Semilinear Parabolic Equation with an Integral Overdetermination Condition .....	249
<i>Amal Benguesmia, Iqbal M. Batiha, Taki-Eddine Oussaeif, Adel Ouannas and Waseem G. Alshanti</i>	
Some Generalized Nonlinear Volterra-Fredholm Type Integral Inequalities with Delay of Several Variables and Applications .....	261
<i>Ammar Boudeliou</i>	
An Adaptive Step Size for Chaotic Local Search Algorithm .....	273
<i>Aziza Filali and Tayeb Hamaizia</i>	
On the Dynamics and FSHP Synchronization of a New Chaotic 3-D System with Three Nonlinearities .....	283
<i>Fareh Hannachi and Rami Amira</i>	
Numerical Solution of the Black-Scholes Partial Differential Equation for the Option Pricing Model Using the ADM-Kamal Method .....	295
<i>M. D. Johansyah, I. Sumiati, E. Rusyaman, Sukono, M. Muslikh, M. A. Mohamed and A. Sambas</i>	
A Novel Adaptive Method Based on New Minorant-Majorant Functions without Line Search for Semidefinite Optimization .....	310
<i>S. Leulmi and A. Leulmi</i>	
Electronic Nose for Classifying Civet Coffee and Non-Civet Coffee .....	323
<i>D. B. Magfira, R. Sarno, F. A. Susanto, T. Herlambang, K. Oktafianto, W. Hartawan and I. W. Farid</i>	
Global Existence for the 3-D Generalized Micropolar Fluid System in Critical Fourier-Besov Spaces with Variable Exponent .....	338
<i>F. Ouidirne, H. Srhiri, C. Allalou and M. Oukessou</i>	
The Regularization Method for Solving Sub-Riemannian Geodesic Problems .....	348
<i>R. Saffidine and N. Bensalem</i>	

Founded by A.A. Martynyuk in 2001.

Registered in Ukraine Number: KB No 5267 / 04.07.2001.

# NONLINEAR DYNAMICS AND SYSTEMS THEORY

An International Journal of Research and Surveys

*Impact Factor from SCOPUS for 2022: SJR – 0.293, SNIP – 0.784 and CiteScore – 1.5*

**Nonlinear Dynamics and Systems Theory** (ISSN 1562–8353 (Print), ISSN 1813–7385 (Online)) is an international journal published under the auspices of the S.P. Timoshenko Institute of Mechanics of National Academy of Sciences of Ukraine and Curtin University of Technology (Perth, Australia). It aims to publish high quality original scientific papers and surveys in areas of nonlinear dynamics and systems theory and their real world applications.

## AIMS AND SCOPE

**Nonlinear Dynamics and Systems Theory** is a multidisciplinary journal. It publishes papers focusing on proofs of important theorems as well as papers presenting new ideas and new theory, conjectures, numerical algorithms and physical experiments in areas related to nonlinear dynamics and systems theory. Papers that deal with theoretical aspects of nonlinear dynamics and/or systems theory should contain significant mathematical results with an indication of their possible applications. Papers that emphasize applications should contain new mathematical models of real world phenomena and/or description of engineering problems. They should include rigorous analysis of data used and results obtained. Papers that integrate and interrelate ideas and methods of nonlinear dynamics and systems theory will be particularly welcomed. This journal and the individual contributions published therein are protected under the copyright by International InforMath Publishing Group.

## PUBLICATION AND SUBSCRIPTION INFORMATION

**Nonlinear Dynamics and Systems Theory** will have 5 issues in 2023, printed in hard copy (ISSN 1562–8353) and available online (ISSN 1813–7385), by InforMath Publishing Group, Nesterov str., 3, Institute of Mechanics, Kiev, MSP 680, Ukraine, 03057. Subscription prices are available upon request from the Publisher, EBSCO Information Services (<mailto:journals@ebSCO.com>), or website of the Journal: <http://e-ndst.kiev.ua>. Subscriptions are accepted on a calendar year basis. Issues are sent by airmail to all countries of the world. Claims for missing issues should be made within six months of the date of dispatch.

## ABSTRACTING AND INDEXING SERVICES

Papers published in this journal are indexed or abstracted in: Mathematical Reviews / MathSciNet, Zentralblatt MATH / Mathematics Abstracts, PASCAL database (INIST–CNRS) and SCOPUS.



# Weights Optimization Using Firefly Algorithm for Dengue Fever Optimal Control Model by Vaccination, Treatment, and Abateseae

A. Y. Asih<sup>1</sup>, B. Gunawan<sup>2\*</sup>, N. Hidayati<sup>2</sup>, T. Herlambang<sup>3</sup>,  
D. Rahmalia<sup>4</sup>, and K. Oktafianto<sup>5</sup>

<sup>1</sup> Department of Public Health, Universitas Nahdlatul Ulama Surabaya, Indonesia.

<sup>2\*</sup> Department of Food Nutrition, Institute of Health and Business Surabaya, Indonesia.

<sup>3</sup> Department of Information System, Universitas Nahdlatul Ulama Surabaya, Indonesia.

<sup>4</sup> Department of Mathematics, University of Islam Darul Ulum, Lamongan, Indonesia.

<sup>5</sup> Department of Mathematics, University of PGRI Ronggolawe, Tuban, Indonesia.

Received: October 8, 2021; Revised: July 25, 2023

**Abstract:** Indonesia is one of tropical countries where dengue fever disease can spread through *Aedes aegypti* mosquitoes and sometimes cause deaths. There are many control strategies to bound the spread of dengue fever: vaccination for controlling susceptible humans, treatment for controlling infected humans, and abateseae (larvacides for killing the mosquito larvae). Optimal control is used for minimizing the number of infected humans, larvae, infected mosquitoes, the cost of vaccination, the cost of treatment, and the cost of abateseae. Due to the cost of the objective function depending on weights, in this research, we will apply the Firefly Algorithm (FA) to optimize the weights minimizing the cost of the objective function. The FA is based on the behavior of flashing characteristics of fireflies. Simulations have been applied and we can obtain the comparison of the number of humans and mosquitoes with and without control. In addition, we also obtain the optimal weight related to the number of infected humans, the number of larvae, the number of infected mosquitoes, the cost of vaccination, the cost of treatment, and the cost of abateseae, respectively.

**Keywords:** dengue fever; optimal control; firefly algorithm; vaccination; treatment; abateseae.

**Mathematics Subject Classification (2010):** 49L12, 65L06.

---

\* Corresponding author: <mailto:gunawanb1011@gmail.com>

## 1 Introduction

Indonesia is one of tropical countries where dengue fever disease can spread through *Aedes aegypti* mosquitoes and sometimes cause deaths. Based on the data of the Directorate of Animal Disease Control Source, Ministry of Health Department of the Republic of Indonesia, in 2011, there were 126,908 cases of dengue with 1,125 deaths [14].

Dengue fever disease is caused by *Aedes aegypti* mosquitoes. The mosquitoes have 4 life stages: egg, larva, pupa and adult (mosquito). Mosquitoes can live and reproduce inside and outside the home. The mosquitoes are most frequently found in tropical and subtropical areas of the world. *Aedes aegypti* historically is considered to be a primary vector of viral diseases such as dengue fever, chikungunya and yellow fever. Generally, the habitats of *Aedes aegypti* are the areas lacking piped water systems and depend on water storage containers to lay their eggs. Male and female mosquitoes feed on nectar of plants. However, female mosquitoes need blood in order to produce eggs, and they are active in the daytime. *Aedes aegypti* prefers biting people but it also bites dogs and other domestic animals, mostly mammals. Only female mosquitoes bite to obtain blood for laying eggs.

The purpose of modelling epidemics is to provide policies designed to control the spread of the disease [7]. There are many control strategies to bound the spread of dengue fever: vaccination for controlling susceptible humans, treatment for controlling infected humans, and abateseae (larvacides for killing the mosquito larvae). Optimal control is used for minimizing the number of infected humans, larvae, infected mosquitoes, the cost of vaccination, the cost of treatment, and the cost of abateseae [6].

From the previous researches, a mathematical model to look for stability of the disease or for controlling the disease has been constructed [13]. In [16], the dengue fever control has been applied by vaccination to control the number of susceptible humans to be recovered humans. However, in Indonesia, dengue fever controls have been applied by vaccination to control the number of susceptible humans to be recovered humans, and fogging for devastating the mosquitoes [17]. In this paper, we construct a mathematical model for controlling dengue fever by vaccination for controlling susceptible humans, treatment for controlling infected humans, and abateseae (larvacides for killing the mosquito larvae) for controlling larvae.

In the earlier research from Michalewicz, by heuristic optimization like the Genetic Algorithm (GA), we can determine an optimal control minimizing the objective function based on the natural selection of chromosomes [5]. In this research, the Firefly Algorithm (FA) will be used. The FA was discovered by Xin-She Yang in 2008. It is based on the behavior of flashing characteristics of fireflies. These insects communicate, search for a prey, and find mates using bioluminescence with varying flashing patterns. One of the characteristics of fireflies is the less bright one will move toward the brighter one. A brighter firefly indicates a better objective function as a fitness function [4].

In the optimal control problem, weight selection is applied by trial and error [2]. Due to the cost of the objective function depending on weights [8], [11], in this research, we will apply the Firefly Algorithm to optimize the weights minimizing the cost of the objective function. In the previous research, the Ant Colony Optimization (ACO) has been applied for SEIR contagious disease [6], [9], [10]. The artificial Bee Colony (ABC) has been applied for influenza disease [7].

Simulations have been applied and we can obtain the comparison of the number of humans and mosquitoes with and without control. In addition, we also obtain optimal

weights related to the number of infected humans, the number of larvae, the number of infected mosquitoes, the cost of vaccination, the cost of treatment, and the cost of abateseae, respectively.

## 2 Optimal Control Dengue Fever Model

Generally, the disease can be modeled as a SIR (Susceptible, Infected, Recovered) epidemic model [6]. In the SIR epidemic model, there are three compartments of individuals: susceptible, infected, and recovered. A susceptible individual can be an infected individual after making contact with an infected individual based on disease transmission rate. An infected individual can be a recovered individual when the symptoms of the disease have gone based on recovery rate [1], [12].

### 2.1 Mathematical model of dengue fever

The dengue fever model is the development of a standard SIR epidemic model. In the dengue fever model, there are two different populations such as mosquito as a vector and human as a host. The compartments of the dengue fever model can be seen in Figure 1 where in the mosquito as a vector one, there are larvae (mosquitoes in aquatic phase)  $A_m$ , susceptible mosquitoes  $S_m$ , and infected mosquitoes  $I_m$ , while in the human as a host one, there are susceptible humans  $S_h$ , infected humans  $I_h$ , and recovered humans  $R_h$ . The mathematical model of dengue fever can be constructed in equations (1) - (8):

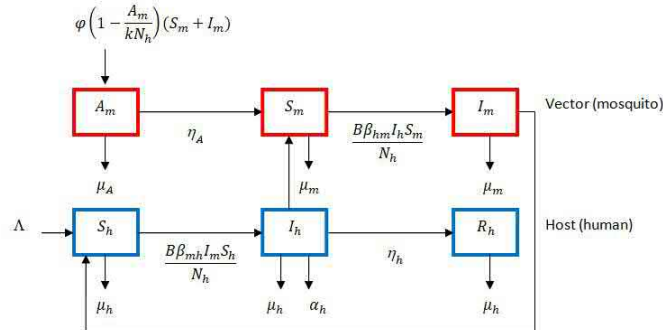


Figure 1: Compartments of the Dengue Fever Model.

$$\frac{dS_h}{dt} = \Lambda - B\beta_{mh} \frac{I_m}{N_h} S_h - \mu_h S_h - u_1 S_h, \tag{1}$$

$$\frac{dI_h}{dt} = B\beta_{mh} \frac{I_m}{N_h} S_h - \eta_h I_h - \mu_h I_h - \alpha_h I_h - u_2 I_h, \tag{2}$$

$$\frac{dR_h}{dt} = \eta_h I_h + u_1 S_h + u_2 I_h - \mu_h R_h, \tag{3}$$

$$\frac{dA_m}{dt} = \varphi \left( 1 - \frac{A_m}{kN_h} \right) (S_m + I_m) - \eta_A A_m - \mu_A A_m - u_3 A_m, \tag{4}$$

$$\frac{dS_m}{dt} = \eta_A A_m - B\beta_{hm} \frac{I_h}{N_h} S_m - \mu_m S_m, \tag{5}$$

$$\frac{dI_m}{dt} = B\beta_{hm}\frac{I_h}{N_h}S_m - \mu_m I_m, \quad (6)$$

$$N_h(t) = S_h(t) + I_h(t) + R_h(t), \quad (7)$$

$$N_m(t) = S_m(t) + I_m(t), \quad (8)$$

with the positive solutions

$$S_h(t) \geq 0, I_h(t) \geq 0, R_h(t) \geq 0, A_m(t) \geq 0, S_m(t) \geq 0, I_m(t) \geq 0.$$

The parameters used in the model above are:

$\Lambda$  : The recruitment rate (birth or immigration) of the human population.

$\mu_h$  : The natural death rate of humans.

$\mu_m$  : The natural death rate of mosquitoes (adult phase).

$\mu_A$  : The natural death rate of mosquitoes (aquatic phase).

$B$  : The average daily biting (per day) of the mosquito.

$\beta_{mh}$  : The transmission probability (per bite) from infected mosquitoes to humans.

$\beta_{hm}$  : The transmission probability (per bite) from infected humans to mosquitoes.

$\varphi$  : The number of eggs at each deposit per capita (per day).

$\eta_h$  : The recovery rate of the human population.

$\eta_A$  : The maturation rate from larvae to adult mosquitoes (per day).

$\alpha_h$  : The death by the disease rate of humans.

In the human population, the model can be explained as follows. At the susceptible compartment, the recruitment rate (birth or immigration) can increase the number of susceptible. However, the disease transmission rate due to the contact with infected mosquitoes through bitings and the natural death rate can decrease the number of susceptible. At the infected compartment, the disease transmission rate due to the contact with infected mosquitoes through bitings can increase the number of infected. However, the natural death rate, death by the disease rate, and recovery rate can decrease the number of infected. At the recovered compartment, the recovery rate can increase the number of recovered. However, the natural death rate can decrease the number of recovered.

In the mosquito population including larva in aqua phase, the model can be explained as follows. At the larvae compartment, the recruitment rate can increase the number of larvae. However, the maturation rate and natural death rate can decrease the number of larvae. At the susceptible compartment, the maturation rate of larvae can increase the number of susceptible. However, the disease transmission rate due to the contact with infected humans through bitings and the natural death rate can decrease the number of susceptible. At the infected compartment, the disease transmission rate due to the contact with infected humans through bitings can increase the number of infected. However, the natural death rate can decrease the number of infected.

In addition, there are the control function of susceptible humans vaccinated,  $u_1$ , the control function of infected humans treated,  $u_2$ , and the control function of larvae killed by abateseae,  $u_3$ . The effectiveness range of  $u_1, u_2$  and  $u_3$  is  $[0, 1]$ , where the value 0 means the control functions fail or are not applied, and the value 1 means the control functions are successful or applied entirely.

The objective function which will be minimized is

$$J(u, v) = \int_0^{t_f} (W_1 I_h(t)^2 + W_2 A_m(t)^2 + W_3 I_m(t)^2 + W_4 u_1(t)^2 + W_5 u_2(t)^2 + W_6 u_3(t)^2) dt \tag{9}$$

with the weights  $W_1 > 0, W_2 > 0, W_3 > 0, W_4 > 0, W_5 > 0, W_6 > 0$ . From the model, we want to minimize the number of infected humans, the number of larvae, the number of infected mosquitoes, the cost of vaccination, the cost of treatment, and the cost of abateseae.

The goal is finding  $u_1^*, u_2^*, u_3^*$  such that

$$J(u_1^*, u_2^*, u_3^*) = \min(J(u_1, u_2, u_3)). \tag{10}$$

### 2.2 Pontryagin’s maximum principle

If  $u_1^*, u_2^*, u_3^*$  are the optimal control, there exist the adjoint variables

$$(\lambda_1 \quad \lambda_2 \quad \lambda_3 \quad \lambda_4 \quad \lambda_5 \quad \lambda_6)$$

which satisfy the following [3]:

$$\frac{d\lambda_1}{dt} = -\frac{\partial H}{\partial S_h} = \lambda_1 B\beta_{mh} \frac{I_m}{N_h} + \lambda_1 \mu_h + \lambda_1 u_1 - \lambda_2 B\beta_{mh} \frac{I_m}{N_h} - \lambda_3 u_1, \tag{11}$$

$$\begin{aligned} \frac{d\lambda_2}{dt} = -\frac{\partial H}{\partial I_h} = & \lambda_2 \eta_h + \lambda_2 \mu_h + \lambda_2 \alpha_h + \lambda_2 u_2 - \lambda_3 \eta_h - \lambda_3 u_2 + \\ & \lambda_5 B\beta_{hm} \frac{S_m}{N_h} - \lambda_6 B\beta_{hm} \frac{S_m}{N_h} - 2W_1 I_h, \end{aligned} \tag{12}$$

$$\frac{d\lambda_3}{dt} = -\frac{\partial H}{\partial R_h} = \lambda_3 \mu_h, \tag{13}$$

$$\frac{d\lambda_4}{dt} = -\frac{\partial H}{\partial A_m} = \lambda_4 \varphi \frac{S_m + I_m}{kN_h} + \lambda_4 \eta_A + \lambda_4 \mu_A + \lambda_4 u_3 - \lambda_5 \eta_A - 2W_2 A_m, \tag{14}$$

$$\frac{d\lambda_5}{dt} = -\frac{\partial H}{\partial S_m} = -\lambda_4 \varphi + \lambda_4 \varphi \frac{A_m}{kN_h} + \lambda_5 B\beta_{hm} \frac{I_h}{N_h} + \lambda_5 \mu_m - \lambda_6 B\beta_{hm} \frac{I_h}{N_h}, \tag{15}$$

$$\begin{aligned} \frac{d\lambda_6}{dt} = -\frac{\partial H}{\partial I_m} = & \lambda_1 B\beta_{mh} \frac{S_h}{N_h} - \lambda_2 B\beta_{mh} \frac{S_h}{N_h} - \lambda_4 \varphi + \\ & \lambda_4 \varphi \frac{A_m}{kN_h} + \lambda_6 \mu_m - 2W_3 I_m, \end{aligned} \tag{16}$$

with the final conditions  $\lambda_1(T) = \lambda_2(T) = \lambda_3(T) = \lambda_4(T) = \lambda_5(T) = \lambda_6(T) = 0$ , where the Hamiltonian is

$$\begin{aligned} H = & W_1 I_h(t)^2 + W_2 A_m(t)^2 + W_3 I_m(t)^2 + W_4 u_1(t)^2 + W_5 u_2(t)^2 + W_6 u_3(t)^2 \\ & \lambda_1 \left( \Lambda - B\beta_{mh} \frac{I_m}{N_h} S_h - \mu_h S_h - u_1 S_h \right) + \\ & \lambda_2 \left( B\beta_{mh} \frac{I_m}{N_h} S_h - \eta_h I_h - \mu_h I_h - \alpha_h I_h - u_2 I_h \right) + \\ & \lambda_3 (\eta_h I_h + u_1 S_h + u_2 I_h - \mu_h R_h) + \end{aligned}$$

$$\begin{aligned} & \lambda_4 \left( \varphi \left( 1 - \frac{A_m}{kN_h} \right) (S_m + I_m) - \eta_A A_m - \mu_A A_m - u_3 A_m \right) + \\ & \lambda_5 \left( \eta_A A_m - B\beta_{hm} \frac{I_h}{N_h} S_m - \mu_m S_m \right) + \lambda_6 \left( B\beta_{hm} \frac{I_h}{N_h} S_m - \mu_m I_m \right). \end{aligned} \quad (17)$$

Furthermore, we can find the optimal control  $u_1^*, u_2^*, u_3^*$  :

$$\begin{aligned} \frac{\partial H}{\partial u_1} &= 0, \\ 2W_4 u_1 - \lambda_1 S_h + \lambda_3 S_h &= 0, \\ u_1 &= \min \left( 1, \max \left( 0, \frac{(\lambda_1 - \lambda_3) S_h}{2W_4} \right) \right), \\ \frac{\partial H}{\partial u_2} &= 0, \\ 2W_5 u_2 - \lambda_2 I_h + \lambda_3 I_h &= 0, \\ u_2 &= \min \left( 1, \max \left( 0, \frac{(\lambda_2 - \lambda_3) I_h}{2W_5} \right) \right), \\ \frac{\partial H}{\partial u_3} &= 0, \\ 2W_6 u_3 - \lambda_4 A_m &= 0, \\ u_3 &= \min \left( 1, \max \left( 0, \frac{\lambda_4 A_m}{2W_6} \right) \right). \end{aligned} \quad (18)$$

### 2.3 Forward-backward sweep method

The forward backward sweep method applied to the optimal control dengue fever model can be designed as follows [3]. Suppose the state variables and the adjoint variables are

$$\begin{aligned} f_1 &= \frac{dS_h}{dt}, f_2 = \frac{dI_h}{dt}, f_3 = \frac{dR_h}{dt}, f_4 = \frac{dA_m}{dt}, f_5 = \frac{dS_m}{dt}, f_6 = \frac{dI_m}{dt}, \\ g_1 &= \frac{d\lambda_1}{dt}, g_2 = \frac{d\lambda_2}{dt}, g_3 = \frac{d\lambda_3}{dt}, g_4 = \frac{d\lambda_4}{dt}, g_5 = \frac{d\lambda_5}{dt}, g_6 = \frac{d\lambda_6}{dt}. \end{aligned}$$

The algorithm to compute the objective function as the fitness function with the parameter weights  $W_1 > 0, W_2 > 0, W_3 > 0, W_4 > 0, W_5 > 0, W_6 > 0$  is:

*control\_dengue*( $W_1, W_2, W_3, W_4, W_5, W_6$ ) while (process has not converged yet)  $u_{old} = 0$ .

1. Compute the solution of state variables forward with the initial condition  $x(0) = (S_h(0), I_h(0), R_h(0), A_m(0), S_m(0), I_m(0))$  using the Runge-Kutta fourth-order method:

$$k_{1i} = f_i(t, x_i(t), u_1(t), u_2(t), u_3(t)), i = 1, 2, \dots, 6,$$

$$\begin{aligned} k_{2i} &= f_i \left( t + \frac{h}{2}, x_i(t) + \frac{h}{2} k_{1i}, \frac{u_1(t) + u_1(t+h)}{2}, \right. \\ & \left. \frac{u_2(t) + u_2(t+h)}{2}, \frac{u_3(t) + u_3(t+h)}{2} \right), i = 1, 2, \dots, 6, \end{aligned}$$

$$k_{3i} = f_i \left( t + \frac{h}{2}, x_i(t) + \frac{h}{2}k_{2i}, \frac{u_1(t) + u_1(t+h)}{2}, \frac{u_2(t) + u_2(t+h)}{2}, \frac{u_3(t) + u_3(t+h)}{2} \right), i = 1, 2, \dots, 6,$$

$$k_{4i} = f(t+h, x_i(t) + hk_{3i}, u_1(t+h), u_2(t+h), u_3(t+h)), i = 1, 2, \dots, 6,$$

$$x_i(t+h) = x_i(t) + \frac{h}{6}(k_{1i} + 2k_{2i} + 2k_{3i} + k_{4i}), i = 1, 2, \dots, 6.$$

2. Compute the solution of adjoint variables backward with the final condition  $\lambda(0) = (\lambda_1(T), \lambda_2(T), \lambda_3(T), \lambda_4(T), \lambda_5(T), \lambda_6(T))$  using the Runge-Kutta fourth order method:

$$k_{1i} = g_i(t, x_i(t), \lambda_1(t), u_2(t), u_3(t)), i = 1, 2, \dots, 6,$$

$$k_{2i} = g_i \left( t - \frac{h}{2}, \frac{x_i(t) + x_i(t-h)}{2}, \lambda_i(t) - \frac{h}{2}k_{1i}, \frac{u_1(t) + u_1(t-h)}{2}, \frac{u_2(t) + u_2(t-h)}{2}, \frac{u_3(t) + u_3(t-h)}{2} \right), i = 1, 2, \dots, 6,$$

$$k_{3i} = g_i \left( t - \frac{h}{2}, \frac{x_i(t) + x_i(t-h)}{2}, \lambda_i(t) - \frac{h}{2}k_{2i}, \frac{u_1(t) + u_1(t-h)}{2}, \frac{u_2(t) + u_2(t-h)}{2}, \frac{u_3(t) + u_3(t-h)}{2} \right), i = 1, 2, \dots, 6,$$

$$k_{4i} = g_i(t-h, x_i(t-h), \lambda_i(t) - hk_{3i}, u_1(t-h), u_2(t-h), u_3(t-h)), i = 1, 2, \dots, 6.$$

$$\lambda_i(t-h) = \lambda_i(t) + \frac{h}{6}(k_{1i} + 2k_{2i} + 2k_{3i} + k_{4i}), i = 1, 2, \dots, 6.$$

3. Compute the optimal control  $u_1^*, u_2^*, u_3^*$  using equations (18).
4. Update the optimal control

$$u_1 \leftarrow \frac{u_1 + u_{1,old}}{2}, u_2 \leftarrow \frac{u_2 + u_{2,old}}{2}, u_3 \leftarrow \frac{u_3 + u_{3,old}}{2} \tag{19}$$

End

5. Compute the objective function as the fitness function

$$J(u_1, u_2, u_3) = \sum_{k=0}^{T-1} (W_1 I_h(k)^2 + W_2 A_m(k)^2 + W_3 I_m(k)^2 + W_4 u_1(k)^2 + W_5 u_2(k)^2 + W_6 u_3(k)^2). \tag{20}$$

### 3 Firefly Algorithm

The Firefly Algorithm (FA) was discovered by Xin-She Yang in 2008. It is based on the behavior of flashing characteristics of fireflies. These insects communicate, search for a prey, and find mates using bioluminescence with varying flashing patterns. The FA is based on the rules [4]:

1. All fireflies are unisex so they attract one another.
2. Attractiveness is proportional to firefly brightness. For any couple of flashing fireflies, the less bright one will move toward the brighter one. Attractiveness is proportional to brightness and they both decrease as their distance increases. If there is no a brighter one than a particular firefly, it will move randomly.

The brightness of a firefly is affected or determined by the landscape of the objective function. In the FA, the attractiveness of a firefly is assumed to be determined by its brightness which is related to the objective function. The brightness of a firefly at a particular location  $x$  can be chosen as  $f(x)$ , where  $f(x)$  is the objective function. However, if the attractiveness  $\beta$  is relative, it should be judged by the other fireflies. Thus, it will vary with the distance  $r_{ij}$  between the firefly  $i$  and the firefly  $j$ .

In this algorithm, the weights used are  $W_1, W_2, W_3, W_4, W_5, W_6$  related to the number of infected humans, the number of larvae, the number of infected mosquitoes, the cost of vaccination, the cost of treatment, and the cost of abateseae, respectively.

The overall algorithm for optimizing the weights  $W_1, W_2, W_3, W_4, W_5, W_6$  using the FA is as follows:

1. Generate the initial population position of fireflies  $x^i = (W_1^i, W_2^i, W_3^i, W_4^i, W_5^i, W_6^i)$ ,  $i = 1, 2, \dots, \max pop$ , and compute the fitness value

$$f(x^i) = control\_dengue (W_1^i, W_2^i, W_3^i, W_4^i, W_5^i, W_6^i) \quad i = 1, 2, \dots, \max pop.$$

2. Determine the best firefly in the population with its position

$$i^{\min} \leftarrow \arg \min_i (f(x^i), i = 1, 2, \dots, \max pop), \quad (21)$$

$$x^{i^{\min}} \leftarrow \arg \min_{x^i} (f(x^i), i = 1, 2, \dots, \max pop). \quad (22)$$

3. Do the iteration as follows:

for  $i = 1 : \max pop$   
 for  $j = 1 : \max pop$   
 if ( $f(x)^j < f(x^i)$ ).

- a. Compute the distance between the firefly  $i$  and the firefly  $j$

$$r_{ij} = \|x^i - x^j\| = \sqrt{\sum_{t=1}^T (x_t^i - x_t^j)^2}.$$

- b. Compute the attractiveness function of a firefly  $\beta \leftarrow \beta_0 e^{-\gamma r_{ij}}$ .

- c. Generate  $u_i = \alpha (rand - \frac{1}{2})$ , with  $rand \sim U(0, 1)$ .

d. Update the movement of the firefly  $i$

$$x^i \leftarrow (1 - \beta)x^i + \beta x^j + u_i$$

end

end

end

Generate  $u_{i\min} = \alpha (rand - \frac{1}{2})$ , with  $rand \sim U(0, 1)$ .

Update the movement of the best firefly

$$x^{i\min} \leftarrow x^{i\min} + u_{i\min}.$$

4. Repeat step 3 until stopping criteria is achieved.

#### 4 Simulation Results

Parameters used in the FA simulations are  $\beta_0 = 1, \gamma = 5, \alpha = 0.1$  with the number of fireflies being 10 and maximum iterations being 50. Parameters used in the dengue fever model are [15], [16]:

Parameters	Value
The recruitment rate (birth or immigration) of the human population $\Lambda$	3
The natural death rate of humans $\mu_h$	$\frac{1}{(70 \times 365)}$
The natural death rate of mosquitoes (adult phase) $\mu_m$	0.0741
The natural death rate of mosquitoes (aquatic phase) $\mu_A$	0.2
The average daily biting (per day) of the mosquito $B$	0.5
The transmission probability (per bite) from infected mosquitoes to humans $\beta_{mh}$	0.38
The transmission probability (per bite) from infected humans to mosquitoes $\beta_{hm}$	0.38
The number of eggs at each deposit per capita (per day) $\varphi$	3
The recovery rate of the human population $\eta_h$	0.17
The maturation rate from larvae to adult mosquitoes (per day) $\eta_A$	0.0541
The death by the disease rate of humans $\alpha_h$	0.000457

**Table 1:** Parameters of the Dengue Fever Model.

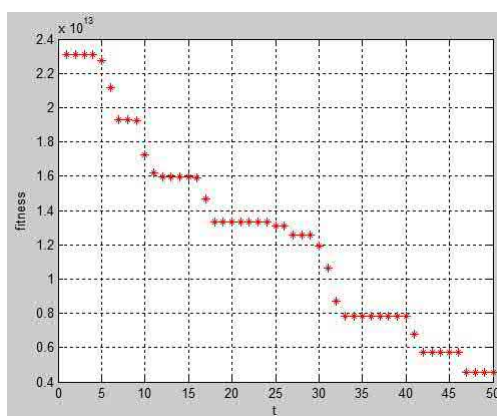
The simulations of the optimal control dengue fever model can be seen in Figures 3-5, while Figure 2 is the FA simulation.

Figure 2 shows the optimization process of the FA. At the first iteration, the positions of fireflies are random. In the optimization process, we update the brightness of fireflies so that the fireflies move toward the brighter firefly with the minimum fitness function. Optimal weights obtained are  $W_1 = 0.641, W_2 = 0.110, W_3 = 6.040, W_4 = 5.581, W_5 = 7.443, W_6 = 1.990$  with the minimum fitness being  $4.529 \times 10^{12}$ .

Figure 3 shows the numerical solution for larvae with and without control. The number of larvae with control is lower than that without control because of the abateseae effect which decreases the number of larvae. The decrease of larvae will cause the decrease of the number of susceptible mosquitoes and infected mosquitoes.

Initial Value	Value
Susceptible humans $S_h(0)$	39850
Infected humans $I_h(0)$	50
Recovered humans $R_h(0)$	100
Larvae $A_m(0)$	50
Susceptible mosquitoes $S_m(0)$	1500
Infected mosquitoes $I_m(0)$	100

**Table 2:** Initial Value of Dengue Fever Model.



**Figure 2:** The FA Optimization Process.

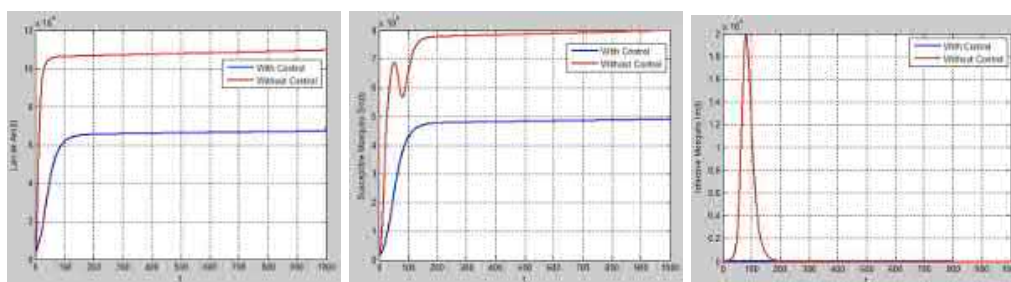


**Figure 3:** Numerical Solutions for Mosquitoes as a Vector. (a) Larvae. (b) Susceptible Mosquitoes. (c) Infected Mosquitoes.

Figure 4(a) shows the numerical solution for susceptible humans with and without control. The number of susceptible humans with control is lower than that without control because of the vaccination effect which decreases the number of susceptible humans. Figure 4(b) shows the numerical solution for infected humans with and without control. The number of infected humans with control is lower than that without control because of the treatment effect which decreases the number of infected humans. Figure 4(c) shows the numerical solution for recovered humans with and without control. The

number of recovered humans with control is higher than that without control because of the vaccination and treatment effect which increases the number of recovered humans.

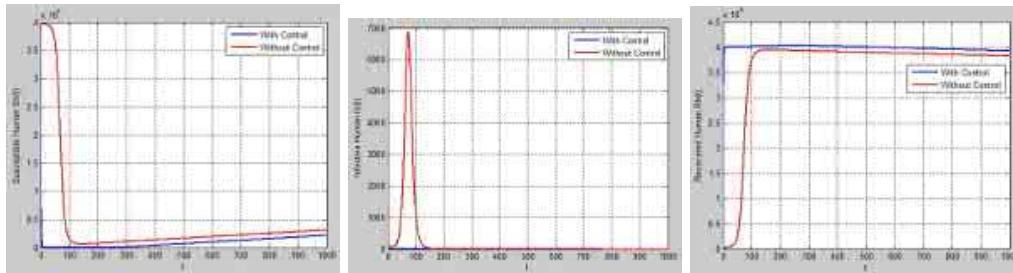


**Figure 4:** Numerical Solutions for Humans as a Host. (a) Susceptible Humans. (b) Infected Humans. (c) Recovered Humans.

Figure 5 shows the control function of vaccination, the control function of treatment and the control function of abateseae. Each of the control functions has the range of effectiveness between 0 to 1, where the value 0 means the control functions fail or are not applied and the value 1 means the control functions are successful or applied entirely.

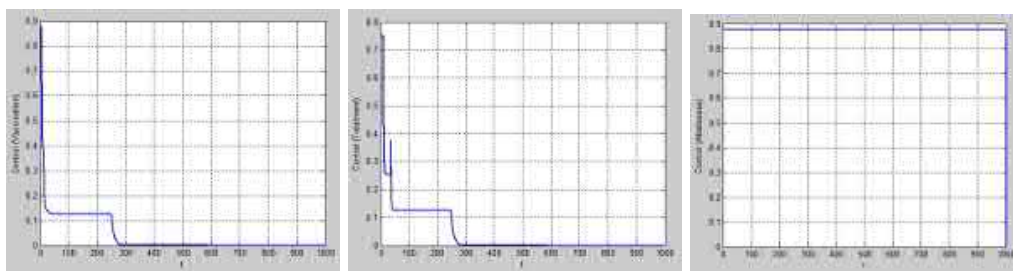


**Figure 5:** Control Function Solutions. (a) Vaccination. (b) Treatment. (c) Abateseae.

## 5 Conclusion

The FA can optimize the weights of the optimal control dengue fever model. From the simulations, the positions of fireflies are random. In the optimization process, we update the brightness of fireflies so that the fireflies move toward the brighter firefly with the minimum fitness function. When the FA has obtained optimal weights related to the number of infected humans, the number of larvae, the number of infected mosquitoes, the cost of vaccination, the cost of treatment, and the cost of abateseae, respectively, the optimal weights are applied in dengue fever simulation. Based on the parameters of the dengue fever model, we can compare the numerical solutions for larvae, susceptible mosquitoes, infected mosquitoes in the mosquito population and the susceptible humans, infected humans, and recovered human in the human population when the vaccination, treatment, and abateseae controls are applied.

## References

- [1] F. Brauer and C. Castillo-Chavez. *Mathematical Models in Population Biology and Epidemiology*. Springer, New York, 2012.
- [2] J. B. Burl. *Linear Optimal Control*. CA : Addison-Wesley, Menlo Park, 1999.
- [3] S. Lenhart and J. T. Workman. *Optimal Control Applied to Biological Models*. CRC Press, London, 2007.
- [4] X. S. Yang, Z. Chui and R. Xiao. *Swarm Intelligence and Bio-Inspired Computation*. Elsevier, 2013.
- [5] Z. Michalewicz, J. B. Krawczyk and C. Z. Janikow. A Modified Genetic Algorithm for Optimal Control Problem. *Computers Math Application*. **23** (1992) 83–94.
- [6] D. Rahmalia, and T. Herlambang. Application Ant Colony Optimization on Weight Selection of Optimal Control SEIR Epidemic Model. *Proceeding The 7th Annual Basic Science International Conference* (2017) 196–199.
- [7] D. Rahmalia and T. Herlambang. Weight Optimization of Optimal Control Influenza Model Using Artificial Bee Colony. *International Journal of Computing Science and Applied Mathematics* **4** (2018) 27–31.
- [8] T. Herlambang, D. Rahmalia and T. Yulianto. Particle Swarm Optimization (PSO) and Ant Colony Optimization (ACO) for Optimizing PID Parameters on Autonomous Underwater Vehicle (AUV) Control System. *Journal of Physics : Conference Series* **1211** (2019) 123039.
- [9] T. Herlambang, D. Rahmalia, H. Nurhadi, D. Adzkiya and S. Subchan. Optimization of Linear Quadratic Regulator with Tracking Applied to Autonomous Underwater Vehicle (AUV) Using Cuckoo Search. *Nonlinear Dynamics and Systems Theory* **20** (3) (2021) 282–298.
- [10] T. Herlambang, S. Subchan, H. Nurhadi and D. Adzkiya. Motion Control Design of UN-USAITS AUV Using Sliding PID. *Nonlinear Dynamics and Systems Theory* **20** (1) (2020) 51–60.
- [11] A. Khernane. Numerical Approximation of the Exact Control for the Vibrating Rod with Improvement of the Final Error by Particle Swarm Optimization. *Nonlinear Dynamics and Systems Theory* **20** (2) (2021) 179–190.
- [12] E. R. M. Putri, M. Iqbal, M. L. Shahab, H. N. Fadhillah, I. Mukhlash, D. K. Arif, E. Apriliani and H. Susanto. COVID-19 Outbreak Prediction in Indonesia Based on Machine Learning and SIRD-Based Hybrid Methods. *Nonlinear Dynamics and Systems Theory* **21** (5) (2021) 494–509.
- [13] D. Rahmalia. Pemodelan Matematika dan Analisis Stabilitas dari Penyebaran Penyakit Flu Burung. *Unisda Journal of Mathematics and Computer Science (UJMC)* **1** (2015) 11–19.
- [14] R. Widyaningrum, S. Partiw, A. Rahman and A. Sudiarno. Prediction of Dengue Fever Epidemic Spreading Using Dynamics Transmission Vector Model. *Indonesian Journal of Tropical and Infectious Disease* **5** (2014) 41–48.
- [15] R. W. S. Hendron and M. B. Bonsall. The Interplay of Vaccination and Vector Control on Small Dengue Networks. *Journal of Theoretical Biology* **407** (2016) 349–361.
- [16] H. S. Rodrigues, M. T. Monteiro and D. F. M. Optimal Control of a Dengue Epidemic Model with Vaccination. *AIP Conference Proceedings* **1389** (2011).
- [17] I. Fitria, W. Winarni, S. Pancahayani and S. Subchan. An Optimal Control Strategies Using Vaccination and Fogging in Dengue Fever Transmission Model. *AIP Conference Proceedings* **1867** (2017).



# Inverse Problem of a Semilinear Parabolic Equation with an Integral Overdetermination Condition

Amal Benguesmia<sup>1</sup>, Iqbal M. Batiha<sup>2,3\*</sup>, Taki-Eddine Oussaeif<sup>1</sup>, Adel  
Ouannas<sup>1</sup> and Waseem G. Alshanti<sup>2</sup>

<sup>1</sup> *Department of Mathematics and Computer Science, University of Larbi Ben M'hidi,  
Oum El Bouaghi, Algeria.*

<sup>2</sup> *Department of Mathematics, Al Zaytoonah University of Jordan, Amman 11733, Jordan.*

<sup>3</sup> *Nonlinear Dynamics Research Center (NDRC), Ajman University, Ajman, UAE.*

Received: February 9, 2023; Revised: May 27, 2023

**Abstract:** The solvability of the semilinear parabolic problem with integral overdetermination condition for an inverse problem is investigated in this work. Accordingly, we solve the generated direct problem by using the so-called “energy inequality” method and then the inverse problem is handled with the use of the fixed point technique.

**Keywords:** *inverse problem; nonlocal integral condition; fixed point theorem.*

**Mathematics Subject Classification (2010):** 35R30, 35K58, 70K60.

## 1 Introduction

The goal of this research was to investigate the solvability of a pair of functions  $\{y, f\}$  that satisfy the following semilinear parabolic problem:

$$y_t - a \frac{\partial^2 y}{\partial x^2} + by + cy^3 = f(t)h(x, t), \quad (x, t) \in \Omega \times (0, T), \quad (1)$$

with the initial condition

$$y(x, 0) = \varphi(x), \quad x \in \Omega, \quad (2)$$

the boundary condition

$$y(x, t) = 0, \quad (x, t) \in \partial\Omega \times (0, T), \quad (3)$$

---

\* Corresponding author: <mailto:i.batiha@zu.edu.jo>

and the nonlocal overdetermination condition

$$\int_{\Omega} y(x, t)v(x)dx = E(t), \quad t \in (0, T), \quad (4)$$

where  $\Omega$  is a bounded domain of  $\mathbb{R}^n$  with smooth boundary  $\partial\Omega$ , the functions  $g$ ,  $\varphi$ , and  $E$  are well-known and  $\beta$  is a positive constant. In this case, supplementary or additional information about the solution of the main problem comes in the form of integral condition (4).

Inverse boundary value problems exist in a variety of domains, including seismology, biology and physics [1,2]. Inverse problems for parabolic equations satisfying the nonlocal overdetermination condition were first investigated in [3–5], whereas the references [6–8] discussed this subject for equations with time-independent coefficient under first and third-order boundary conditions. Several solvability investigations of the inverse problem and others were carried out in [9–12]. The theory of the existence and uniqueness of the inverse problem has been examined by many authors, see [13–17] and also [18–20]. In the present work, a new study for the inverse problem of a semilinear parabolic equation is presented. The existence and uniqueness of the classical solution to problem (1)-(4) are analysed by a fixed point technique.

## 2 Preliminaries

Let us now give certain notations and rules that we will use:

$$g^*(t) = \int_{\Omega} v(x)h(x, t)dx, \quad Q = \Omega \times (0, T).$$

We use also the well-known inequality (Cauchy's  $\varepsilon$ -inequality)

$$2|ab| \leq \varepsilon a^2 + \frac{1}{\varepsilon} b^2, \quad a, b \in \mathbb{R}.$$

**Lemma 2.1** (*Gronwall's Lemma*) *Let  $f \in L^\infty(0, T)$ ,  $g \in L^1(0, T)$  and  $f(t) \geq 0, g(t) \geq 0$ . If we have*

$$f(t) \leq c + \int_0^t f(s)g(s)ds,$$

then

$$f(t) \leq c \exp\left(\int_0^t g(s)ds\right).$$

**Lemma 2.2** (*Poincare Inequality*) *If  $\Omega$  is bounded in at least one direction, then there exists a constant  $c = c_{\Omega, p} > 0$  such that*

$$\int_{\Omega} |u|^p dx \leq c \left( \sum_{i=1}^n \int_{\Omega} \left| \frac{\partial u}{\partial x_i} \right|^p dx \right),$$

or, what is equivalent,

$$\|u\|_{L^p(\Omega)} \leq c' \|\nabla u\|_{(L^p(\Omega))^n}, \quad \forall u \in W_0^{1,p}(\Omega),$$

where  $c'$  is a constant dependant on  $c$  given by

$$c' = c^{\frac{1}{p}}.$$

### 3 Existence and Uniqueness of the Solution to the Direct Problem

#### 3.1 Setting of the problem

In the rectangle  $Q = (0, 1) \times (0, T) = \Omega \times (0, T)$ , with  $T < \infty$ , we consider the semilinear parabolic problem

$$(P) \quad \begin{cases} y_t - a \frac{\partial^2 y}{\partial x^2} + by + cy^3 = f(x, t), & (x, t) \in \Omega \times (0, T), \\ y(x, 0) = \varphi(x), & x \in \Omega, \\ y(x, t) = 0, & (x, t) \in \partial\Omega \times (0, T), \end{cases}$$

$$\mathcal{L}y = y_t - a \frac{\partial^2 y}{\partial x^2} + by + cy^3 = f(x, t), \tag{5}$$

with the initial condition

$$ly = y(x, 0) = \varphi(x), \quad x \in \Omega, \tag{6}$$

and the Dirichlet boundary condition

$$y(x, t) = 0, \quad (x, t) \in \partial\Omega \times (0, T), \tag{7}$$

where the functions  $f(x, t)$  and  $y_0(x)$  are known functions and  $a, b, c$  are also given constants that verify the following hypothesis:

$$A1 : a \geq 0, b \geq 0, c \geq 0.$$

The operator  $L$  is defined from  $E$  to  $F$ , where  $E$  is the Banach space, which contains all functions  $y(x, t)$  with finite norms

$$\|y\|_E^2 = \|y\|_{L^\infty(0,T,L^2(\Omega))}^2 + \left\| \frac{\partial y}{\partial x} \right\|_{L^2(Q)}^2 + \|y\|_{L^2(Q)}^2 + \|y\|_{L^4(Q)}^4.$$

Besides,  $F$  represents the Hilbert space, which includes all elements  $\mathcal{F} = (f, \varphi)$  for which the norm

$$\|\mathcal{F}\|_F^2 = \|f\|_{L^2(Q)}^2 + \|\varphi\|_{L^2(\Omega)}^2$$

is finite.

#### 3.1.1 A priori estimate

**Theorem 3.1** *Let condition A1 be satisfied. Then for any function  $y \in D(L)$ , we have the inequality*

$$\|y\|_E \leq C \|Ly\|_F,$$

where  $C$  is a positive constant independent of  $y$  and  $D(L)$  denotes the domain of definition of the operator  $L$ , which can be defined by

$$D(L) = \{y \mid y, y_t, \frac{\partial y}{\partial x}, \frac{\partial^2 y}{\partial x^2} \in L^2(Q), y \in L^4(Q)\}.$$

**Proof.** Taking the scalar product in  $L^2(Q)$  of (5) and  $My = y$ , we have

$$\begin{aligned} \langle \mathcal{L}y, My \rangle_{L^2(Q)} &= \langle y_t, y \rangle_{L^2(Q)} - a \langle \frac{\partial^2 y}{\partial x^2}, y \rangle_{L^2(Q)} + b \langle y, y \rangle_{L^2(Q)} + c \langle y^3, y \rangle_{L^2(Q)} \\ &= \langle f, y \rangle_{L^2(Q)}. \end{aligned} \tag{8}$$

Integrating (3.1.1) and applying Cauchy's  $\varepsilon$ -inequality yield

$$\begin{aligned} \frac{1}{2} \|y(\cdot, \tau)\|_{L^2(\Omega)}^2 + a \|\frac{\partial y}{\partial x}\|_{L^2(Q)}^2 + b \|y\|_{L^2(Q)}^2 + c \|y\|_{L^4(Q)}^4 \\ \leq \frac{1}{2\varepsilon} \|f\|_{L^2(Q)}^2 + \frac{1}{2} \|\varphi\|_{L^2(\Omega)}^2 + \frac{\varepsilon}{2} \int_0^T \|y\|_{L^2(\Omega)}^2 dt. \end{aligned}$$

Using Gronwall's lemma and the fact that the right-hand side is not related to  $\tau$ , we substitute the left-hand side with its upper bound with respect to  $\tau$  from 0 to  $T$  to obtain

$$\|y\|_{L^\infty(0,T,L^2(\Omega))}^2 + \|\frac{\partial y}{\partial x}\|_{L^2(Q)}^2 + \|y\|_{L^2(Q)}^2 + \|y\|_{L^4(Q)}^4 \leq C(\|f\|_{L^2(Q)}^2 + \|\varphi\|_{L^2(\Omega)}^2),$$

where

$$C = \frac{\max(\frac{c'}{2}, \frac{c'}{2\varepsilon})}{\min(\frac{1}{2}, a, b, c)} \quad \text{and} \quad c' = \exp(\frac{\varepsilon T}{2}).$$

Consequently, we have

$$\|y\|_E \leq C \|Ly\|_F. \tag{9}$$

**Proposition 3.1** *The operator  $L$  from  $E$  to  $F$  has a closure.*

**Proof.** Let  $(y_n)_{n \in \mathbb{N}} \subset D(L)$  be a sequence such that

$$y_n \longrightarrow 0 \quad \text{in } E$$

and

$$Ly_n \longrightarrow (f, \varphi) \quad \text{in } F. \tag{10}$$

Herein, we should prove that

$$f \equiv 0, \varphi \equiv 0 \quad \text{in } F.$$

The convergence of  $y_n$  to 0 in  $E$  entails that

$$y_n \longrightarrow 0 \quad \text{in } D'(Q). \tag{11}$$

According to the continuity of the derivation of  $D'(Q)$  and the continuity distribution of the function  $y^2$ , relation (11) involves

$$\mathcal{L}y_n \longrightarrow 0 \quad \text{in } D'(Q). \tag{12}$$

Also, the convergence of  $Ly_n$  to  $f$  in  $L^2(Q)$  gives

$$\mathcal{L}y_n \longrightarrow f \quad \text{in } D'(Q). \tag{13}$$

By means of the uniqueness of the limit in  $D'(Q)$ , we can deduce from (12) and (13) that  $f \equiv 0$ . Therefore, it can be generated from (10) that

$$ly_n \longrightarrow \varphi \quad \text{in } L^2(\Omega).$$

On the other hand, we have

$$\|y_n\|_E \geq \|y_n\|_{L^\infty(0,T,L^2(\Omega))}^2,$$

i.e.,

$$\|y_n\|_E \geq \|\varphi\|_{L^2(\Omega)}^2.$$

Immediately, we have

$$y_n \longrightarrow 0 \quad \text{in } E,$$

which implies

$$\|y_n\|_E^2 \longrightarrow 0 \quad \text{in } \mathbb{R}.$$

So, we get  $\varphi \equiv 0$ , and as a result, the operator  $L$  is closable.

**Definition 3.1** Let  $\bar{L}$  be the closure of  $L$  and  $D(\bar{L})$  be the definition domain of  $\bar{L}$ . The solution of the equation

$$\bar{L}y = F$$

is called a strong solution to problem (5)-(7). Then a priori estimate (9) can be extended to the strong solution, i.e., we have the following inequality:

$$\|y\|_E \leq C\|\bar{L}y\|_F, \forall y \in D(\bar{L}). \tag{14}$$

**Corollary 3.1** The range  $R(\bar{L})$  of the operator  $\bar{L}$  is closed in  $F$  and equal to the closure  $\overline{R(L)}$  of  $R(L)$ .

**Proof.** First, we prove the uniqueness of the solution if it exists. Let  $y_1$  and  $y_2$  be two different solutions. If we put  $\eta = y_1 - y_2$ , then  $\eta$  satisfies

$$(P') \quad \begin{cases} \eta_t - a \frac{\partial^2 \eta}{\partial x^2} + c(y_1^3 - y_2^3) + b\eta = 0, & (x, t) \in Q, \\ \eta(x, 0) = 0, & x \in \Omega, \\ \eta(x, t) = 0, & (x, t) \in \partial\Omega \times (0, T) \end{cases} \tag{15}$$

$$\eta_t - a \frac{\partial^2 \eta}{\partial x^2} + c(y_1^3 - y_2^3) + b\eta = 0, \quad (x, t) \in Q. \tag{16}$$

By multiplying (16) by  $\eta$  and integrating the result over  $\Omega$ , we get

$$\int_{\Omega} \eta_t(x, t) \cdot \eta(x, t) dx - a \int_{\Omega} \frac{\partial^2 \eta}{\partial x^2} \cdot \eta(x, t) dx + c \int_{\Omega} (y_1^3 - y_2^3)(y_1 - y_2) dx + b \int_{\Omega} \eta^2(x, t) dx = 0.$$

Consequently, we can get

$$\frac{1}{2} \frac{d}{dt} \|\eta\|_{L^2(\Omega)}^2 + a \left\| \frac{\partial \eta}{\partial x} \right\|_{L^2(\Omega)}^2 + b \|\eta\|_{L^2(\Omega)}^2 + c \int_{\Omega} (y_1^3 - y_2^3)(y_1 - y_2) dx = 0. \tag{17}$$

As the function  $\lambda^3$  is a monotone function over  $\Omega$ , we can conclude that the last term of the left-hand side of (17) is positive, so it follows that

$$\frac{d}{dt} \|\eta\|_{L^2(\Omega)}^2 \leq 0,$$

which implies that for all  $t \in (0, T)$ , we have  $y_1(t) = y_2(t)$  in  $E$ . Now, we will return to the proof of Corollary 3.1. To this end, we let  $z \in R(\bar{L})$ . Then there exists a Cauchy sequence  $(z_n)_{n \in \mathbb{N}}$  in  $R(L)$  such that

$$\lim_{n \rightarrow +\infty} z_n = z.$$

So, there exists a corresponding sequence  $(y_n)_{n \in \mathbb{N}}$  in  $D(L)$  such that  $Ly_n = z_n$ . Now, let  $\varepsilon, n \geq n_0$  and  $m, m' \in \mathbb{N}$  such that  $m \geq m'$  and  $y_m, y_{m'}$  are two solutions, i.e.,

$$Ly_m = f \quad \text{and} \quad Ly_{m'} = f.$$

We put  $\phi = y_m - y_{m'}$  and we apply to  $\phi$  the same procedure that we used to demonstrate the uniqueness of the solution in the previous step. This yields  $\phi = 0$ . It means that for all  $t \in (0, T)$ , we have

$$0 \leq \|y_m(t) - y_{m'}(t)\|_E \leq 0 \tag{18}$$

$$\Leftrightarrow \forall \varepsilon \geq 0, \quad \exists n_0 \in \mathbb{N} \setminus \forall m, m' \geq n_0 : \|y_m(t) - y_{m'}(t)\|_E \leq \varepsilon.$$

As a result,  $(y_n)_n$  is a Cauchy sequence in the Banach space  $E$ . So, there is  $y \in E$  such that

$$\lim_{n \rightarrow +\infty} y_n = y.$$

By virtue of the definition of  $\bar{L}$  (i.e.,  $\lim_{n \rightarrow +\infty} y_n = y$  if  $\lim_{n \rightarrow +\infty} Ly_n = \lim_{n \rightarrow +\infty} z_n = z$ , and so  $\lim_{n \rightarrow +\infty} \bar{L}y_n = z$  as  $\bar{L}$  is closed, which implies that  $\bar{L}y = z$ ), the function  $y$  verifies

$$y \in D(\bar{L}), \quad \bar{L}y = z.$$

Thus  $z \in R(\bar{L})$ , and so  $\overline{R(L)} \subset R(\bar{L})$ . In the same regard, we can also deduce that  $R(\bar{L})$  is closed because it is a Banach space. It remains to prove the reverse inclusion. For this purpose, we observe that  $z \in R(\bar{L})$ , and then there exists a sequence of  $(z_n)_n$  in  $F$  consisting of the elements of the set  $R(\bar{L})$  such that

$$\lim_{n \rightarrow +\infty} z_n = z.$$

As a result, there exists a corresponding sequence  $(v_n)_n \subset D(\bar{L})$  such that

$$\lim_{n \rightarrow +\infty} \bar{L}v_n = z_n.$$

On the other hand, we have  $(v_n)_n$  is a Cauchy sequence in  $F$ . So, there is  $v \in E$  such that

$$\lim_{n \rightarrow +\infty} v_n = v, \quad v \in E.$$

This implies

$$\lim_{n \rightarrow +\infty} \bar{L}v_n = z.$$

Consequently,  $z \in \overline{R(L)}$ , and hence we conclude that  $R(\bar{L}) \subset \overline{R(L)}$ .

**3.1.2 Solvability of the direct problem**

To prove the existence of the solution, we must prove that  $R(L)$  is dense in  $F$  for all  $y \in E$  and for arbitrary  $\mathcal{F} = (f, \varphi) \in F$ .

**Theorem 3.2** *Suppose that A1 is satisfied. Then for each  $\mathcal{F} = (f, \varphi) \in F$ , there is a unique strong solution  $y = L^{-1}\mathcal{F} = \overline{L^{-1}}\mathcal{F}$  to problem (P).*

**Proof.** First, we prove that  $R(L)$  is dense in  $F$  for all  $y \in D(L)$  for the exceptional case when  $D(L)$  is reduced to  $D_0(L)$ , where

$$D_0(L) = \{y, y \in D(L) : ly = 0\}.$$

**Proposition 3.2** *Let the conditions of Theorem 3.2 be satisfied. If for  $w \in L^2(Q)$  and for each  $y \in D_0(L)$ , we have*

$$\int_Q \mathcal{L}y \cdot w dxdt = 0, \tag{19}$$

then  $w$  vanishes almost everywhere in  $Q$ .

**Proof.** The scalar product of  $F$  is defined as follows:

$$(Ly, W)_F = \int_Q \mathcal{L}y \cdot w dxdt, W = (w, 0) \in D(L). \tag{20}$$

If we put  $y = w$ , the equality (19) can be written as follows:

$$\int_Q y_t(t, x) \cdot y(t, x) dxdt - a \int_Q \frac{\partial^2 y}{\partial x^2} \cdot y(t, x) dxdt + b \int_Q y^2(t, x) dxdt + c \int_Q y^4(t, x) dxdt = 0. \tag{21}$$

Integrating (21) by parts yields

$$a \|\frac{\partial y}{\partial x}\|_{L^2(Q)}^2 + b \|y\|_{L^2(Q)}^2 + c \|y\|_{L^4(Q)}^4 = \frac{-1}{2} \|y\|_{L^2(\Omega)}^2.$$

So, we can deduce that  $\|y\|_{L^2(Q)}^2 \leq 0$ , i.e.,  $y \equiv 0$  in  $Q$ , and hence  $w \equiv 0$ . Now, we return to the proof of Theorem 3.2. To this end, we suppose that  $W = (w, w_1) \in R^{\perp}(L)$ . This implies

$$(Ly, W)_F = \int_Q \mathcal{L}y \cdot w dxdt + \int_{\Omega} ly \cdot w_1 dx = 0, \forall y \in D(L). \tag{22}$$

By means of the last proposition and by putting  $y \in D_0(L)$ , we obtain  $w \equiv 0$ . Thus, (22) becomes

$$\int_{\Omega} ly \cdot w_1 dx = 0, \forall y \in D(L). \tag{23}$$

The range of the trace operator  $l$  is dense in the Hilbert space  $F$ , then the equality (23) implies that  $w_1 = 0$ . As a result, we can conclude that  $W = 0$ , and this completes the proof of Theorem 3.2.

#### 4 Existence and Uniqueness of Solution of the Inverse Problem

In this section, we will suppose that the functions appearing in the problem data are measurable and satisfy the following conditions:

$$(H) \quad \begin{cases} h \in C(0, T, L^2(\Omega)), v \in V = \{v, \frac{\partial v}{\partial x} \in L^2(\Omega), v \in L^4(\Omega)\}, & E \in W_2^2(0, T), \\ \|h(x, t)\| \leq m; |g^*(t)| \geq r > 0, & \text{for } r \in \mathbb{R}, \quad (x, t) \in Q, \\ \varphi(x) \in W_2^1(\Omega). \end{cases} .$$

The relation between  $f$  and  $y$  is given by the following linear operator:

$$A : L^2(0, T) \longrightarrow L^2(0, T), \quad (24)$$

with the value

$$Af(t) = \frac{1}{g^*} \left\{ a \int_{\Omega} \frac{\partial y}{\partial x} \frac{\partial v}{\partial x} dx + c \int_{\Omega} y^3(t, x)v(x)dx \right\}. \quad (25)$$

As a result, the preceding relationship between  $f$  and  $y$  may be expressed as a second-order linear equation for the function  $f$  over  $L^2(0, T)$  such that

$$f = Af + \mu, \quad (26)$$

where

$$\mu = \frac{E' + bE}{g^*}. \quad (27)$$

**Theorem 4.1** *Assume that the input of data of the inverse problem (1)-(4) verifies condition (H). Then the following statements are equivalent:*

- *If the inverse problem (1)-(4) is solved, then so is equation (26).*
- *If equation (26) has a solution and the compatibility condition  $E(0) = \int_{\Omega} \varphi(x)v(x)dx$  is true, then the inverse problem (1)-(4) has also a solution.*

**Proof.**

- Assume that the inverse problem (1)-(4) is solved. We denote its solution by  $\{y, f\}$ . Now, multiplying (1) by  $v$  and then integrating the result over  $\Omega$  yield

$$\begin{aligned} \frac{d}{dt} \int_{\Omega} y(t, x)v(x)dx + a \int_{\Omega} \frac{\partial y}{\partial x} \frac{\partial v}{\partial x} dx + b \int_{\Omega} y(x, t)v(x)dx + c \int_{\Omega} y^3(t, x)v(x)dx \\ = f(t)g^*(t). \end{aligned} \quad (28)$$

Using (4) and (24) implies

$$\frac{E' + bE}{g^*} + Af = f.$$

This gives that  $f$  solves equation (26).

- According to the assumption, the equation (25) has a solution, say  $f$ . By substituting  $f$  into equation (1), the resulting relationships (1)-(3) can be then treated as a direct problem with a unique solution. It is yet up to us to show that  $y$  verifies the integral overdetermination (4). By the equation (28), the function  $y$  is subject to the following relation:

$$E' + bE + a \int_{\Omega} \frac{\partial y}{\partial x} \frac{\partial v}{\partial x} dx + c \int_{\Omega} y^3(t, x)v(x)dx = f(t)g^*(t). \tag{29}$$

Subtracting equation (28) from (29) yields

$$\frac{d}{dt} \int_{\Omega} y(t, x)v(x)dx + b \int_{\Omega} y(x, t)v(x)dx = E' + bE. \tag{30}$$

Now, integrating the above differential equation and using the compatibility condition  $E(0) = \int_{\Omega} \varphi(x)v(x)dx$  lead us to the conclusion that  $y$  satisfies the integral condition (4). As a result, we can conclude that  $\{y, f\}$  is the solution of the inverse problem (1)-(4).

In what follows, we aim to introduce some properties connected to the operator  $A$ .

**Lemma 4.1** *If (H1) holds, then there exists a positive  $\delta$  for which the operator  $A$  is a contracting operator in  $L^2(0, T)$ .*

**Proof.** We obtain from (25) the following estimate:

$$|Af(t)|^2 \leq \frac{2}{r^2} [a^2 \|\frac{\partial y}{\partial x}\|_{L^2(\Omega)}^2 \|\frac{\partial v}{\partial x}\|_{L^2(\Omega)}^2 + \gamma \|v\|_{L^4(\Omega)}^2 \|y\|_{L^4(\Omega)}^4],$$

where  $\gamma = \|y\|_{L^\infty(0, T, L^4(\Omega))}^2 \geq 0$ . Now, integrating the above equality over  $(0, T)$  yields

$$\int_0^T |Af(t)|^2 \leq \frac{2}{r^2} \max(a^2 \|\frac{\partial v}{\partial x}\|_{L^2(\Omega)}^2, \gamma \|v\|_{L^4(\Omega)}^2) \int_0^T (\|\frac{\partial y}{\partial x}\|_{L^2(\Omega)}^2 + \|y\|_{L^4(\Omega)}^4) dt. \tag{31}$$

So, we get

$$\|Af\|_{L^2(0, T)} \leq K \left( \int_0^T (\|\frac{\partial y}{\partial x}\|_{L^2(\Omega)}^2 + \|y\|_{L^4(\Omega)}^4) dt \right)^{\frac{1}{2}},$$

where

$$K = \frac{1}{r} \sqrt{2 \max(a^2 \|\frac{\partial v}{\partial x}\|_{L^2(\Omega)}^2, \gamma \|v\|_{L^4(\Omega)}^2)}.$$

By multiplying both sides of (1) by  $y$  in  $L^2(Q)$  and then by integrating the resulting expression by parts with the use of Cauchy's  $\varepsilon$ -inequality and the Poincare inequality, we get

$$\frac{1}{2} \|y\|_{L^2(\Omega)}^2 + (a - \frac{c''\varepsilon}{2}) \|\frac{\partial y}{\partial x}\|_{L^2(Q)}^2 + b \|y\|_{L^2(Q)}^2 + c \|y\|_{L^4(Q)}^4 \leq \frac{m^2}{2\varepsilon} \|f\|_{L^2(0, T)}^2 + \frac{1}{2} \|\varphi\|_{L^2(\Omega)}^2, \tag{32}$$

with  $a - \frac{c''\varepsilon}{2} > 0$ . With the help of passing to the maximum and omitting some terms, we get

$$\int_0^T (\|\frac{\partial y}{\partial x}\|_{L^2(\Omega)}^2 + \|y\|_{L^4(\Omega)}^4) dt \leq M' \|f\|_{L^2(0, T)}^2, \tag{33}$$

where

$$M' = \frac{\frac{m^2}{2\varepsilon}}{\min(a - \frac{c''\varepsilon}{2}, c)}.$$

It means that

$$\left( \int_0^T (\|\frac{\partial y}{\partial x}\|_{L^2(\Omega)}^2 + \|y\|_{L^4(\Omega)}^4) dt \right)^{\frac{1}{2}} \leq M'' \|f\|_{L^2(0,T)}, \quad (34)$$

where  $M'' = \sqrt{M'}$ . Consequently, we get

$$\|Af\|_{L^2(0,T)} \leq \delta \|f\|_{L^2(0,T)}, \quad (35)$$

with  $\delta = KM''$ . It is obvious from the above assertion that there exists a positive  $\delta$  such that  $\delta \leq 1$ . Thus, inequality (35) demonstrates that the operator  $A$  is a contracting mapping in  $L^2(0, T)$ .

**Theorem 4.2** *Let the compatibility condition  $E(0) = \int_{\Omega} \varphi(x)v(x)dx$  and the condition (H) hold. Then the following statements are correct:*

- *With any initial iteration  $f_0 \in L^2(0, T)$ , the following approximations are correct:*

$$f_{n+1} = \mathcal{A}f_n, \quad (36)$$

*which converge to  $f$  in the  $L^2(0, T, L^2(0, T))$ -norm.*

- *The inverse problem (1)-(4) has a unique solution  $\{y, f\}$ .*

**Proof.**

- We have the following operator  $\mathcal{A} : L^2(0, T) \rightarrow L^2(0, T, L^2(0, T))$ , which is defined by

$$\mathcal{A}f = Af + \frac{E' + bE}{g^*}, \quad (37)$$

where the operator  $A$  and the function  $g^*$  come from (25). As a result of (36), relation (26) can be expressed as

$$f = \mathcal{A}f. \quad (38)$$

As a result, it is sufficient to show that the operator  $\mathcal{A}$  has a fixed point in the space  $L^2(0, T, L^2(0, T))$ . Accordingly, we can have

$$\mathcal{A}f_1 - \mathcal{A}f_2 = Af_1 - Af_2 = A(f_1 - f_2).$$

From estimate (35), we can deduce that

$$\|\mathcal{A}f_1 - \mathcal{A}f_2\|_{L^2(0,T)} \leq \delta \|f_1 - f_2\|_{L^2(0,T,L^2(0,T))}. \quad (39)$$

Based on (38),  $\mathcal{A}$  is a contracting mapping on  $L^2(0, T, L^2(0, T))$ . As a result,  $\mathcal{A}$  has a unique fixed point  $f$  in  $L^2(0, T, L^2(0, T))$  and the successive approximations (36) converge to  $f$  in  $L^2(0, T, L^2(0, T))$ -norm, which is independent of the initial iteration  $f_0 \in L^2(0, T, L^2(0, T))$ .

- This demonstrates that equations (38) and (26) have a unique solution  $f$  in  $L^2(0, T, L^2(0, T))$ . The existence of a solution to the main problem is proved by Theorem 4.1, but it has to be proven that this solution is unique. Using the demonstration by contradiction, we assume that there are two distinct solutions  $\{y_1, f_1\}$  and  $\{y_2, f_2\}$  to problem (1)-(4). First, we claim that  $f_1 \neq f_2$  almost everywhere on  $(0, T)$ . If  $f_1 = f_2$ , then by applying the uniqueness theorem to the related direct problem (5)-(7), we find  $y_1 = y_2$  almost everywhere in  $Q$ . Given that both pairs have verified (28), we infer that the functions  $f_1$  and  $f_2$  are two distinct solutions to equation (38), which contradicts the uniqueness of the functions.

**Corollary 4.1** *If the conditions of Theorem 4.2 are satisfied, then the solution  $f$  varies continuously with respect to the data  $\mu$  of the equation (26).*

**Proof.** Let  $\mu$  and  $\vartheta$  be two sets of data that satisfy the assumptions of Theorem 4.2 and let  $f$  and  $g$  be two solutions of the equation (26), which correspond to  $\mu$  and  $\vartheta$ , respectively. As a result of (26), we have

$$f = Af + \mu, \quad g = Ag + \vartheta.$$

By calculating the difference  $f - g$  and by using (35), we can have:

$$\|f - g\|_{L^2(0, T, L^2(0, T))} \leq \frac{1}{1 - \delta} \|\mu - \vartheta\|_{L^2(0, T)}.$$

Therefore, the proof of this corollary is completed.

## 5 Conclusion

The novel contribution of this manuscript has been successfully made by investigating the solvability of the semilinear parabolic problem with the integral overdetermination condition for an inverse problem. In addition, we have solved the direct problem by using the "energy inequality" method and accordingly, we have dealt with the inverse problem by using the fixed point technique.

## References

- [1] I. M. Batiha, Z. Chebana, T. E. Oussaeif, A. Ouannas and I. H. Jebril. On a weak solution of a fractional-order temporal equation. *Mathematics and Statistics* **10** (5) (2022) 1116–1120.
- [2] T. E. Oussaeif, B. Antara, A. Ouannas, I. M. Batiha, K. M. Saad, H. Jahanshahi, A. M. Aljuaid and A. A. Aly. Existence and uniqueness of the solution for an inverse problem of a fractional diffusion equation with integral condition. *Journal of Function Spaces* **2022** (2022) Article ID 7667370.
- [3] M. Ivanchov. *Inverse Problems for Equations of Parabolic Type*. VNTL Publishers, Lviv, Ukraine, 2003.
- [4] F. Kanca and M. Ismailov. Inverse problem of finding the time-dependent coefficient of heat equation from integral overdetermination condition data. *Inverse Problems in Science and Engineering* **20** (2012) 463–476.
- [5] O. Taki-Eddine and B. Abdelfatah. On determining the coefficient in a parabolic equation with nonlocal boundary and integral condition. *Electronic Journal of Mathematical Analysis and Applications* **6** (2018) 94–102.

- [6] T. E. Oussaeif and A. Bouziani. Inverse problem of a hyperbolic equation with an integral overdetermination condition. *Electronic Journal of Differential Equations* **2016** (138) (2016) 1–7.
- [7] T. E. Oussaeif and A. Bouziani. An inverse coefficient problem for a parabolic equation under nonlocal boundary and integral overdetermination conditions. *Internat. J. PDE Appl.* **2** (3) (2014) 38–43.
- [8] O. Taki-Eddine and B. Abdelfatah. On determining the coefficient in a parabolic equation with nonlocal boundary and integral condition. *Electronic Journal of Mathematical Analysis and Applications* **6** (2018) 94–102.
- [9] N. Anakira, Z. Chebana, T. E. Oussaeif, I. M. Batiha and A. Ouannas. A study of a weak solution of a diffusion problem for a temporal fractional differential equation. *Nonlinear Functional Analysis and Applications* **27** (3) (2022) 679–689.
- [10] I. M. Batiha, A. Ouannas, R. Albadarneh, A. A. Al-Nana and S. Momani. Existence and uniqueness of solutions for generalized Sturm–Liouville and Langevin equations via Caputo–Hadamard fractional-order operator. *Engineering Computations* **39** (7) (2022) 2581–2603.
- [11] Z. Chebana, T. E. Oussaeif, A. Ouannas and I. Batiha. Solvability of Dirichlet problem for a fractional partial differential equation by using energy inequality and Faedo-Galerkin method. *Innovative Journal of Mathematics* **1** (1) (2022) 34–44.
- [12] A. Zraiqat and L. K. Al-Hwawcha. On exact solutions of second order nonlinear ordinary differential equations. *Applied Mathematics* **6** (6) (2015) 953–957.
- [13] J. R. Cannon. An inverse problem of finding a parameter in a semi-linear heat equation. *J. Math. Anal. Appl.* **145** (1990) 470–484.
- [14] A. Bouziani. Solution forte d’un problème mixte avec condition non locales pour une classe d’équations hyperboliques. *Bull. de la Classe des Sciences, Académie Royale de Belgique* **8** (1997) 53–70.
- [15] I. M. Batiha, Z. Chebana, T. E. Oussaeif, A. Ouannas, S. Alshorm and A. Zraiqat. Solvability and dynamics of superlinear reaction diffusion problem with integral condition. *IAENG International Journal of Applied Mathematics* **53** (1) (2023) 113–121.
- [16] I. M. Batiha, L. Ben Aoua, T. E. Oussaeif, A. Ouannas, S. Alshorman, I. H. Jebril and S. Momani. Common fixed point theorem in non-Archimedean menger PM-spaces using CLR property with application to functional equations. *IAENG International Journal of Applied Mathematics* **53** (1) (2023) 113–121.
- [17] I. M. Batiha, N. Barrouk, A. Ouannas and W. G. Alshanti. On global existence of the fractional reaction-diffusion system’s solution. *International Journal of Analysis and Applications* **21** (1) (2023) 11.
- [18] M. Mardiyana, S. Sutrima, R. Setiyowati and R. Respatiwan. Solvability of equations with time-dependent potentials. *Nonlinear Dynamics and Systems Theory* **22** (3) (2022) 291–302.
- [19] B. El-Aqqad, J. Oudaani and A. El Mouatasim. Existence, uniqueness of weak Solution to the thermoelastic plates. *Nonlinear Dynamics and Systems Theory* **22** (3) (2022) 263–280.
- [20] A. Bouzelmate and M. EL Hathout. Asymptotic analysis of a nonlinear elliptic equation with a gradient term. *Nonlinear Dynamics and Systems Theory* **22** (3) (2022) 243–262.



# Some Generalized Nonlinear Volterra-Fredholm Type Integral Inequalities with Delay of Several Variables and Applications

Ammar Boudeliou \*

*Department of Mathematics, University of Constantine 1,  
BP, 325, Ain El Bey Street, 25017, Algeria.*

Received: March 4, 2023; Revised: July 21, 2023

**Abstract:** In the present paper, some new explicit bounds on solutions to a class of new nonlinear retarded integral inequalities of Volterra-Fredholm type for the functions of  $n$ -independent variables are established, which generalize some known integral inequalities. The derived results can be used as useful tools in the study of certain integral and differential equations of Volterra-Fredholm type. An application is given to illustrate the usefulness of our results.

**Keywords:** *delay integral inequality; Volterra-Fredholm type integral inequalities; explicit bounds;  $n$ -independent variables.*

**Mathematics Subject Classification (2010):** 26D15, 45B05, 45D05, 70K20.

## 1 Introduction

It is well known that the Gronwall-Bellman integral inequality [3, 8] and its various generalizations which provide explicit bounds on unknown functions have played an important role in the study of existence, uniqueness, boundedness, and other qualitative properties of solutions of differential equations, integral equations and have been applied in the stability analysis of solutions to dynamic equations on time scale [1, 12]. Recently, many authors have further improved more general forms of this inequality [2, 4, 6]. In the past few decades, many such new interesting retarded integral inequalities of Volterra-Fredholm type were established [10, 15].

---

\* Corresponding author: [mailto:ammar\\_boudeliou@umc.edu.dz](mailto:ammar_boudeliou@umc.edu.dz)

In [13] and [14], respectively, Pachpatte has established the following useful linear Volterra-Fredholm type integral inequalities with delay:

$$u(t) \leq k + \int_{\alpha(t_0)}^{\alpha(t)} a(t, s) \left[ f(s)u(s) + \int_{\alpha(t_0)}^s c(s, \tau)u(\tau)d\tau \right] ds + \int_{\alpha(t_0)}^{\alpha(T)} b(t, s)u(s)ds, \quad (1)$$

$$u(x, y) \leq c + \int_{\alpha(x_0)}^{\alpha(x)} \int_{\beta(y_0)}^{\beta(y)} a(x, y, s, t)u(s, t)dtds + \int_{\alpha(x_0)}^{\alpha(M)} \int_{\beta(y_0)}^{\beta(N)} b(x, y, s, t)u(s, t)dtds. \quad (2)$$

In [11], Ma and Pečarić discussed the following nonlinear retarded Volterra-Fredholm integral inequality:

$$\begin{aligned} u(x, y) \leq & k + \int \int_{\alpha(x_0)}^{\alpha(x)} \int_{\beta(x_0)}^{\beta(x)} \sigma_1(s, t) \left[ f(s, t)\omega(u(s, t)) \right. \\ & \left. + \int_{\alpha(x_0)}^s \int_{\beta(x_0)}^t \sigma_2(\tau, \xi)\omega(u(\tau, \xi)) d\xi d\tau \right] dtds \\ & + \int_{\alpha(x_0)}^{\alpha(M)} \int_{\beta(x_0)}^{\beta(M)} \sigma_1(s, t) \left[ f(s, t)\omega(u(s, t)) \right. \\ & \left. + \int_{\alpha(x_0)}^s \int_{\beta(x_0)}^t \sigma_2(\tau, \xi)\omega(u(\tau, \xi)) d\xi d\tau \right] dtds. \end{aligned} \quad (3)$$

El-Deeb and Ahmed [5] have established the following useful Volterra-Fredholm type integral inequality with delay which generalizes some results obtained in [9]:

$$\omega^p(t) \leq c(t) + \int_a^{\alpha(t)} g(s)\omega(s)ds + \int_a^b f(s)\omega^p(s)ds. \quad (4)$$

However, in certain situations such as some classes of delay differential or integral equations of Volterra-Fredholm type, it is desirable to find some new delay inequalities in order to achieve a diversity of desired goals. In this paper, we discuss a class of retarded integral inequalities of Volterra-Fredholm type. We use some analysis techniques to get the explicit estimations of the unknown function in the inequality. Finally, we give an application to illustrate the usefulness of our results.

## 2 Main Results

Throughout this paper, we use the following notations:  $I = [x^0, T] = I_1 \times \dots \times I_n$ , where  $I_i = [x_i^0, T_i]$ ,  $i = 1, \dots, n$ , and  $x^0 = (x_1^0, \dots, x_n^0)$ ,  $T = (T_1, \dots, T_n) \in \mathbb{R}^n$ ,  $\Delta = \{(x, s) \in I^2 : x^0 \leq s \leq x \leq T\}$ . If  $x = (x_1, \dots, x_n)$  and  $y = (y_1, \dots, y_n)$  belong to  $\mathbb{R}^n$ , we write  $x \leq y$  ( $x < y$ ) if and only if  $x_i \leq y_i$  ( $x_i < y_i$ ),  $i = 1, \dots, n$ . We also adopt the notation  $x = (x_1, x_2, \dots, x_n) = (x_1, x^1)$ , where  $x^1 = (x_2, \dots, x_n)$ ,  $(x^0)^1 = (x_2^0, \dots, x_n^0)$ , and

- $D_i = \frac{\partial}{\partial x_i}$ ,  $i = 1, \dots, n$ ,
- $dx^1 = dx_n \dots dx_2$ ,
- $\int_{x^0}^x \dots ds = \int_{x_1^0}^{x_1} \dots \int_{x_n^0}^{x_n} \dots ds_n \dots ds_1 = \int_{x_1^0}^{x_1} \int_{(x^0)^1}^{x^1} \dots ds^1 ds_1$ ,

- $\int_{\alpha(x^0)}^{\alpha(x)} \dots ds = \int_{\alpha(x_1^0)}^{\alpha_1(x_1)} \dots \int_{\alpha(x_n^0)}^{\alpha_n(x_n)} \dots ds_n \dots ds_1.$

In the following, we establish some new generalized Volterra-Fredholm type integral inequalities in  $n$ -independent variables.

**Theorem 2.1** *Let  $u(x) \in C(I, \mathbb{R}_+)$ ,  $f(x, s), \gamma_1(x, s), \gamma_2(x, s) \in C(\Delta, \mathbb{R}_+)$  and  $f, \gamma_1, \gamma_2$  be nondecreasing in  $x$  for each  $s \in I, \alpha(x) = (\alpha_1(x_1), \dots, \alpha_n(x_n)) \in C^1(I, I)$ , where  $\alpha_i(x_i) \in C^1(I_i, I_i)$  are nondecreasing functions on  $I_i$  with  $\alpha_i(x_i) \leq x_i, i = 1, \dots, n$ . Let  $\psi, \omega, \omega_1 \in C(\mathbb{R}_+, \mathbb{R}_+)$  be nondecreasing with  $\{\psi, \omega, \omega_1\}(u) > 0$  for  $u > 0$ , and  $\lim_{u \rightarrow +\infty} \psi(u) = +\infty$  and  $F_1(v) = \int_{v_0}^v \frac{ds}{\omega(\psi^{-1}(s))\omega_1(\psi^{-1}(s))}, v \geq v_0 > 0, F_1(+\infty) = +\infty$ . If  $u(x)$  satisfies*

$$\begin{aligned} \psi(u(x)) \leq & u_0 + \int_{\alpha(x^0)}^{\alpha(x)} \gamma_1(x, s)\omega(u(s)) \left[ f(x, s)\omega_1(u(s)) + \int_{\alpha(x^0)}^s \gamma_2(s, \tau)\omega_1(u(\tau))d\tau \right] ds \\ & + \int_{\alpha(x^0)}^{\alpha(T)} \gamma_1(x, s)\omega(u(s)) \left[ f(x, s)\omega_1(u(s)) \right. \\ & \left. + \int_{\alpha(x^0)}^s \gamma_2(s, \tau)\omega_1(u(\tau))d\tau \right] ds \end{aligned} \tag{5}$$

for  $x \in I$ , where  $u_0 \geq 0$  is a constant and

$$H_1(t) = F_1(2t - u_0) - F_1(t) \tag{6}$$

is increasing for  $t \geq u_0$ , then

$$\begin{aligned} u(x) \leq & \psi^{-1} \left\{ F_1^{-1} \left( F_1 \left[ H_1^{-1} \left( \int_{\alpha(x^0)}^{\alpha(T)} \gamma_1(x, s) \left[ f(x, s) + \int_{\alpha(x^0)}^s \gamma_2(s, \tau)d\tau \right] ds \right) \right] \right. \right. \\ & \left. \left. + \int_{\alpha(x^0)}^{\alpha(x)} \gamma_1(x, s) \left[ f(x, s) + \int_{\alpha(x^0)}^s \gamma_2(s, \tau)d\tau \right] ds \right) \right\} \end{aligned} \tag{7}$$

for  $x \in I, F_1^{-1}$  and  $H_1^{-1}$  are the inverse functions of  $F_1$  and  $H_1$ , respectively.

**Proof.** Let  $u_0 > 0$  and fix any arbitrary  $X = (X_1, \dots, X_n) \in I$ , then for  $x^0 \leq x \leq X \leq T$ , we define a positive and nondecreasing function  $z(x)$  on  $I$  by the right-hand side of (5) for  $x \in I$ , so we have

$$u(x) \leq \psi^{-1}(z(x)), \tag{8}$$

and

$$\begin{aligned} D_1 \dots D_n z(x) \leq & \gamma_1(X, \alpha(x))\omega(\psi^{-1}(z(\alpha(x)))) \left[ f(X, \alpha(x))\omega_1(\psi^{-1}(z(\alpha(x)))) \right. \\ & \left. + \int_{\alpha(x^0)}^{\alpha(x)} \gamma_2(\alpha(x), \tau)\omega_1(\psi^{-1}(z(\tau)))d\tau \right] \alpha'(x) \\ \leq & \gamma_1(X, \alpha_1(x_1), \dots, \alpha_n(x_n))(\omega\omega_1)(\psi^{-1}(z(\alpha_1(x_1), \dots, \alpha_n(x_n)))) \\ & \left[ f(X, \alpha_1(x_1), \dots, \alpha_n(x_n)) + \int_{\alpha_1(x_1^0)}^{\alpha_1(x_1)} \dots \int_{\alpha_n(x_n^0)}^{\alpha_n(x_n)} \gamma_2(\alpha(x), \tau_1, \dots, \tau_n) \right. \\ & \left. d\tau_n \dots d\tau_1 \right] \alpha'_1(x_1) \dots \alpha'_n(x_n). \end{aligned}$$

So

$$\frac{D_1 \dots D_n z(x)}{(\omega \omega_1)(\psi^{-1}(z(x)))} \leq \gamma_1(X, \alpha_1(x_1), \dots, \alpha_n(x_n)) \left[ f(X, \alpha_1(x_1), \dots, \alpha_n(x_n)) + \int_{\alpha_1(x_1^0)}^{\alpha_1(x_1)} \dots \int_{\alpha_n(x_n^0)}^{\alpha_n(x_n)} \gamma_2(\alpha(x), \dots, \alpha_n(x_n), \tau_1, \dots, \tau_n) d\tau_n \dots d\tau_1 \right] \alpha'_1(x_1) \times \dots \times \alpha'_n(x_n),$$

then

$$D_n \left( \frac{D_1 \dots D_{n-1} z(x)}{(\omega \omega_1)(\psi^{-1}(z(x)))} \right) \leq \gamma_1(X, \alpha_1(x_1), \dots, \alpha_n(x_n)) \left[ f(X, \alpha_1(x_1), \dots, \alpha_n(x_n)) + \int_{\alpha_1(x_1^0)}^{\alpha_1(x_1)} \dots \int_{\alpha_n(x_n^0)}^{\alpha_n(x_n)} \gamma_2(\alpha_1(x_1), \dots, \alpha_n(x_n), \tau_1, \dots, \tau_n) d\tau_n \dots d\tau_1 \right] \alpha'_1(x_1) \times \dots \times \alpha'_n(x_n). \quad (9)$$

Keeping  $x_1, \dots, x_{n-1}$  fixed in (9), setting  $x_n = s_n$  and integrating with respect to  $s_n$  from  $x_n^0$  to  $x_n$ , we get

$$\frac{D_1 \dots D_{n-1} z(x)}{(\omega \omega_1)(\psi^{-1}(z(x)))} \leq \int_{\alpha_n(x_n^0)}^{\alpha_n(x_n)} \gamma_1(X, \alpha_1(x_1), \dots, \alpha_{n-1}(x_{n-1}), s_n) \left[ f(X, \alpha_1(x_1), \dots, \alpha_{n-1}(x_{n-1}), s_n) + \int_{\alpha_1(x_1^0)}^{\alpha_1(x_1)} \dots \int_{\alpha_n(x_n^0)}^{s_n} \gamma_2(\alpha_1(x_1), \dots, \alpha_{n-1}(x_{n-1}), s_n, \tau_1, \dots, \tau_n) d\tau_n \dots d\tau_1 \right] \alpha'_1(x_1) \times \dots \times \alpha'_{n-1}(x_{n-1}) ds_n.$$

Repeating this, we find (after  $n - 1$  steps)

$$\frac{D_1 z(x)}{\omega \omega_1(\psi^{-1}(z(x)))} \leq \int_{\alpha_2(x_2^0)}^{\alpha_2(x_2)} \dots \int_{\alpha_n(x_n^0)}^{\alpha_n(x_n)} \gamma_1(X, \alpha_1(x_1), s_2, \dots, s_n) \left[ f(X, \alpha_1(x_1), s_2, \dots, s_n) + \int_{\alpha_1(x_1^0)}^{\alpha_1(x_1)} \int_{\alpha_2(x_2^0)}^{s_2} \dots \int_{\alpha_n(x_n^0)}^{s_n} \gamma_2(\alpha_1(x_1), s_2, \dots, s_n, \tau_1, \dots, \tau_n) d\tau_n \dots d\tau_1 \right] \alpha'_1(x_1) ds_n \dots ds_2. \quad (10)$$

Keeping  $x^1 = (x_2, \dots, x_n)$  fixed in (10), replacing  $x_1$  by  $s_1$  and then integrating with respect to  $s_1$  from  $x_1^0$  to  $x_1$ , we obtain

$$z(x) \leq F_1^{-1} \left( F_1(z(x_1^0, x^1)) + \int_{\alpha(x^0)}^{\alpha(x)} \gamma_1(X, s) \left[ f(X, s) + \int_{\alpha(x^0)}^s \gamma_2(s, \tau) d\tau \right] ds \right) \quad (11)$$

for  $x \in I$ . From the equation

$$z(x_1^0, x^1) = u_0 + \int_{\alpha(x^0)}^{\alpha(T)} \gamma_1(X, s) \omega(u(s)) \left[ f(X, s) \omega_1(u(s)) + \int_{\alpha(x^0)}^s \gamma_2(s, \tau) \omega_1(u(\tau)) d\tau \right] ds,$$

we observe that

$$z(T) = 2z(x_1^0, x^1) - u_0 = u_0 + 2 \int_{\alpha(x^0)}^{\alpha(T)} \gamma_1(X, s) \omega(u(s)) \left[ f(X, s) \omega_1(u(s)) + \int_{\alpha(x^0)}^s \gamma_2(s, \tau) \omega_1(u(\tau)) d\tau \right] ds.$$

Using (11), we get

$$2z(x_1^0, x^1) - u_0 \leq F_1^{-1} \left( F_1(z(x_1^0, x^1)) + \int_{\alpha(x^0)}^{\alpha(T)} \gamma_1(X, s) \left[ f(X, s) + \int_{\alpha(x^0)}^s \gamma_2(s, \tau) d\tau \right] ds \right),$$

or

$$F_1(2z(x_1^0, x^1) - u_0) - F_1(z(x_1^0, x^1)) \leq \int_{\alpha(x^0)}^{\alpha(T)} \gamma_1(X, s) \left[ f(X, s) + \int_{\alpha(x^0)}^s \gamma_2(s, \tau) d\tau \right] ds, \tag{12}$$

then  $H_1(z(x_1^0, x^1)) \leq \int_{\alpha(x^0)}^{\alpha(T)} \gamma_1(X, s) \left[ f(X, s) + \int_{\alpha(x^0)}^s \gamma_2(s, \tau) d\tau \right] ds$ . Since  $H_1$  is increasing, for  $t \geq u_0$ , we get

$$z(x_1^0, x^1) \leq H_1^{-1} \left( \int_{\alpha(x^0)}^{\alpha(T)} \gamma_1(X, s) \left[ f(X, s) + \int_{\alpha(x^0)}^s \gamma_2(s, \tau) d\tau \right] ds \right). \tag{13}$$

Since  $X \in I$  is chosen arbitrary, now substituting (13) into (11) and from (8), we obtain the desired inequality (7). If  $u_0 = 0$ , we carry out the above procedure with  $\varepsilon > 0$  instead of  $u_0$  and subsequently let  $\varepsilon \rightarrow 0$ .  $\square$

**Remark 2.1** For  $\gamma_1 = 1, \gamma_2 = 0, \psi(u) = \omega_1(u) = u, \omega(u) = 1$  and  $x^2 = (x_3, \dots, x_n)$  fixed, inequality (5) reduces to inequality (2).

**Remark 2.2** For  $\psi(u) = u, \gamma_1(x, s) = \gamma_1(s), \gamma_2(s, \tau) = \gamma_2(\tau), f(x, s) = f(s), \omega(u) = 1$  and  $x^1$  fixed, (5) reduces to (3). Further, for  $\psi(u) = u, \gamma_1(x, s) = \gamma_1(s), \gamma_2(s, \tau) = \gamma_2(\tau), f(x, s) = f(s), \omega(u) = 1$  and  $x^2$  fixed, Theorem 2.1 reduces to Theorem 3.1 in [11].

**Theorem 2.2** Let  $u, f, g, h \in C(I, \mathbb{R}_+)$  and  $\alpha(x) = (\alpha_1(x_1), \dots, \alpha_n(x_n)) \in C^1(I, I)$ , where  $\alpha_i(x_i) \in C^1(I_i, I_i)$  are nondecreasing functions on  $I_i$  with  $\alpha_i(x_i) \leq x_i, i = 1, \dots, n$ . Let  $\omega_1, \omega_2, \omega_3, \frac{\omega_3}{\omega_2} \in C(\mathbb{R}_+, \mathbb{R}_+)$  be nondecreasing with  $\omega_i(u) > 0 (i = 1, 2, 3)$  for  $u > 0$ , and

$$G_1(r) = \int_{r_0}^r \frac{ds}{\omega_1 \omega_2(s)}, G_2(r) = \int_{r_0}^r \frac{\omega_2(G_1^{-1}(s)) ds}{\omega_3(G_1^{-1}(s))}, r \geq r_0 > 0, G_1(\infty) = G_2(\infty) = \infty, \tag{14}$$

$$H_1(u) = G_2(G_1(2u - u_0)) - G_2 \left( G_1(u) + \int_{\alpha(x^0)}^{\alpha(T)} f(s) g(s) ds \right) - \int_{\alpha(x^0)}^{\alpha(T)} f(s) \left( \int_{\alpha(x^0)}^s h(\tau) d\tau \right) ds \tag{15}$$

is increasing, and  $H_1(u) = 0$  has a solution  $c$  for  $u \geq u_0$ . If  $u(x)$  satisfies

$$\begin{aligned} u(x) \leq & u_0 + \int_{\alpha(x^0)}^{\alpha(x)} f(s)\omega_1(u(s)) \left[ g(s)\omega_2(u(s)) + \int_{\alpha(x^0)}^s h(\tau)\omega_3(u(\tau))d\tau \right] ds \\ & + \int_{\alpha(x^0)}^{\alpha(T)} f(s)\omega_1(u(s)) \left[ g(s)\omega_2(u(s)) + \int_{\alpha(x^0)}^s h(\tau)\omega_3(u(\tau))d\tau \right] ds, \end{aligned} \quad (16)$$

then

$$u(x) \leq G_1^{-1} \left\{ G_2^{-1} \left[ G_2 \left( G_1(c) + \int_{\alpha(x^0)}^{\alpha(x)} f(s)g(s)ds \right) + \int_{\alpha(x^0)}^{\alpha(x)} f(s) \left( \int_{\alpha(x^0)}^s h(\tau)d\tau \right) ds \right] \right\} \quad (17)$$

for  $x \in I$ , where  $G_1^{-1}, G_2^{-1}$  are the inverse functions of  $G_1, G_2$ , respectively.

**Proof.** Let  $u_0 > 0$  and  $z(x)$  denote the function on the right-hand side of (16), which is positive and nondecreasing function on  $I$ . Then we have

$$u(x) \leq z(x), \quad (18)$$

and

$$z(x_1^0, x^1) = u_0 + \int_{\alpha(x^0)}^{\alpha(T)} f(s)\omega_1(u(s)) \left[ g(s)\omega_2(u(s)) + \int_{\alpha(x^0)}^s h(\tau)\omega_3(u(\tau))d\tau \right] ds.$$

Differentiating  $z(x)$  with respect to  $x$ , using (18), we have

$$D_1 \dots D_n z(x) \leq \alpha'(x) f(\alpha(x)) \omega_1(z(\alpha(x))) \left[ g(\alpha(x)) \omega_2(z(\alpha(x))) + \int_{\alpha(x^0)}^{\alpha(x)} h(\tau) \omega_3(z(\tau)) d\tau \right]$$

by the monotonicity of  $\omega_1, \omega_2$ , and  $z$  and the property of  $\alpha$ . From the above inequality, we have

$$\frac{D_1 \dots D_n z(x)}{(\omega_1 \omega_2)(z(x))} \leq \alpha'(x) f(\alpha(x)) \left[ g(\alpha(x)) + \int_{\alpha(x^0)}^{\alpha(x)} h(\tau) \frac{\omega_3(z(\tau))}{\omega_2(z(\tau))} d\tau \right],$$

or

$$\begin{aligned} D_n \left( \frac{D_1 \dots D_{n-1} z(x)}{\omega_1 \omega_2(z(x))} \right) \leq & \alpha'_1(x_1) \dots \alpha'_n(x_n) f(\alpha_1(x_1), \dots, \alpha_n(x_n)) \left[ g(\alpha_1(x_1), \dots, \alpha_n(x_n)) \right. \\ & \left. + \int_{\alpha_1(x_1^0)}^{\alpha_1(x_1)} \dots \int_{\alpha_n(x_n^0)}^{\alpha_n(x_n)} h(\tau_1, \dots, \tau_n) \frac{\omega_3(z(\tau_1, \dots, \tau_n))}{\omega_2(z(\tau_1, \dots, \tau_n))} d\tau_n \dots d\tau_1 \right]. \end{aligned}$$

Keeping  $x_1, \dots, x_{n-1}$  fixed, integrating both sides of the above inequality from  $x_n^0$  to  $x_n$ , we obtain

$$\begin{aligned} \frac{D_1 \dots D_{n-1} z(x)}{\omega_1 \omega_2(z(x))} \leq & \int_{\alpha_n(x_n^0)}^{\alpha_n(x_n)} f(\alpha_1(x_1), \dots, \alpha_{n-1}(x_{n-1}), s_n) \left[ g(\alpha_1(x_1), \dots, \alpha_{n-1}(x_{n-1}), s_n) \right. \\ & \left. + \int_{\alpha_1(x_1^0)}^{\alpha_1(x_1)} \dots \int_{\alpha_{n-1}(x_{n-1}^0)}^{\alpha_{n-1}(x_{n-1})} \int_{\alpha_n(x_n^0)}^{s_n} h(\tau_1, \dots, \tau_n) \frac{\omega_3(z(\tau_1, \dots, \tau_n))}{\omega_2(z(\tau_1, \dots, \tau_n))} \right. \\ & \left. d\tau_n \dots d\tau_1 \right] \alpha'_1(x_1) \times \dots \times \alpha'_{n-1}(x_{n-1}) ds_n. \end{aligned}$$

Continuing this process, we obtain (after  $n - 1$  steps)

$$\frac{D_1 z(x)}{\omega_1 \omega_2(z(x))} \leq \int_{\alpha_2(x_2^0)}^{\alpha_2(x_2)} \dots \int_{\alpha_n(x_n^0)}^{\alpha_n(x_n)} f(\alpha_1(x_1), s_2, \dots, s_n) \left[ g(\alpha_1(x_1), s_2, \dots, s_n) + \int_{\alpha_1(x_1^0)}^{\alpha_1(x_1)} \int_{\alpha_2(x_2^0)}^{s_2} \dots \int_{\alpha_n(x_n^0)}^{s_n} h(\tau_1, \dots, \tau_n) \frac{\omega_3(z(\tau_1, \dots, \tau_n))}{\omega_2(z(\tau_1, \dots, \tau_n))} d\tau_n \dots d\tau_1 \right] \alpha_1'(x_1) ds^1.$$

Integrating the above inequality from  $x_1^0$  to  $x_1$ , using (14), we obtain

$$\begin{aligned} G_1(z(x)) &\leq G_1(z(x_1^0, x^1)) + \int_{\alpha(x^0)}^{\alpha(x)} f(s) \left[ g(s) + \int_{\alpha(x^0)}^s h(\tau_1, \dots, \tau_n) \frac{\omega_3(z(\tau))}{\omega_2(z(\tau))} d\tau \right] ds \\ &\leq G_1(z(x_1^0, x^1)) + \int_{\alpha(x^0)}^{\alpha(X)} f(s)g(s) ds \\ &\quad + \int_{\alpha(x^0)}^{\alpha(x)} f(s) \left( \int_{\alpha(x^0)}^s h(\tau_1, \dots, \tau_n) \frac{\omega_3(z(\tau))}{\omega_2(z(\tau))} d\tau \right) ds \end{aligned} \tag{19}$$

for all  $x \in [x^0, X]$ ,  $X \in I$ , and  $X$  is chosen arbitrarily. Let  $v(x)$  denote the function on the right-hand side of (19), which is positive and nondecreasing in each variable  $x \in [x^0, X]$ .

From (19), we have

$$z(x) \leq G_1^{-1}(v(x)), \quad \forall x \in [x^0, X], \tag{20}$$

$$v(x_1^0, x^1) = G_1(z(x_1^0, x^1)) + \int_{\alpha(x^0)}^{\alpha(X)} f(s)g(s) ds.$$

Differentiating  $v(x)$  with respect to  $x$ , by the monotonicity of  $v$ ,  $G_1^{-1}$ , and  $\frac{\omega_3}{\omega_2}$ , the property of  $\alpha$ , and (20), we have

$$D_1 \dots D_n v(x) \leq \alpha'(x) f(\alpha(x)) \frac{\omega_3(G_1^{-1}(v(x)))}{\omega_2(G_1^{-1}(v(x)))} \int_{\alpha(x^0)}^{\alpha(x)} h(\tau_1, \dots, \tau_n) d\tau$$

for all  $x \in [x^0, X]$ . Then we have

$$\begin{aligned} \frac{\omega_2(G_1^{-1}(v(x))) D_1 \dots D_n v(x)}{\omega_3(G_1^{-1}(v(x)))} &\leq \alpha'(x) f(\alpha(x)) \int_{\alpha(x^0)}^{\alpha(x)} h(\tau_1, \dots, \tau_n) d\tau, \\ D_n \left( \frac{\omega_2(G_1^{-1}(v(x))) D_1 \dots D_{n-1} v(x)}{\omega_3(G_1^{-1}(v(x)))} \right) &\leq \alpha'(x) f(\alpha(x)) \int_{\alpha(x^0)}^{\alpha(x)} h(\tau_1, \dots, \tau_n) d\tau. \end{aligned}$$

Keeping  $x_1$  fixed, integrating both sides of the above inequality with respect to  $x_2, \dots, x_n$ , respectively, we obtain (after  $n - 1$  steps)

$$\begin{aligned} \frac{\omega_2(G_1^{-1}(v(x))) D_1 v(x)}{\omega_3(G_1^{-1}(v(x)))} &\leq \int_{\alpha_2(x_2^0)}^{\alpha_2(x_2)} \dots \int_{\alpha_n(x_n^0)}^{\alpha_n(x_n)} f(\alpha_1(x_1), s_2, \dots, s_n) \times \\ &\quad \left( \int_{\alpha_1(x_1^0)}^{\alpha_1(x_1)} \int_{\alpha_2(x_2^0)}^{s_2} \dots \int_{\alpha_n(x_n^0)}^{s_n} h(\tau_1, \dots, \tau_n) d\tau_n \dots d\tau_1 \right) ds^1 \alpha_1'(x). \end{aligned}$$

Integrating both sides of the above inequality from  $x_1^0$  to  $x_1$ , using (14), we obtain

$$G_2(v(x)) \leq G_2(v(x_1^0, x^1)) + \int_{\alpha(x^0)}^{\alpha(x)} f(s) \left( \int_{\alpha(x^0)}^s h(\tau) d\tau \right) ds,$$

or

$$v(x) \leq G_2^{-1} \left[ G_2(v(x_1^0, x^1)) + \int_{\alpha(x^0)}^{\alpha(x)} f(s) \left( \int_{\alpha(x^0)}^s h(\tau) d\tau \right) ds \right], \quad \forall x \in [x^0, X]. \quad (21)$$

From (20) and (21), we have

$$z(x) \leq G_1^{-1}(v(x)) \leq G_1^{-1} \left\{ G_2^{-1} \left[ G_2(v(x_1^0, x^1)) + \int_{\alpha(x^0)}^{\alpha(x)} f(s) \left( \int_{\alpha(x^0)}^s h(\tau) d\tau \right) ds \right] \right\}.$$

Substituting  $v(x_1^0, x^1)$  into the above inequality, and since  $X$  is chosen arbitrarily, we have

$$\begin{aligned} z(x) \leq G_1^{-1} \left\{ G_2^{-1} \left[ G_2 \left( G_1(z(x_1^0, x^1)) + \int_{\alpha(x^0)}^{\alpha(x)} f(s)g(s)ds \right) \right. \right. \\ \left. \left. + \int_{\alpha(x^0)}^{\alpha(x)} f(s) \left( \int_{\alpha(x^0)}^s h(\tau) d\tau \right) ds \right] \right\}. \end{aligned} \quad (22)$$

By the definition of  $z$  and the expression of  $z(x_1^0, x^1)$ , we have  $2z(x_1^0, x^1) - u_0 = z(T)$ .

From (22), we have

$$\begin{aligned} 2z(x_1^0, x^1) - u_0 \leq G_1^{-1} \left\{ G_2^{-1} \left[ G_2 \left( G_1(z(x_1^0, x^1)) + \int_{\alpha(x^0)}^{\alpha(T)} f(s)g(s)ds \right) \right. \right. \\ \left. \left. + \int_{\alpha(x^0)}^{\alpha(T)} f(s) \left( \int_{\alpha(x^0)}^s h(\tau) d\tau \right) ds \right] \right\}, \text{ or} \\ G_2(G_1(2z(x_1^0, x^1) - u_0)) \leq G_2 \left( G_1(z(x_1^0, x^1)) + \int_{\alpha(x^0)}^{\alpha(T)} f(s)g(s)ds \right) \\ + \int_{\alpha(x^0)}^{\alpha(T)} f(s) \left( \int_{\alpha(x^0)}^s h(\tau) d\tau \right) ds. \end{aligned} \quad (23)$$

By the definition of  $H_1$ , the assumption of Theorem 2.2, and (23), we observe that

$$H_1(z(x_1^0, x^1)) \leq 0 = H_1(c). \quad (24)$$

Since  $H_1$  is increasing, from (18), (22), and (24), we have the desired estimation (17). If  $u_0 = 0$ , we carry out the above procedure with  $\varepsilon > 0$  instead of  $u_0$  and subsequently let  $\varepsilon \rightarrow 0$ .  $\square$

**Remark 2.3** If  $\omega_2 = \omega_3$ , and for  $x^2 = (x_3, \dots, x_n)$  fixed,  $G_2(u) = u - u_0$ , and  $G_2^{-1}(u) = u + u_0$ , (17) is equivalent to

$$u(x) \leq G_1^{-1} \left\{ G_1(c) + \int_{\alpha(x^0)}^{\alpha(x)} f(s) \left[ g(s) + \int_{\alpha(x^0)}^s h(\tau) d\tau \right] ds \right\}.$$

Theorem 2.2 reduces to Theorem 3.1 in [11].

**Theorem 2.3** Let  $u, f, \alpha, u_0$  be as in Theorem 2.1,  $a(x, s), b(x, s), c(x, s), g(x, s), d(x, s)$  be the functions of  $C(\Delta, \mathbb{R}_+)$  nondecreasing in  $x$  for each  $s \in I$ , and  $0 < p < 1$  be a constant. If  $u(x)$  satisfies

$$\begin{aligned}
 u(x) \leq & u_0 + \int_{\alpha(x^0)}^{\alpha(x)} a(x, s) \left[ f(x, s)u(s) + \int_{\alpha(x^0)}^s b(s, \tau)u(\tau)d\tau \right] ds \\
 & + \int_{\alpha(x^0)}^{\alpha(T)} c(x, s) \left[ g(x, s)u^p(s) + \int_{\alpha(x^0)}^s d(s, \tau)u^p(\tau)d\tau \right] ds \tag{25}
 \end{aligned}$$

for  $x \in I$ , and

$$\exp \left( \int_{\alpha(x^0)}^{\alpha(T)} \gamma_1^*(x, s) \left[ f^*(x, s) + \int_{\alpha(x^0)}^s \gamma_2^*(s, \tau)d\tau \right] ds \right) < 2, \tag{26}$$

then

$$\begin{aligned}
 u(x) \leq & \left\{ \left( 1 + (c)^{1-p} \right) \exp \left( (1-p) \int_{\alpha(x^0)}^{\alpha(x)} \gamma_1^*(x, s) \left[ f^*(x, s) + \int_{\alpha(x^0)}^s \gamma_2^*(s, \tau)d\tau \right] ds \right) \right. \\
 & \left. - 1 \right\}^{\frac{1}{1-p}} \tag{27}
 \end{aligned}$$

for  $x \in I$ , where  $c$  is the solution of the equation

$$H_2(t) = \frac{1}{1-p} \ln \frac{1 + (2t - u_0)^{1-p}}{1 + t^{1-p}} - \int_{\alpha(x^0)}^{\alpha(T)} \gamma_1^*(x, s) \left[ f^*(x, s) + \int_{\alpha(x^0)}^s \gamma_2^*(s, \tau)d\tau \right] ds = 0 \tag{28}$$

for  $t \geq u_0$ , where  $\gamma_1^*(x, s) = \max \{a(x, s), c(x, s)\}$ ,  $f^*(x, s) = \max \{f(x, s), g(x, s)\}$ , and  $\gamma_2^*(x, s) = \max \{b(x, s), d(x, s)\}$ .

**Proof.** Let  $W \in C(\mathbb{R}_+, \mathbb{R}_+)$  so that  $W(u) = u + u^p$  is nondecreasing, so it is obvious that  $u, u^p \leq W(u)$ . From (25) and the assumptions, we get

$$\begin{aligned}
 u(x) \leq & u_0 + \int_{\alpha(x^0)}^{\alpha(x)} \gamma_1^*(x, s) \left[ f^*(x, s)W(u(s)) + \int_{\alpha(x^0)}^s \gamma_2^*(s, \tau)W(u(\tau))d\tau \right] ds \\
 & + \int_{\alpha(x^0)}^{\alpha(T)} \gamma_1^*(x, s) \left[ f^*(x, s)W(u(s)) + \int_{\alpha(x^0)}^s \gamma_2^*(s, \tau)W(u(\tau))d\tau \right] ds.
 \end{aligned}$$

Fix any arbitrary  $X = (X_1, \dots, X_n) \in I$ , then for  $x^0 \leq x \leq X \leq T$ , define a positive and nondecreasing function  $z(x)$  on  $I$  by

$$\begin{aligned}
 z(x) = & u_0 + \int_{\alpha(x^0)}^{\alpha(x)} \gamma_1^*(X, s) \left[ f^*(X, s)W(u(s)) + \int_{\alpha(x^0)}^s \gamma_2^*(s, \tau)W(u(\tau))d\tau \right] ds \\
 & + \int_{\alpha(x^0)}^{\alpha(T)} \gamma_1^*(X, s) \left[ f^*(X, s)W(u(s)) + \int_{\alpha(x^0)}^s \gamma_2^*(s, \tau)W(u(\tau))d\tau \right] ds,
 \end{aligned}$$

so we have  $u(x) \leq z(x)$ , by the same steps as in the proof of Theorem 2.1, we obtain

$$z(x) \leq F_2^{-1} \left( F_2(z(x_1^0, x^1)) + \int_{\alpha(x^0)}^{\alpha(x)} \gamma_1^*(x, s) \left[ f^*(x, s) + \int_{\alpha(x^0)}^s \gamma_2^*(s, \tau)d\tau \right] ds \right), \tag{29}$$

where

$$F_2(v) = \int_{v_0}^v \frac{ds}{W(s)} = \int_{v_0}^v \frac{ds}{s + s^p} = \frac{1}{1-p} \ln \frac{1 + v^{1-p}}{1 + v_0^{1-p}}, v \geq v_0 > 0, \quad (30)$$

then

$$F_2^{-1}(v) = \left[ (1 + v_0^{1-p}) \exp((1-p)v) - 1 \right]^{\frac{1}{1-p}}. \quad (31)$$

We have

$$H_2(t) = F_2(2t - u_0) - F_2(t) - \int_{\alpha(x^0)}^{\alpha(T)} \gamma_1^*(x, s) \left[ f^*(x, s) + \int_{\alpha(x^0)}^s \gamma_2^*(s, \tau) d\tau \right] ds,$$

so

$$H_2(t) = \frac{1}{1-p} \ln \frac{1 + (2t - u_0)^{1-p}}{1 + t^{1-p}} - \int_{\alpha(x^0)}^{\alpha(T)} \gamma_1^*(x, s) \left[ f^*(x, s) + \int_{\alpha(x^0)}^s \gamma_2^*(s, \tau) d\tau \right] ds,$$

so we have

$$H_2'(t) = \frac{u_0 + 2t^p - (2t - u_0)^p}{[2t - u_0 + (2t - u_0)^p](t + t^p)} > 0 \quad (32)$$

for  $t \geq u_0$  and

$$H_2(u_0) = - \int_{\alpha(x^0)}^{\alpha(T)} \gamma_1^*(x, s) \left[ f^*(x, s) + \int_{\alpha(x^0)}^s \gamma_2^*(s, \tau) d\tau \right] ds < 0, \quad (33)$$

and from (26), we get

$$\lim_{t \rightarrow +\infty} H_2(t) = \ln 2 - \int_{\alpha(x^0)}^{\alpha(T)} \gamma_1^*(x, s) \left[ f^*(x, s) + \int_{\alpha(x^0)}^s \gamma_2^*(s, \tau) d\tau \right] ds > 0. \quad (34)$$

By (32)-(34), we obtain that (28) has a unique solution  $c > u_0$ . Now by (29), (30) and (31), we get (27).  $\square$

### 3 Application

In this section, we apply our results to obtain the estimate of the solution of the retarded Volterra-Fredholm integral equation with delay in  $n$ -independent variables.

**Example 3.1.** Consider the following differential boundary value problem system in  $n$ -independent variables

$$\begin{cases} D_1 \dots D_n z(x) = D_1 \dots D_n f(x) + A(x, s, z(s - \beta(s))) + B(x, s, z(s - \beta(s))), \\ z(x_1, \dots, x_{n-1}, x_n^0) = f(x_1, \dots, x_{n-1}, x_n^0), \dots, z(x_1^0, \dots, x_n) = f(x_1^0, \dots, x_n), \end{cases} \quad (35)$$

where  $z, f \in C^1(I, \mathbb{R})$ ,  $A, B \in C(\Delta \times \mathbb{R}, \mathbb{R})$ ,  $I = [x^0, T] \subset \mathbb{R}^n$ ,

$\Delta = \{(x, s) \in I^2 : x^0 \leq s \leq x \leq T\} \subset \mathbb{R}^n$  and  $\beta \in C^1(I, I)$  is nonincreasing on  $I$  such that  $\beta(x) = (\beta_1(x_1), \dots, \beta_n(x_n))$ ,  $x_i - \beta_i(x_i) \geq 0$ ,  $\beta'_i(x_i) < 1$ , and  $\beta_i(x_i^0) = 0$  for  $i = 1, \dots, n$ ,  $x = (x_1, \dots, x_n)$ ,  $x^0 = (x_1^0, \dots, x_n^0) \in \mathbb{R}^n$ . Integrating both sides of (35) with respect to  $x_1, \dots, x_n$ , respectively, we obtain (after  $n$  steps)

$$z(x) = f(x) + \int_{x^0}^x A(x, s, z(s - \beta(s))) ds + \int_{x^0}^T B(x, s, z(s - \beta(s))) ds. \quad (36)$$

**Theorem 3.1** Assume that the functions  $f, A, B$  in (36) satisfy the conditions

$$|f(x)| \leq u_0, \tag{37}$$

$$|A(x, s, z)| \leq a(x, s) |z|, \tag{38}$$

$$|B(x, s, z)| \leq b(x, s) |z|^p, \tag{39}$$

where  $u_0, a(x, s), b(x, s)$  are as in Theorem 2.3,  $0 < p < 1$  is a constant. Let

$$M_i = \max_{x_i \in I_i} \frac{1}{1 - \beta'_i(x_i)}, i = 1, \dots, n, \tag{40}$$

and

$$\exp \left( M \int_{\alpha(x^0)}^{\alpha(T)} \gamma(x, s) ds \right) < 2, \tag{41}$$

where  $M = M_1 \times \dots \times M_n, \alpha(x) = x - \beta(x) \in C^1(I, I)$  is increasing on  $I, \gamma(x, s) = \max \{a(x, \alpha^{-1}(s)), b(x, \alpha^{-1}(s))\}$ . If  $z(x)$  is a solution of (35) on  $I$ , then

$$|z(x)| \leq \left\{ \left(1 + (c_3)^{1-p}\right) \exp \left( (1-p)M \int_{\alpha(x^0)}^{\alpha(x)} \gamma(x, s) ds \right) - 1 \right\}^{\frac{1}{1-p}} \tag{42}$$

for  $x \in I$ , where  $c_3$  is the solution of the equation

$$\bar{H}_3(t) = \frac{1}{1-p} \ln \frac{1 + (2t - u_0)^{1-p}}{1 + t^{1-p}} - M \int_{\alpha(x^0)}^{\alpha(T)} \gamma(x, s) ds = 0, t \geq u_0.$$

**Proof.** Using the conditions (37)-(39) for (36), we have

$$\begin{aligned} |z(x)| &\leq u_0 + \int_{x^0}^x a(x, s) |z(s - \beta(s))| ds + \int_{x^0}^T b(x, s) |z(s - \beta(s))|^p ds \\ &\leq u_0 + \int_{x^0}^x a(x, s) |z(\alpha(s))| ds + \int_{x^0}^T b(x, s) |z(\alpha(s))|^p ds, \end{aligned}$$

with a suitable change of variables and using (40), we get

$$\begin{aligned} |z(x)| &\leq u_0 + M \int_{\alpha(x^0)}^{\alpha(x)} a(x, \alpha^{-1}(s)) |z(s)| ds + M \int_{x^0}^T b(x, \alpha^{-1}(s)) |z(s)|^p ds \\ &\leq u_0 + M \int_{\alpha(x^0)}^{\alpha(x)} \gamma(x, s) |z(s)| ds + M \int_{x^0}^T \gamma(x, s) |z(s)|^p ds \end{aligned} \tag{43}$$

for  $x \in I$ . The application of Theorem 2.3, with  $f = g = 1, b = d = 0$ , to (43) yields (42).  $\square$

**Remark 3.1** In (35), if we replace  $\mathbb{R}$  by any time scale  $\mathbf{T}$ , we obtain a dynamic boundary value problem system as follows:

$$\begin{cases} z^{\Delta_1 \dots \Delta_n}(x) = f^{\Delta_1 \dots \Delta_n}(x) + A(x, s, z(s)) + B(x, s, z(s)), \\ z(x_1, \dots, x_{n-1}, x_n^0) = f(x_1, \dots, x_{n-1}, x_n^0), \dots, z(x_1^0, \dots, x_n) = f(x_1^0, \dots, x_n), \end{cases} \tag{44}$$

(44) can be restated as follows:

$$z(x) = f(x) + \int_{x^0}^x A(x, s, z(s)) \Delta s + \int_{x^0}^T B(x, s, z(s)) \Delta s,$$

which can be applied in the dynamic analysis of stability of solutions to dynamic Volterra-Fredholm integral equations on time scales.

#### 4 Conclusion

Some new generalized Gronwall-Bellman-Volterra-Fredholm type nonlinear integral inequalities with delay have been established in this paper, which extend some known results obtained in [11, 14]. In the last section, to illustrate the usefulness of our results, we give an application to the research of boundedness of solutions of certain Volterra-Fredholm integral equations in  $n$ -independent variables.

#### Acknowledgment

The author is very grateful to the editor and the anonymous referees for their helpful comments and valuable suggestions.

#### References

- [1] S. V. Babenko and A. A. Martynyuk. Nonlinear dynamic inequalities and stability quasilinear systems on time scales. *IFAC PapersOnLine* **50** (1) (2017) 14879–14883.
- [2] D. Bainov, and P. Simeonov. *Integral inequalities and applications*. Kluwer Academic Publishers, Dordrecht, 1992.
- [3] R. Bellman. The stability of solutions of linear differential equations. *Duke Math. J.* **10** (1943) 643–647.
- [4] A. Boudeliou. On certain new nonlinear retarded integral inequalities in two independent variables and applications. *Appl. Math. Comput.* **335** (2018) 103–111.
- [5] A. A. El-Deeb and R. G. Ahmed. On some generalizations of certain nonlinear retarded integral inequalities for Volterra–Fredholm integral equations and their applications in delay differential equations. *J. Egypt. Math. Soci.* **25** (2017) 279–285.
- [6] S. Dhar and J. T. Neugebauer. Lyapunov-Type Inequalities for a Fractional Boundary Value Problem with a Fractional Boundary Condition. *Nonlinear Dynamics and Systems Theory* **22** (2) (2022) 133–143.
- [7] Q. Feng, F. Meng and B. Fu. Some new generalized Volterra–Fredholm type finite difference inequalities involving four iterated sums. *Appl. Math. Comput.* **219** (2013) 8247–8258.
- [8] T. H. Gronwall. Note on the derivatives with respect to a parameter of the solutions of a system of differential equations. *Ann Math.* **20** (1919) 292–296.
- [9] S. D. Kendre, S. G. Latpate and S. S. Ranmal. Some nonlinear integral inequalities for Volterra-Fredholm Integral equations. *Adv. Inequal. Appl.* **2014** (2014), Article ID 21.
- [10] H. Liu. On some nonlinear retarded Volterra-Fredholm type integral inequalities on time scales and their applications. *J. Inequal. Appl.* (2018) 2018:211.
- [11] Q. H. Ma and J. Pecaric. Estimates on solutions of some new nonlinear retarded Volterra-Fredholm type integral inequalities. *Nonlinear Analysis* **69** (2008) 393–407.
- [12] A. A. Martynyuk. *Stability Theory for Dynamic Equations on Time Scales*. Birkhauser, 2016.
- [13] B. G. Pachpatte. Explicit bound on a retarded integral inequality. *Math. Inequal. Appl.* **7** (2004) 7–11.
- [14] B. G. Pachpatte. On a certain retarded integral inequality and its applications. *JIPAM. J. Inequal. Pure Appl. Math.* **5** (2004) 1–22.
- [15] O. M. Stanzhytskyi, S. G. Karakenova, and R. E. Uteshova. Averaging method and boundary value problems for systems of Fredholm integro-differential equations. *Nonlinear Dynamics and Systems Theory* **21** (1) (2021) 100–113.



# An Adaptive Step Size for Chaotic Local Search Algorithm

Aziza Filali<sup>1</sup> and Tayeb Hamaizia<sup>2\*</sup>

<sup>1</sup> *Department of Mathematics, Faculty of Exact Sciences, University of Constantine 1, Algeria.*

<sup>2</sup> *Department of Mathematics, Faculty of Exact Sciences, University of Constantine 1, Algeria.*

Received: April 5, 2023; Revised: July 25, 2023

**Abstract:** In this paper, a chaotic strategy based on a 2-D chaotic application is proposed. This method reduces the search space of optimized variables and improves the search precision, which has higher search efficiency. In order to solve the problem between fast convergence and low steady-state, a suitable step size control is proposed. The simulation results show that the new algorithm has faster convergence.

**Keywords:** *chaos; global optimization; evolutionary algorithms; step size control; chaos optimization algorithm.*

**Mathematics Subject Classification (2010):** 34D45, 70K55.

## 1 Introduction

Chaos is one of the few concepts in mathematics that cannot usually be defined in a word or statement. The study of chaos has been rapidly developed since Lorenz's influential book [7], and Li and York's pioneer paper [8]. R. L. Devaney has been provided one of the most popular and accepted definitions of chaos, in which chaotic systems exhibit a sensitive dependence on the initial conditions, topological transitivity, and dense periodic orbits [2]. Recently, there has been an increasing interest in controlling and utilizing chaos, particularly among the physicists, mathematicians, engineering and technological communities. The noun "chaos" and the adjective "chaotic" are used to describe the time behavior of a system when this behavior is a sensitive dependence on the initial conditions, aperiodic (it never exactly repeats), and apparently random or "noisy". The key word here is apparently. Underlying this apparent chaotic randomness is an order determined, in some sense, by the equation describing the system [7–9,11]. The

---

\* Corresponding author: <mailto:el.tayyeb@umc.edu.dz>

combination of optimization methods and fundamentals of chaotic systems has attracted an increased interest in various fields in recent years. The chaos optimization algorithm is a new global optimization, which used chaotic variables directly in the search for the optimal solution. Referring to the properties of chaotic systems, it is clear that the ergodicity, self-similarity, regularity, and intrinsic stochastic property of chaos make it more possible to obtain the global optimal solution by the chaos optimization than by the method adopted before. It can more easily escape from local minima than other stochastic algorithms. The optimization algorithms based on the chaos theory are search methodologies that differ from any of the existing traditional stochastic optimization techniques [2–4, 13]. So, the chaos optimization algorithm (COA) is used to greatly reduce computational cost and select the optimal threshold value, and finally, to enhance segmentation performance [5, 6, 12]. The paper is organized as follows: in the next section, we introduce the proposed approach with a new strategy based on two phases of global/local chaotic search using the Gingerbreadman map. In Section 2, illustrative examples with the discussion of the results are presented and conclusions are offered.

## 2 The Principal of Chaos Optimization

Non-linear systems with complex dynamics have lately been the subject of intense research and exploration, giving birth to *chaos theory*. Chaotic systems are deterministic systems that exhibit irregular behavior and sensitive dependence on the initial conditions. Chaos theory studies the behavior of systems that follow deterministic laws but appear random and unpredictable, i.e., dynamical systems. Chaotic variables can go through all states in certain ranges according to their own regularity without repetition [8]. A chaotic map is a map that exhibits some type of chaotic behavior. In this work, we applied a chaotic map that is common in the literature, namely, the Gingerbreadman map. The mathematical form of a chaotic two-dimensional map, which maps the unit square  $I \times I$ , where  $I = [0, 1]$ , onto itself in a one-to-one manner, is chosen. Later on, we will use this map in the chaotic searches.

### 2.1 Chaos model

In most COA methods [3], chaos variables are generated by the logistic map [1, 2]. It is possible to change the form of this map to obtain other chaotic attractors, but in this paper, we assume a Gingerbreadman two-dimensional discrete map can generate chaos variables. The Gingerbreadman map is a discrete-time dynamical system [9–11]. It is one of the most studied examples of dynamical systems that exhibit chaotic behavior. The Gingerbreadman map takes a point  $(x_n, y_n)$  on the plane and maps it to a new point

$$\begin{cases} y_1(k) = 1 - a(y_1(k-1))^2 + by(k-1), \\ y(k) = y_1(k-1), \end{cases} \quad (1)$$

where  $k$  is the iteration number. In this work, the values of  $y$  are normalized in the range  $[0, 1]$  to each decision variable in the uni-dimensional space of the optimization problem. This transformation is given by

$$z_i(k) = \frac{(x_i(k) - L_i)}{(U_i - L_i)}.$$

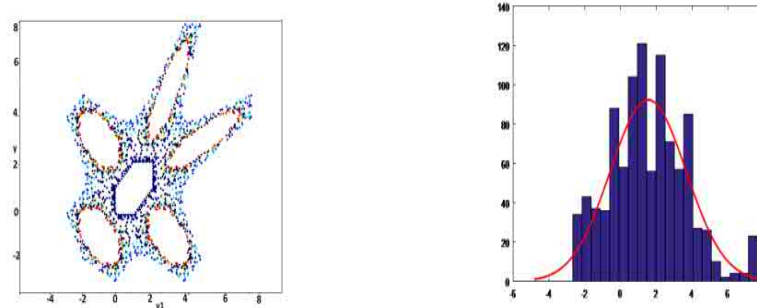


**Figure 1:** A chaotic Gingerbreadman attractor obtained for  $a = 1$  and  $b = 1$ .

The parameters used in this work are  $a = 1$  and  $b = 1$ , these values are suggested by (1). An example of the evolution of a new map is shown in Fig.1. The properties of stochastic sensitivity to the initial value and ergodicity of the two-dimensional map (1) are expressed in Fig.1 by iterating 1000 times.

### 3 Design of the Algorithm

Recently, the idea of using chaotic sequences instead of random sequences has been noticed in the research field such as chaos optimization. Li and Jiang [3] presented a chaos optimization algorithm (COA) that can solve complex optimization problems. The most important advantages of the COA are summarized as: easy implementation, short execution time, and speed-up of the search. Observations, however, reveal that the COA also has some problems including: (i) the COA is effective only for small decision spaces; (ii) the COA easily converges in the early stages of the search process [8]. Figure 2 shows the flowchart of the proposed algorithm.

Consider the following optimization problem on the minimum of functions. If the target function  $f(x_i)$  is continuous and differentiable, the object problem to be optimized is find  $x_i$  to minimize  $f(x_i); x_i \in [L_i, U_i]; i = 1, 2, \dots, n$ .

The main procedures of this algorithm are shown as follows:

#### Input :

$M_g$  : maximum number of iterations of the global search.

$M_l$  : maximum number of iterations of the local search.

$M_l + M_g$  : stopping criterion of the chaotic optimization method in iterations.

$\lambda$  : step size in the chaotic local search.

#### Output :

$X^*$  : best solution from the current run of the chaotic search.

$f^*$  : best objective function (minimization problem).

Then the basic steps of the chaos optimization algorithm based on the chaos variable from chaos map (1) are expressed as follows [2]:

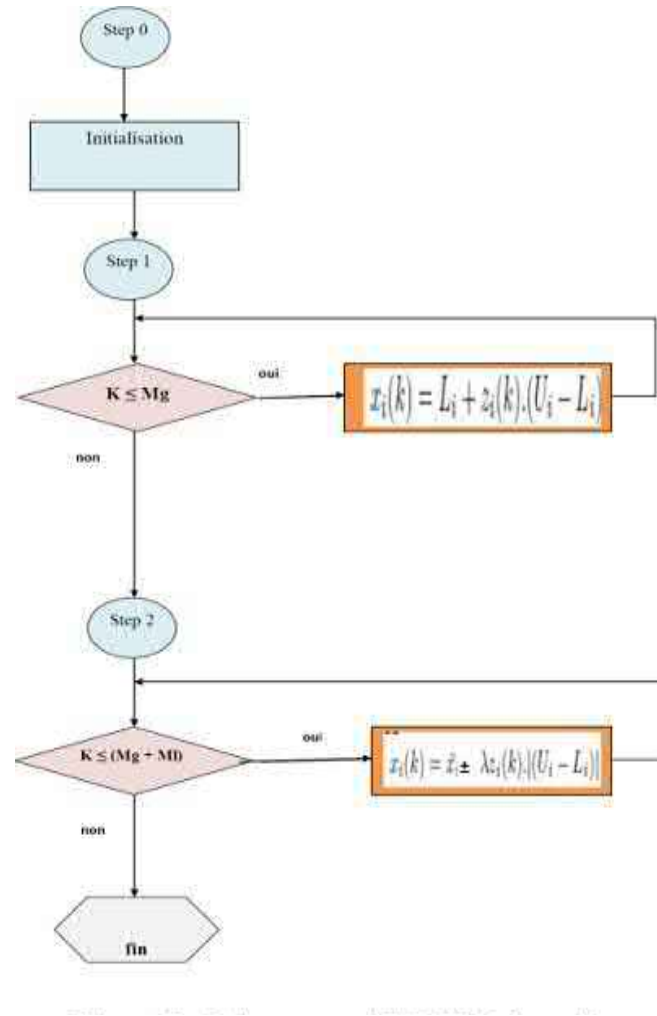


Figure 2: Diagram of the COA.

### 3.1 Step-size control

It is well-established that the convergence of a chaos optimization algorithm directly depends on how it controls the step size. Moreover, the step-size control influences to a large extent the rate at which a chaos optimization algorithm approaches the optimum. The step-size adaptation mechanisms are all based on the idea that the smaller the step size, the higher the probability of sampling good solutions.

## 4 Numerical Results

In order to verify the typical function of this paper to optimize the effectiveness of the algorithm, the 4-target function expression is as follows [14, 15]:

1.  $F_1$  is the Rosenbrock function,

$$F_1 = 100(x_1^2 - x_2)^2 + (1 - x_1)^2. \quad (2)$$

- Search domain :  $-2.048 \leq x_i \leq 2.048, i = 1, 2$ .
- Number of local minima : no local minima except the global one.
- The global minima :  $\bar{x} = (1, 1), f(\bar{x}) = 0$ .

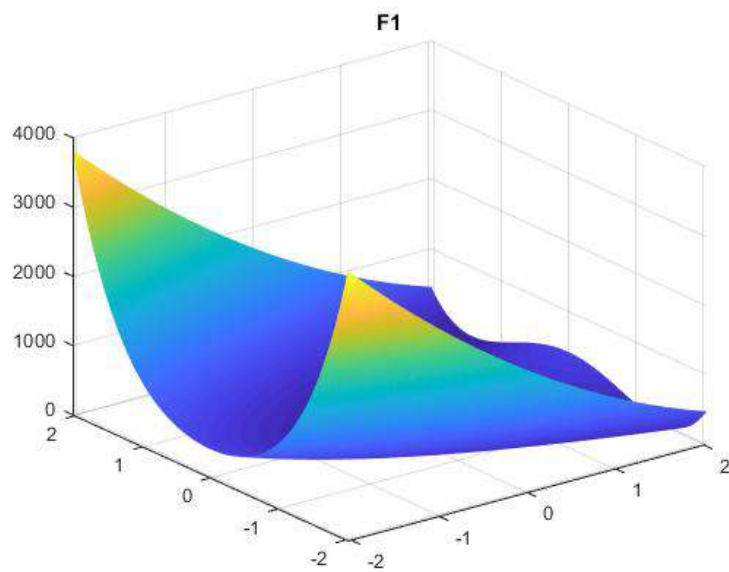


**Figure 3:** The Rosenbrock function.

2.  $F_2$  is the Goldstein-Price function,

$$F_2 = (1 + (x_1 + x_2 + 1)^2(19 - 14x_1 + 3x_1^2 - 14x_2 + 6x_1x_2 + 3x_2^2)) \\ (30 + (2x_1 - 3x_2)^2(18 - 32x_1 + 12x_1^2 + 48x_2 - 36x_1x_2 + 27x_2^2)). \quad (3)$$

- Search domain :  $-2 \leq x_i \leq 2, i = 1, 2$ .
- Number of local minima: several local minima.
- The global minima :  $\bar{x} = (0, 1), f(\bar{x}) = 3$ .

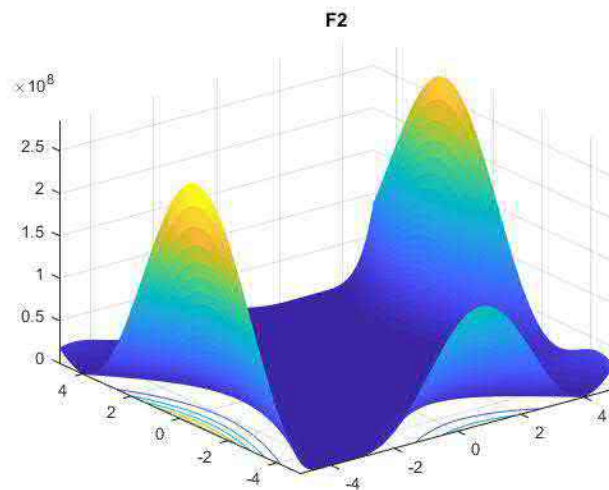


**Figure 4:** The Goldstein-Price function.

3.  $F_3$  is the Easom function,

$$F_3 = -\cos(x_1)\cos(x_2)\exp(-(x_1 - \pi)^2 - (x_2 - \pi)^2). \quad (4)$$

- Search domain :  $-10 \leq x_i \leq 10, i = 1, 2$ .

- Number of local minima : several local minima.
- The global minima :  $\bar{x} = (\pi, \pi)$ ,  $f(\bar{x}) = -1$ .

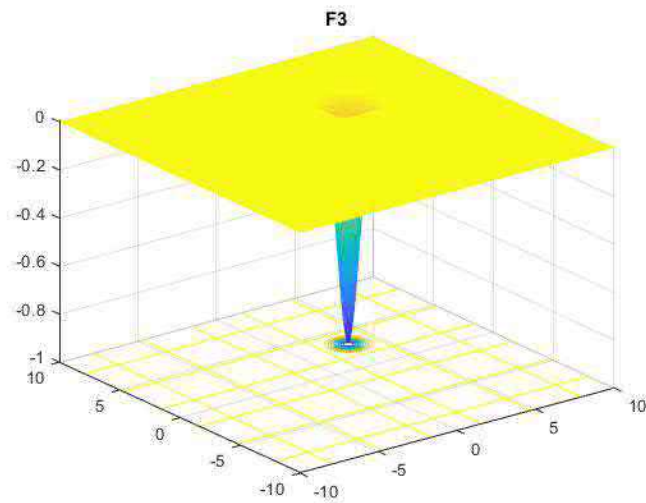


**Figure 5:** The Easom function

4.  $F_4$  is the Schaffer function,

$$F_4 = -0.5 + \left( \frac{((\sin \sqrt{(x_1^2 + x_2^2)})^2 - 0.5)}{(1 + .001(x_1^2 + x_2^2))^2} \right). \quad (5)$$

- Search domain :  $-4 \leq x_i \leq 4$ ,  $i = 1, 2$ .
- Number of local maxima : infinite local maxima.
- The global maximum:  $\bar{x} = (0, 0)$ ,  $f(\bar{x}) = -1$ .

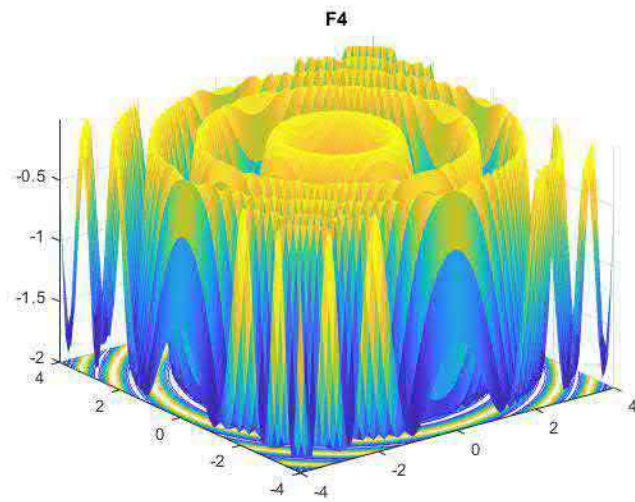


**Figure 6:** The Schaffer function.

Function  $F_1$  is the Rosenbrock function, which has global minima  $\bar{x} = (1, 1)$ , and optimal objective function value  $F_1(\bar{x}) = 0$ . The function  $F_2$  is the Goldstein-Price function, which has infinite local minima and one global minimum  $\bar{x} = (0, 1)$ ;  $F_2(\bar{x}) = 3$ . The function  $F_3$  is the Easom function, which has many local minima and one global minimum  $\bar{x} = (-\pi, \pi)$  and  $F_3(\bar{x}) = -1$ . The function  $F_4$  is the Schaffer function, which has infinite local maxima and one global maximum  $\bar{x} = (0, 0)$ , and  $F_4(\bar{x}) = -1$ . These four nonlinear multimodal functions are often used to test the convergence, efficiency, and accuracy of the optimization algorithms [3].

During the chaotic local search, the step size  $\lambda$  is an important parameter in the convergence behavior of the optimization method, which adjusts small ergodic ranges around. The step size  $\lambda$  is employed to control the impact of the current best solution on the generating of a new trial solution. A small  $\lambda$  tends to perform exploitation to refine results by local search, while a large one tends to facilitate a global exploration of search

space [2, 13]. A suitable value for the step size  $\lambda$  usually provides a balance between global and local exploration abilities and consequently, a reduction of the number of iterations required to locate the optimum solution.

In this work, using the same number of function evaluations :  $M_g + M_l$ , we perform 50 runs with different initial conditions for the mapping of the tested values of step size in the chaotic optimization method based on the Gingerbreadman map which are described as follows:

- $\lambda = 0.1; M_g = 2200; M_l = 300$ .

	Best Value	Mean Value	Std. Dev	$(\bar{x}_1, \bar{x}_2)$	Time
$F_1$	0.0000	0.0003	0.0003	(0.9913, 0.9831)	33.9249s
$F_2$	3.0031	3.0031	0.0000	(0.0032, -0.9978)	34.4000s
$F_3$	-0.9961	-0.9961	0.0000	( 3.1364 , 3.0906)	37.6054s
$F_4$	-0.9993	-0.9989	0.0001	(-0.0310, 0.0080)	35.6340s

**Table 1:** The COA based on the Gingerbreadman map.

- $\lambda = 0.001; M_g = 2200; M_l = 300$ .

	Best Value	Mean Value	Std. Dev	$(\bar{x}_1, \bar{x}_2)$	Time
$F_1$	0.0000	0.0000	0.0000	(1.0001, 1.0002)	33.8875s
$F_2$	3.0000	3.0000	0.0000	(-0.0001, -1.0001)	33.9260s
$F_3$	-1.0000	-0.9997	0.0001	(3.1438 , 3.1411)	37.1161s
$F_4$	-0.9999	-0.9998	0.0001	(-0.0006, -0.0017)	35.7883s

**Table 2:** The COA based on the Gingerbreadman map.

- $0.001 \leq \lambda \leq 0.1; M_g = 2200; M_l = 300$ .

	Best Value	Mean Value	Std. Dev	$(\bar{x}_1, \bar{x}_2)$	Time
$F_1$	0.0000	0.0001	0.0001	(1.0044, 1.0088)	35.2739s
$F_2$	3.0000	3.0027	0.0010	( 0.0024, -0.9985)	35.4629s
$F_3$	-0.9994	-0.9963	0.0008	( 3.1374 , 3.0952)	38.2361s
$F_4$	-0.9996	-0.9989	0.0001	(-0.0290 , 0.0063)	36.9733s

**Table 3:** The COA based on the Gingerbreadman map.

## 5 Conclusion

The chaos optimization method based on the Gingerbreadman map (COGM methodologies) was successfully validated for testing four different cost functions. From the case studies and comparison of the results through three tested COGM approaches it has been shown that the parameter of step size  $\lambda$  is essential for the good convergence profile. In this context, the parameter  $\lambda$  regulates the trade-off between the global and local exploration abilities of the chaotic local search. However, the future works will include a detailed study of self-adaptive heuristics for the step size design.

## References

- [1] T. Hamaizia and R. Lozi. An improved chaotic optimization algorithm using a new global locally averaged strategy. *Journal of Nonlinear Systems and Applications* **3** (2) (2012) 58–63.
- [2] H. Shayeghi, H. A. Shayanfar, S. Jalilzade and A. Safari. A PSO based unified power flow controller for damping of power system oscillations. *Energy Conversion and Management* **50** (10) (2009) 2583–2592.
- [3] B. Li and W. S. Jiang. Chaos optimization method and its application. *Journal of Control Theory and Application* **14** (4) (1997) 613–615.
- [4] R. Caponetto, L. Fortuna, S. Fazzino and M. G. Xibilia. Chaotic sequences to improve the performance of evolutionary algorithms. *IEEE Transactions on Evolutionary Computation* **7** (3) (2003) 289–304.
- [5] W. H. Ho, J. H. Chou and C. Y. Guo. Parameter identification of chaotic systems using improved differential evolution algorithm. *Nonlinear Dyn.* **61** 2941 (2010) 29–41.
- [6] Z. Wei, F. Ge, Y. Lu, L. Li and Y. Yang. Chaotic ant swarm for the traveling salesman problem. *Nonlinear Dyn.* **65** (2011) 271–281.
- [7] T. Y. Li and J. A. Yorke. Period three implies chaos. *Amer. Math. Monthly* **82** (10) (1975) 985–992.
- [8] S. H. Strogatz. *Nonlinear Dynamics and Chaos*. Massachusetts: Perseus Publishing, 2000.
- [9] M. Hénon. A two dimensional mapping with a strange attractor. *Commun. Math. Phys.* **50** (1) (1976) 69–77.
- [10] A. Aziz-Alaoui, C. Robert and C. Grebogi. Dynamics of a Hénon-Lozi map. *Chaos, Solitons Fractals* **12** (11) (2001) 2323–2341.
- [11] M. Misiurewicz. Strange attractors for the lozi mappings. *Annals of the New York academy of sciences, nonlinear dyn.* **357** (1980) 348–358.
- [12] S. Cong, G. Li and X. Feng. An Improved Algorithm of Chaos Optimization. In: *Proc. IEEE Int. Conf. on Control and Automation*, Xiamen, China, 2010, 1196–1200.
- [13] B. Li and W. S. Jiang. Optimizing complex function by chaos search. *Cybernetics and Systems* **29** (4) (1998) 409–419.
- [14] S. K. Mishra. *Some New Test Functions For Global Optimization And Performance of Repulsive Particle Swarm Method*. University Library of Munich, Germany, 2006.
- [15] M. Molga and C. Smutnicki. *Test functions for optimization needs*, 2005, <https://robertmarks.org/Classes/ENGR5358/Papers/functions.pdf>.



# On the Dynamics and FSHP Synchronization of a New Chaotic 3-D System with Three Nonlinearities

Fareh Hannachi<sup>1\*</sup> and Rami Amira<sup>2</sup>

<sup>1</sup> *Echahid Cheikh Larbi Tebessi University, Tebessa, Algeria.*

<sup>2</sup> *Laboratory of Mathematics, Informatics and Systems (LAMIS), Echahid Cheikh Larbi Tebessi University, Tebessa, Algeria.*

Received: January 12, 2023; Revised: May 26, 2023

**Abstract:** This paper reports on a novel chaotic system with three nonlinearities. Firstly, some properties of the system are studied including equilibrium points and their stability, the Lyapunov exponent and Kaplan-Yorke dimension. Also, the system dynamics are studied by numerical mathematical tools, namely, the Lyapunov exponent spectrum, bifurcation diagrams and 0-1 test. Also, we have studied a type of synchronization, a full-state hybrid projective synchronization (FSHPS), between master and slave chaotic systems. We design suitable controllers to achieve this type of synchronization by using the Lyapunov stability criteria of the integer-order linear system. Finally, the effectiveness of the proposed scheme for this type of synchronization is demonstrated by an illustrative example with numerical simulation in Matlab.

**Keywords:** *chaotic system; strange attractor; Lyapunov exponent; Lyapunov stability theory; adaptive control; synchronization.*

**Mathematics Subject Classification (2010):** 34C28, 34D08, 37B25, 37B55, 37D45, 93D05, 93D20.

## 1 Introduction

In the fields of nonlinear systems dynamics and Chaos theory, a chaotic system is a nonlinear deterministic system that displays a complex, unpredictable behavior and extreme sensitivity to initial conditions. Chaotic systems are applied in many disciplines such as biology, ecology, economics, science and engineering [1-4], etc. They have many different and common application areas such as neural networks, image and sound encryption, robotics, cryptography and secure communication [5-13]. In 1963, Lorenz discovered the

---

\* Corresponding author: <mailto:fareh.hannachi@univ-tebessa.dz>

first 3-d chaotic system [14]. After that, several chaotic systems have been designed by many researchers, they are: the Rossler, Chen, Zhou, Vaidyanathan, Yu-Wang, Hannachi systems [15-20], etc. After the work done by Pecora and Carroll [21], the chaos synchronization between chaotic systems has been extensively studied by different theoretical and experimental methods and due to the powerful and multiple applications of synchronization using chaotic systems in various fields such as secure communication, telecommunication, cryptography and encryption [22-26], the study of chaos and synchronization in dynamical systems has attracted a considerable attention, and an intense competition has begun among researchers for finding new chaotic systems and developing different types and methods of synchronization for those systems. The synchronization of chaotic systems has been presented in diverse works, where different techniques were employed to synchronize two chaotic systems. In recent years, we find that diverse types and methods of synchronization have been developed, among them there are the active control [27-28], sliding mode control [29-31], backstepping control [32], adaptive control [33-36], function projective synchronization [37], modified projective synchronization [38], hybrid projective synchronization [39], full state hybrid projective synchronization [40], inverse full state hybrid projective synchronization [41]. In this work, a new 3-D chaotic system with three nonlinearities is introduced. Basic dynamical properties of this new chaotic system are studied, namely, the equilibrium points and their stability, dissipativity and Lyapunov exponent, Lyapunov exponent spectrum, Kaplan-Yorke dimension, bifurcations. Also, we have studied a type of synchronization, a full-state hybrid projective synchronization (FSHPS), using the new systems. We design suitable controllers to achieve this type of synchronization by using the Lyapunov stability criteria of the integer-order linear system. Finally, the effectiveness of the proposed scheme for this type of synchronization is demonstrated by an illustrative example with numerical simulation in Matlab.

This paper is organized as follows. In Section 2, a description of the novel chaotic system is given. In Sections 3, the FSHP synchronization using the new chaotic system is investigated. The new system and another new system are used in Section 4 to demonstrate the effectiveness of the proposed method. Finally, the conclusion is given in Section 4.

### 1.1 Description of the novel chaotic system

A novel 3-D autonomous chaotic system is expressed as follows:

$$\begin{cases} \frac{dx}{dt} = a(y - x), \\ \frac{dy}{dt} = cx - y - xz, \\ \frac{dz}{dt} = e^{xy} - y^2 - bz, \end{cases} \quad (1)$$

where  $x, y, z$  are the state variables and  $a, b, c$  are the positive real parameters.

There are eight terms on the right-hand side but it mainly relies on three nonlinearities, namely,  $e^{xy}$ ,  $y^2$  and  $xz$ , respectively.

System (1) can generate a new double scroll strange attractor for the parameters  $a = 10, b = 3, c = 35$  with the initial conditions  $[1, 1, 1]$  as displayed in Figs.2-3. We note the new chaotic attractor is different from that of the Lorenz system or any existing systems.

## 1.2 Basic properties

In this section, some basic properties of the system (1) are given. We start with the equilibrium points of the system and check their stability at the initial values of the parameters  $a, b, c$ .

## 1.3 Equilibrium points

Put the equations of the system (1) equal to zero, i.e.,

$$\begin{cases} a(y - x) = 0, \\ cx - y - xz = 0, \\ e^{xy} - y^2 - bz = 0. \end{cases} \quad (2)$$

A simple calculation yields the unique equilibrium point

$$p_1 = \left(0, 0, \frac{1}{3}\right). \quad (3)$$

## 1.4 Stability

In order to check the stability of the equilibrium points, we derive the Jacobian matrix at a point  $p(x, y, z)$  of the system (1):

$$J(p) = \begin{pmatrix} -a & a & 0 \\ c - z & -1 & -x \\ ye^{xy} & -2y + xe^{xy} & -b \end{pmatrix}. \quad (4)$$

For  $p_1$ , we obtain three eigenvalues:

$$\lambda_1 = \frac{1}{6}\sqrt{3}\sqrt{4403} - \frac{11}{2}, \lambda_2 = -\frac{1}{6}\sqrt{3}\sqrt{4403} - \frac{11}{2}, \lambda_3 = -3. \quad (5)$$

Since all the eigenvalues are real, the Hartma-Grobman theorem implies that  $p_1$  is a saddle point which is unstable according to the Lyapunov theorem on stability.

### 1.4.1 Lyapunov exponents and Kaplan-Yorke dimension

For the chosen parameter values of  $a, b, c$ , the Lyapunov exponents of the novel chaotic system (1) are obtained using Matlab with the initial conditions  $(x(0), y(0), z(0)) = (1, 1, 1)$  as

$$L_1 = 0.955333, L_2 = -0.00158345, L_3 = -14.9537. \quad (6)$$

Since the spectrum of Lyapunov exponents (6) has a maximal positive value  $L_1$ , it follows that the 3-D novel system (1) is a chaotic system. Moreover, the sum of all the Lyapunov exponents is negative, which implies that the system is dissipative. The Kaplan-Yorke dimension of system (1) is calculated as

$$D_{KL} = 2 + \frac{L_1 + L_2}{|L_3|} = 2.0638. \quad (7)$$

The Lyapunov exponents spectrum and the chaotic attractor of system (1) in 2-D and 3-D are shown in Figs.1-3.

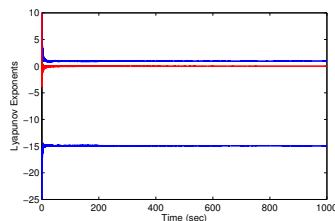


Figure 1: Lyapunov exponents spectrum.

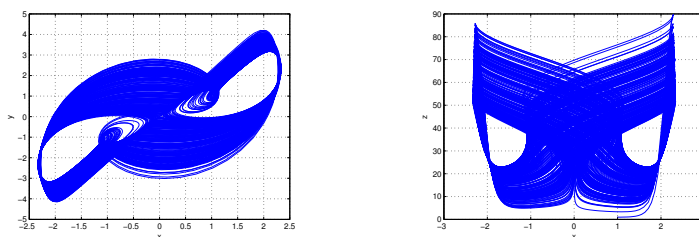


Figure 2: Chaotic attractor of system (1) in the x-y and x-z plane.

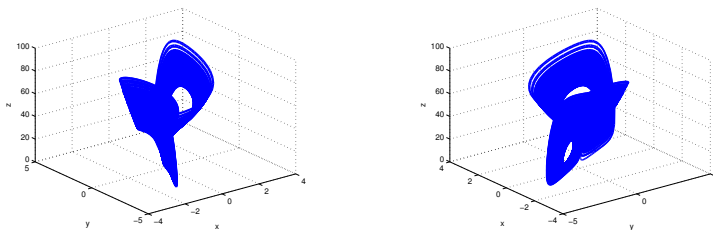


Figure 3: 3-D view of the chaotic attractor of system (1) in the x-y-z and y-x-z space.

## 2 Dynamics of the System

In this section, we investigate numerically the dynamical behavior of the system (1) using the largest Lyapunov exponents spectrum and bifurcation diagrams.

Figs.4-6 show the largest Lyapunov exponents spectrum and the bifurcation diagrams of system (1) with respect to the parameters  $a$ ,  $b$ ,  $c$ , respectively. Obviously, when  $a \in [0, 20]$ ,  $b \in [0, 10]$ ,  $c \in [20, 40]$ , the behavior of system (1) is either chaotic, periodic or converges to an equilibrium. When  $a \in ]1.07, 1.3[ \cup ]4, 8.7[ \cup ]9.3, 11.2[$ ,  $b \in [2.6, 3.2] \cup [3.5, 10]$ ,  $c \in [22.23, 22.6] \cup [23, 40]$ , the maximum Lyapunov exponent is positive, implying that the new system (1) is chaotic in this range of parameters. For  $a \in [11.47, 20]$ ,  $b \in [1.25, 2.5]$ ,  $c \in [20, 21.9]$ , the maximum Lyapunov exponent almost always equals zero, implying that the new system (1) has a periodic orbit. The maximum Lyapunov exponent is negative when  $a \in [0, 1.06] \cup [1.43, 4[ \cup ]11.2, 11.46[$ ,  $b \in [2.3267697, 2.3886929] \cup$

$[3.2490194, 3.2743673] \cup [3.3644489, 3.437006] \cup [3.4626194, 3.4800358]$ ,  $c \in ]21.9, 22] \cup [22.8, 22.87]$ , which means that the trajectories of the new system (1) is fall to converge to equilibria. Figs.7 shows the different behavior of system (1): for  $a = 3.02$  converging to an equilibrium, for  $c = 32$  chaotic, for  $c = 21.9$  and  $b = 1.75$  periodic.

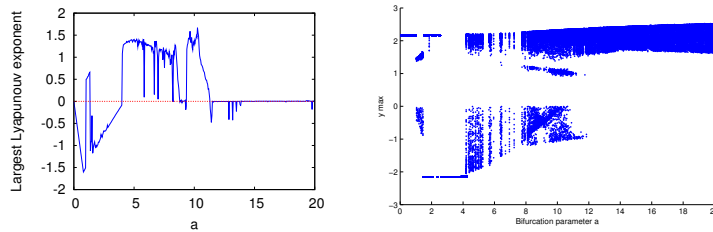


Figure 4: Lyapunov exponents spectrum and bifurcation diagram for  $a \in [0, 20]$ .

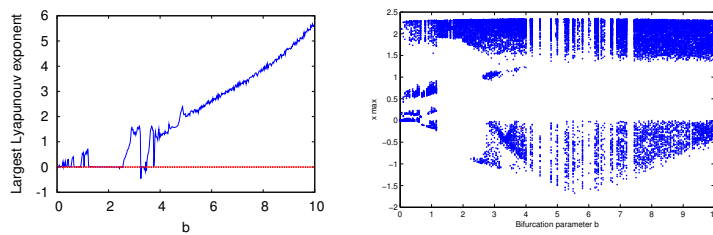


Figure 5: Lyapunov exponents spectrum and bifurcation diagram for  $b \in [0, 10]$ .

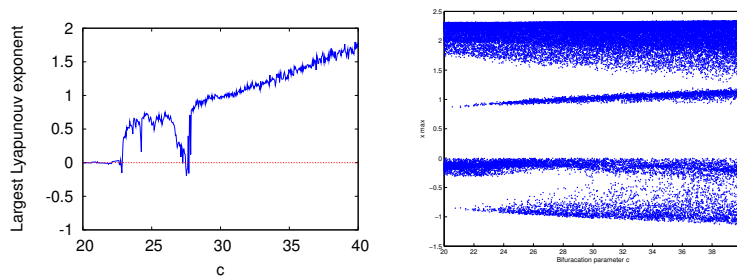
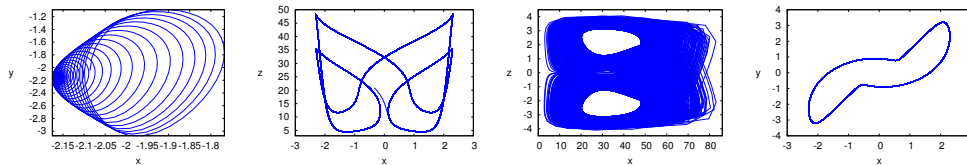


Figure 6: Lyapunov exponents spectrum and bifurcation diagram for  $c \in [20, 40]$ .

### 2.1 0-1 test for system (1)

The 0-1 test was proposed by Gottwald and Melbourne, it is a test approach for distinguishing regular and chaotic dynamics in deterministic dynamical systems [42]. This test depends on the rapport  $k_c$ , if it is close to one, then the system has a chaotic behavior and if it is close to zero, then the system has a regular behavior.



**Figure 7:** Different behavior of system (1): For  $a=3.02$  converging to an equilibrium, for  $c=32$  chaotic, for  $c=21.9$  and  $b=1.75$  periodic.

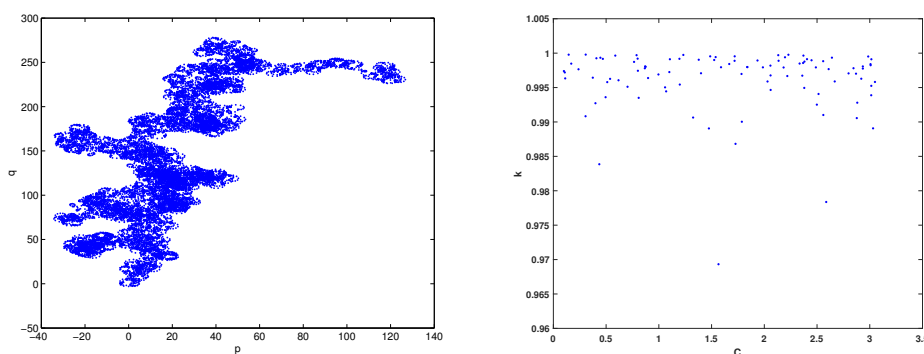


**Figure 8:** Brownian motion in the (p-q) plane and Kc Plot for the new system (1).

In Matlab, we choose the random constant ( $C \in [0; \pi]$ ), as a result, we find the rapport  $k_c = 0.9990$  which is close to one as shown in Fig.8, moreover, we obtain a Brownian motion in the (p-q) plane, which means that the novel system (1) has a chaotic behavior as shown in Fig.8.

### 3 Master-Slave Synchronization of Non-Identical 3-D Novel Chaotic Systems Using FSHP Method

We consider the drive system given by

$$\dot{x}_i(t) = f_i(X(t)), i = 1, \dots, n, \quad (8)$$

where  $X(t) = (x_1, x_2, \dots, x_n)^T$  is the state vector of the system (8),  $f_i : \mathbb{R}^n \rightarrow \mathbb{R}^n$  for  $i = 1, \dots, n$  are nonlinear functions, and the response system is the system given by

$$\dot{y}_i(t) = \sum_{j=1}^n b_{ij} y_j(t) + g_i(Y(t)) + u_i, i = 1, \dots, n, \quad (9)$$

where  $Y(t) = (y_1, y_2, \dots, y_n)^T$  is the state vector of the system (9),  $g_i : \mathbb{R}^n \rightarrow \mathbb{R}^n$  for  $i = 1, \dots, n$  are the nonlinear functions,  $u_i$  are the controllers to be designed so that the system (8) and the system (9) are synchronized.

Now, we introduce the definition of FSHPs [40] between master and slave systems.

**Definition 3.1** FSHPs occurs between master and slave systems (8) and (9) when there are controllers  $u_i, i=1,2,\dots,n$ , and given real numbers  $(\alpha_{ij})_{1 \leq i,j \leq n}$  such that the synchronization errors

$$e_i(t) = y_i(t) - \sum_{j=1}^n \alpha_{ij} x_j(t), \quad i = 1, \dots, n, \tag{10}$$

satisfy  $\lim_{t \rightarrow +\infty} e_i(t) = 0$ .

Full-state hybrid projective synchronization (FSHPS) is one of the most noticeable types. It has been widely used in the synchronization of chaotic systems. In this type of synchronization, each slave system state achieves synchronization with the linear combination of master and system states. The state errors for (8) and (9) are

$$e_i = y_i - \sum_{j=1}^n \alpha_{ij} x_j, \quad i = 1, \dots, n. \tag{11}$$

Consequently, the error dynamic system is given by

$$\dot{e}_i = \left( \sum_{j=1}^n b_{ij} y_j(t) + g_i(Y(t)) \right) + U_i - \sum_{j=1}^n \alpha_{ij} f_j(X(t)), \quad i = 1, \dots, n. \tag{12}$$

The error system can be described as

$$\dot{e}_i = \sum_{j=1}^n b_{ij} e_j(t) + \left( \sum_{j=1}^n b_{ij} y_j(t) - \sum_{j=1}^n b_{ij} e_j(t) + g_i(Y(t)) \right) + U_i - \sum_{j=1}^n \alpha_{ij} f_j(X(t)), \tag{13}$$

$i = 1, \dots, n$ , i.e.,

$$\dot{e}_i = \sum_{j=1}^n b_{ij} e_j(t) + R_i + U_i, \quad i = 1, \dots, n, \tag{14}$$

where

$$R_i = \left( \sum_{j=1}^n b_{ij} y_j(t) - \sum_{j=1}^n b_{ij} e_j(t) + g_i(Y(t)) \right) - \sum_{j=1}^n \alpha_{ij} f_j(X(t)), \quad i = 1, \dots, n. \tag{15}$$

Rewrite error system (14) in the compact form

$$\dot{e} = Be + R + U, \tag{16}$$

where  $B = (b_{ij})_{n \times n}$  and  $e = (e_1, e_2, \dots, e_n)^T, R = (R_i)_{1 \leq i \leq n}, U = (U_i)_{1 \leq i \leq n}$ .

**Theorem 3.1** FSHPS between the master system (8) and the slave system (9) will occur under the following control law:

$$U = -(R + Ce) \tag{17}$$

with  $C$  being a feedback gain matrix selected so that  $B - C$  is a negative definite matrix.

**Proof.** By inserting (17) into (16), we get

$$\dot{e} = (B - C)e. \quad (18)$$

If we choose matrix  $C$  so that  $B - C$  is negative, then all the eigenvalues  $\lambda_i, i = 1, 2, 3$ , of  $(B - C)$  stay in the left-half plane, i.e.,  $Re(\lambda_i) < 0$ , which ensures, according to the Lyapunov stability theory, that error system (18) is asymptotically stable. Hence the synchronization between the sytem (8) and the sytem (9) is achieved.

#### 4 Illustrative Example

In this section, the new system (1) and another new system (19) are used to demonstrate the effectiveness of the proposed method.

As a driving system, we considier the chaotic system [20] given by

$$\begin{cases} \frac{dx_1}{dt} = a(x_2 - x_1), \\ \frac{dx_2}{dt} = cx_1 - x_1x_3, \\ \frac{dx_3}{dt} = -x_1x_2 + b(x_1 - x_3), \end{cases} \quad (19)$$

where  $a = 13, b = 2.5, c = 50$ , and as a response system, we consider the controlled system of system (1) given by

$$\begin{cases} \frac{dy_1}{dt} = a(y_2 - y_1) + u_1, \\ \frac{dy_2}{dt} = cy_1 - y_2 - y_1y_3 + u_2, \\ \frac{dy_3}{dt} = e^{y_1y_2} - y_2^2 - by_3 + u_3, \end{cases} \quad (20)$$

where  $a = 10, b = 3, c = 35$ .

According to the above method, for FSHPS, we have

$$B = \begin{pmatrix} -10 & 10 & 0 \\ 35 & -1 & 0 \\ 0 & 0 & -3 \end{pmatrix} \quad (21)$$

and the choice of  $C = \begin{pmatrix} 0 & 10 & 0 \\ 35 & 4 & 0 \\ 0 & 0 & -2 \end{pmatrix}$  and  $(\alpha_{ij})_{1 \leq i, j \leq 4} = \begin{pmatrix} 1 & 8 & 5 \\ 7 & 2 & 1 \\ 6 & 0 & -3 \end{pmatrix}$  yields

$$\begin{cases} R_1 = 10e_1 - 10e_2 - 399.5x_1 - 13x_2 + 12.5x_3 - 10y_1 + 10y_2 + 5x_1x_2 + 8x_1x_3, \\ R_2 = e_2 - 35e_1 - 11.5x_1 - 91x_2 + 2.5x_3 + 35y_1 - y_2 + x_1x_2 + 2x_1x_3 - y_1y_3, \\ R_3 = 3e_3 + 85.5x_1 - 78x_2 - 7.5x_3 - 3y_3 + e^{y_1y_2} - y_2^2 - 3x_1x_2 \end{cases} \quad (22)$$

and

$$\begin{aligned} (U_1, U_2, U_3)^T &= -\left(R + C(e_1, e_2, e_3)^T\right) \\ &= \begin{pmatrix} 399.5x_1 - 10e_1 + 13x_2 - 12.5x_3 + 10y_1 \\ \quad -10y_2 - 5x_1x_2 - 8x_1x_3 \\ 11.5x_1 - 5e_2 + 91x_2 - 2.5x_3 - 35y_1 \\ \quad + y_2 - x_1x_2 - 2x_1x_3 + y_1y_3 \\ 78x_2 - 85.5x_1 - e_3 + 7.5x_3 + 3y_3 - e^{y_1y_2} \\ \quad + y_2^2 + 3x_1x_2 \end{pmatrix}. \end{aligned} \quad (24)$$

The error system is given by

$$\begin{pmatrix} \dot{e}_1 \\ \dot{e}_2 \\ \dot{e}_3 \end{pmatrix} = \begin{pmatrix} -10 & 0 & 0 \\ 0 & -5 & 0 \\ 0 & 0 & -1 \end{pmatrix} \begin{pmatrix} e_1 \\ e_2 \\ e_3 \end{pmatrix}, \tag{25}$$

then the eigenvalues of the matrix  $(B - C)$  are given by  $\lambda_1 = -10, \lambda_2 = -5, \lambda_3 = -1$ , which all are negatives. Hence the error system is asymptotically stable [43] and the synchronization between the two systems (19) and (20) is achieved.

We used the classical fourth-order Runge-Kutta method with the step size  $h = 10^{-6}$  to solve the system of differential equations (25). The initial conditions of the drive system (19) and the response system (20) are chosen as  $(x_1(0), x_2(0), x_3(0)) = (20, 10, -10)$ ,  $(y_1(0), y_2(0), y_3(0)) = (-20, -10, -50)$ , respectively.  $(e_1(0), e_2(0), e_3(0)) = (-70, -160, -200)$ ,  $(z_1(0), z_2(0), z_3(0)) = (50, 150, 150)$  with  $z_i = \sum_{j=1}^3 \alpha_{ij}x_j, i = 1, 2, 3$ .

In Fig.10, the time-history of the synchronization errors  $e_1(t); e_2(t); e_3(t)$  is depicted.

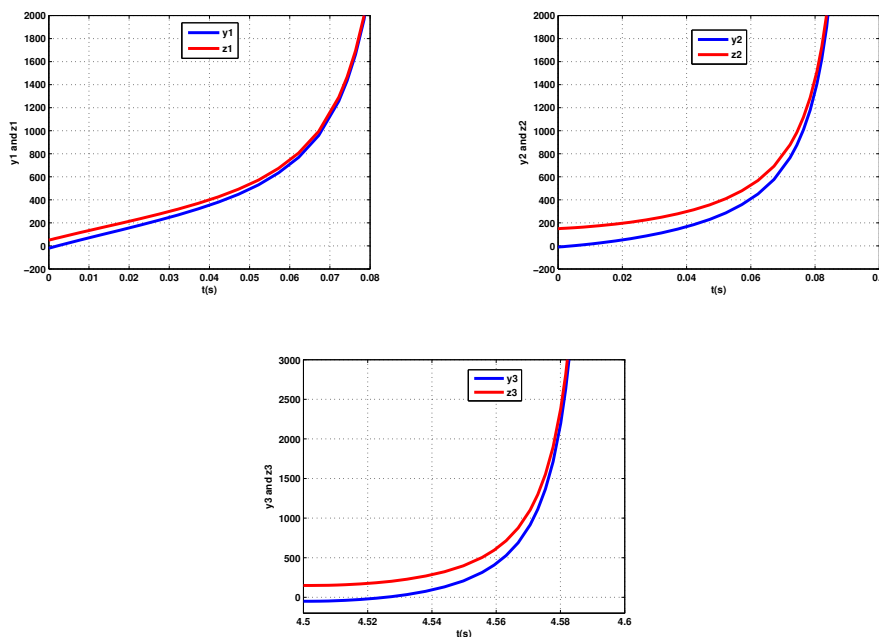
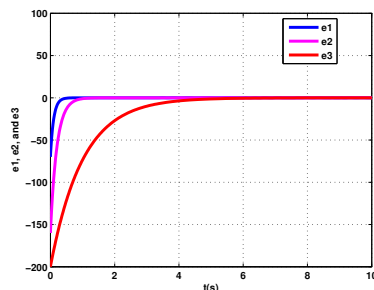


Figure 9: Synchronization between  $z_i, y_i, i = 1, 2, 3$ .

### 5 Conclusion

In this work, a new 3-D chaotic system with three nonlinearities is introduced. Basic dynamical properties of this new chaotic system are studied including equilibrium points and their stability, dissipativity, the Lyapunov exponent, Kaplan-Yorke dimension, Lyapunov exponent spectrum and bifurcation diagrams. Moreover, the synchronization problem for



**Figure 10:** The time-history of the synchronization errors  $e_1(t)$ ;  $e_2(t)$ ;  $e_3(t)$ .

globally synchronizing the non-identical 3-D chaotic systems is solved using the FSHP method and Lyapunov stability criteria of the integer-order linear system. Numerical simulations using MATLAB have been shown to illustrate our results for the new chaotic system and the considered synchronization scheme.

## 6 Concluding remarks

The main important points in this work are:

- The new chaotic attractor is different from that of the Lorenz system or any existing systems.
- The dynamics of the novel system is investigated by means of the largest Lyapunov exponents spectrum and bifurcation diagrams of the system with respect to the system parameters.
- We achieved FSHP synchrony between non-identical 3-D chaotic systems using the new system and the Lyapunov stability theory.

The novel system and the obtained results of this work have many applications in many fields such as secure communication and signal encryption. Therefore, further research of the system is still important and will be taken into consideration in a future work.

## Acknowledgment

The author would like to thank the editor-in-chief and the referees for their valuable suggestions and comments.

## References

- [1] M. Kyriazis. Applications of chaos theory to the molecular biology of aging. *Experimental Gerontology* **26** (6) (1991) 569–572.
- [2] J. C. Sprott , J. A. Vano, J. C.Wildenberg, M. B. Anderson and J. K. Noel. Coexistence and chaos in complex ecologies. *Physics Letters A* **335** (2-3) (2005) 207–212.

- [3] D. Guegan. Chaos in economics and finance. *Annual Reviews in Control* **33** (1) (2009) 89–93.
- [4] S. Vaidyanathan and C. Volos. *Advances and Applications in Chaotic Systems*. Springer, Berlin, New York, 2016.
- [5] G. He, Z.Cao, P.Zhu, H. Ogura. Controlling chaos in a chaotic neural network. *Neural Networks* **16** (8) (2003) 1195–1200.
- [6] E. Kaslik and S. Sivasundaram. Nonlinear dynamics and chaos in fractional-order neural networks. *Neural Networks* **32** (2012) 245–256.
- [7] E. B. Corrochano, Y. Mao and G. Chen. Chaos-based image encryption. In: *Handbook of geometric computing*. Springer, Berlin, Heidelberg, 2005, 231–265.
- [8] C. Volos, A. Akgul, V. T. Pham, I. Stouboulos and I. Kyprianidis. A simple chaotic circuit with a hyperbolic sine function and its use in a sound encryption scheme. *Nonlinear Dynamics* **89** (2) (2017) 1047–1061.
- [9] U. Nehmzow and K. Walker. Quantitative description of robot–environment interaction using chaos theory. *Robotics and Autonomous Systems* **53** (3-4) (2005) 177–193.
- [10] S. Iqbal, X. Zang, Y.Zhu and J. Zhao. Bifurcations and chaos in passive dynamic walking: A review. *Robotics and Autonomous Systems* **62** (6) (2014) 889–909.
- [11] N. Smaoui and A. Kanso. Cryptography with chaos and shadowing. *Chaos, Solitons and Fractals* **42** (4) (2009) 2312–2321.
- [12] S. Wang, J. Kuang, J. Li, Y. Luo, H. Lu and G. Hu. Chaos-based secure communications in a large community. *Physical Review E* **66** (6) (2002) 065202.
- [13] A. A. Zaher and A. Abu-Rezq. On the design of chaos-based secure communication systems. *Communications in Nonlinear Science and Numerical Simulation* **16** (9) (2011) 3721–3737.
- [14] E. N. Lorenz. Deterministic nonperiodic flow. *Journal of atmospheric sciences* **20** (2) (1963) 130–141.
- [15] O. E. RöSSLer. An equation for continuous chaos. *Physics Letters A* **57** (5) (1976) 397–398.
- [16] G. Chen and T. Ueta. Yet another chaotic attractor. *International Journal of Bifurcation and chaos* **9** (07) (1999) 1465–1466.
- [17] W. Zhou, Y.Xu, H. Lu and L. Pan. On dynamics analysis of a new chaotic attractor. *Physics Letters A* **372** (36) (2008) 5773–5777.
- [18] S. Vaidyanathan. A new six-term 3-D chaotic system with an exponential nonlinearity. *Far East Journal of Mathematical Sciences* **79** (2013) 135–143.
- [19] F. Yu and C. Wang. A novel three dimension autonomous chaotic system with a quadratic exponential nonlinear term. *Engineering, Technology and Applied Science Research* **2** (2) (2012) 209–215.
- [20] F. Hannachi. Analysis and Adaptive Control Synchronization of a Novel 3-D Chaotic System. *Nonlinear Dynamics and Systems Theory* **19** (1) (2019) 68–78.
- [21] L. M. Pecora and T. L. Carroll. Synchronization in chaotic systems. *Physical Review Letters* **64** (1990) 821–825.
- [22] A. A. Koronovskii, O. I. Moskalenko, A. E. Hramov. On the use of chaotic synchronization for secure communication. *Physics-Uspeski* **52** (12) (2009) 1213.
- [23] W. Kinzel, A. Englert and I. Kanter. On chaos synchronization and secure communication. *Philosophical Transactions of the Royal Society A: Mathematical, Physical and Engineering Sciences* **368** (1911) (2010) 379–389.
- [24] S. Banerjee. *Chaos Synchronization and Cryptography for Secure Communications: Applications for Encryption: Applications for Encryption*. IGI global, 2010.

- [25] C. K. Volos, I. M. Kyprianidis and I. N. Stouboulos. Image encryption process based on chaotic synchronization phenomena. *Signal Processing* **93** (5) (2013) 1328–1340.
- [26] L. Keuninckx, M. C. Soriano, I. Fischer, C. R. Mirasso, R. M. Nguimdo and G. Van der Sande. Encryption key distribution via chaos synchronization. *Scientific reports* **7** (1) (2017) 1–14.
- [27] S. M. Hamidzadeh and R. Esmaelzadeh. Control and synchronization chaotic satellite using active control. *International journal of computer applications* **94** (10) (2014)
- [28] P. P. Singh, J. P. Singh and B. K. Roy. Synchronization and anti-synchronization of Lu and Bhalekar–Gejji chaotic systems using nonlinear active control. *Chaos, Solitons and Fractals* **69** (2014) 31–39.
- [29] J. Sun, Y. Shen, X. Wang et al. Finitetime combination-combination synchronization of four different chaotic systems with unknown parameters via sliding mode control. *Nonlinear Dynamics* **76** (1) (2014) 383–397.
- [30] Y. Toopchi and J. Wang. Chaos control and synchronization of a hyperchaotic Zhou system by integral sliding mode control. *Entropy* **16** (12) (2014) 6539–6552.
- [31] F. Hannachi. Adaptive Sliding Mode Control Synchronization of a Novel, Highly Chaotic 3-D System with Two Exponential Nonlinearities. *Nonlinear Dynamics and Systems Theory* **20** (1) (2020) 38–50.
- [32] X. Wu and J. Lu. Parameter identification and backstepping control of uncertain Lu system. *System, Chaos, Solitons and Fractals* **18** (1) (2003) 721–729.
- [33] H. Adloo and M. Roopaei. Review article on adaptive synchronization of chaotic systems with unknown parameters. *Nonlinear Dynamics* **65** (1) (2011) 141–159.
- [34] F. Hannachi. Analysis, dynamics and adaptive control synchronization of a novel chaotic 3-D system. *SN Applied Sciences* **1** (2) (2019) 158.
- [35] S. Vaidyanathan, Q. Zhu, and A. T. Azar, Adaptive control of a novel nonlinear double convection chaotic system. In: *Fractional Order Control and Synchronization of Chaotic Systems*. Springer, Cham, 2017, 357–385.
- [36] S. Vaidyanathan and Volos, C. Analysis and adaptive control of a novel 3-D conservative no-equilibrium chaotic system. *Archives of Control Sciences* **25** (3) (2015) 333–353.
- [37] R. Zhang, Y. Yang, Z. Xu and M. Hu. Function projective synchronization in drive–response dynamical network. *Physics Letters A* **374** (30) (2010) 3025–3028.
- [38] G. H. Li. Modified projective synchronization of chaotic system. *Chaos, Solitons and Fractals* **32** (5) (2007) 1786–1790.
- [39] N. Jia and T. Wang. Chaos control and hybrid projective synchronization for a class of new chaotic systems. *Computers and Mathematics with Applications* **62** (12) (2011) 4783–4795.
- [40] M. Hu, Z. Xu and R. Zhang. Full state hybrid projective synchronization in continuous-time chaotic (hyperchaotic) systems. *Communications in Nonlinear Science and Numerical Simulation* **13** (2) (2008) 456–464.
- [41] A. Ouannas and G. Grassi. Inverse full state hybrid projective synchronization for chaotic maps with different dimensions. *Chinese Physics B* **25** (9) (2016) 090503.
- [42] G. A. Gottwald and I. Melbourne. A new test for chaos in deterministic systems. *Proceedings of the Royal Society of London. Series A: Mathematical, Physical and Engineering Sciences* **460** (2042) (2004) 603–611.
- [43] W. Hahn. *Stability of Motion*. Springer, Berlin, New York, 1967.



# Numerical Solution of the Black-Scholes Partial Differential Equation for the Option Pricing Model Using the ADM-Kamal Method

M. D. Johansyah<sup>1\*</sup>, I. Sumiati<sup>1</sup>, E. Rusyaman<sup>1</sup>, Sukono<sup>1</sup>, M. Muslikh<sup>2</sup>,  
M. A. Mohamed<sup>3</sup> and A. Sambas<sup>3,4</sup>

<sup>1</sup> Department of Mathematics, Faculty of Mathematics and Natural Sciences, Universitas Padjadjaran, Indonesia.

<sup>2</sup> Department of Mathematics, Faculty of Mathematics and Natural Sciences, Universitas Brawijaya, Indonesia.

<sup>3</sup> Faculty of Informatics and Computing, University Sultan Zainal Abidin, Gong Badak, 21300, Terenggan, Malaysia.

<sup>4</sup> Department of Mechanical Engineering, Universitas Muhammadiyah Tasikmalaya, Tasikmalaya, Jawa Barat 46196, Indonesia

Received: February 8, 2023; Revised: June 6, 2023

**Abstract:** Option contracts are financial derivatives developed as investment alternatives which are useful for minimizing the risk of loss. One of the most well-known models for calculating option prices is the Black-Scholes equation. This equation is a partial differential equation (PDE) of the order of natural and fractional numbers. In this paper, we have proposed a combined method of the Adomian Decomposition Method (ADM) and the Kamal Integral Transform (KIT) to solve the Black-Scholes Fractional Partial Differential Equation (FPDE) for the Option Pricing Model (OPM). The Black-Scholes FPDE approach solution can be used to build a buy and sell option pricing model. Numerical simulation results show that this method has an accurate performance in determining option pricing.

**Keywords:** price of buy and sell options; fractional partial differential equation; Black-Scholes; Kamal integral transform; Adomian decomposition method.

**Mathematics Subject Classification (2010):** 70K75, 93A10, 35Q91, 34A08, 34K37.

---

\* Corresponding author: <mailto:muhamad.deni@unpad.ac.id>

## 1 Introduction

Since its applications in numerous industries began to gain traction several decades ago, fractional-order calculus has made significant stride in many areas such as high-tech industry [1], spherical tank system for level process [2], heat and mass transfer for the elliptic inclined plate [3], web transport systems in process industries [4], image encryption process [5,6], robotic manipulators [7], photovoltaic solar energy [8], manufacturing industrial natural gas consumption [9], Field-Programmable Gate Array [10], lesser date moth system [11], magnetic levitation system [12] and spiral-plate heat exchanger [13].

Numerous economic models employ fractional order models of real dynamical objects and processes. For instance, a business cycle model includes an investment function and a general liquidity preference function [14], an IS-LM macroeconomic system [15], a financial risk chaotic system [16,17], an economic growth model [18,19] and Ivancevic option pricing model [20].

The Black-Scholes equation (BSE) is among the most important mathematical models for option pricing. Black and Scholes [21] first introduced the Black-Scholes PDE employed for calculating the price of European type call and put options, in which the underlying financial asset is the stock price without dividend payments. The symbol  $C = C(S,t)$  denotes the price of the European call option at time  $t$  and the asset price  $S$ . Let  $E$  be the exercise price,  $\sigma$  be the price volatility of the asset,  $T$  be the maturity date or time, and  $r$  be the rate of interest at which there is no risk of loss. The BSE and the boundary conditions for pricing European type call options are as follows [22]:

$$\frac{\partial C}{\partial t} + \frac{1}{2}\sigma^2 S^2 \frac{\partial^2 C}{\partial S^2} + rS \frac{\partial C}{\partial S} - rC = 0, \quad (1)$$

where  $C$  is option,  $\sigma$  is the volatility of the underlying asset,  $r$  is the risk-free interest rate,  $C(0,t) = 0$ ,  $C(S,t) \sim S$  for  $S \rightarrow \infty$ , and  $C(S,T) = \max\{S - E, 0\}$ . It follows that the diffusion equation is similar to equation (1) but with more parameters. In order to simplify equation (1), make the following conversion:

$$S = Ee^x, t = T - \frac{2\tau}{\sigma^2}, \text{ and } C(S,t) = Ev(x,\tau), \quad (2)$$

which reduces to the following PDE:

$$\frac{\partial v}{\partial \tau} = \frac{\partial^2 v}{\partial x^2} + (k-1) \frac{\partial v}{\partial x} - kv, \quad (3)$$

where  $k = \frac{2r}{\sigma^2}$  and the main criteria becomes  $v(x,0) = \max\{e^x - 1, 0\}$ .

Many Black-Scholes PDE for the option pricing model have been studied and solved. The semidiscretization technique was employed by Company *et al.* [23] to evaluate the computational efficiency of the Black-Scholes option pricing PDEs. They found that when incorporating transaction costs into a model of option pricing, the semidiscretization approach provides a highly accurate approximation. Song and Wang [24] explored the Black-Scholes time-fractional equation-based option pricing problems, where the fractional derivative is referred to as a modified Riemann-Liouville fractional derivative. The successful use of the finite difference method demonstrates the efficiency of this approach and the reduction in computational effort needed to solve fractional PDE. Wang [25] investigated the degenerate Black-Scholes equation, which governs option pricing by using a novel numerical strategy. The author has employed implicit temporal stepping and

fitted finite volume spatial discretization. Edeki *et al.* [26] extended the idea from the classical Differential Transformation Method (DTM) for the Black–Scholes equation to define the Projected DTM Method (PDTM) for European Option Valuation. Due to the fact that the PDTM requires less computing work than the traditional DTM and other semi-analytical approaches, it is demonstrated that it is more effective, reliable, and superior. He and Lin [27], using a new two-step solution approach, investigated the prices of European option using the stochastic volatility finite moment log-stable model. Additionally, numerical examples are provided to illustrate the efficiency and accuracy of the newly developed formula. The generalized Black-Scholes PDE, which appears in European option pricing, can be solved numerically using a method proposed by Mohammadi [28]. The author demonstrates how the numerical outcomes demonstrate the method’s effectiveness and validate the predicted behavior of the rates of convergence. Based on the idea of homotopy perturbation, the Sumudu transform, and He’s polynomials, Elbeleze *et al.* [29] investigated the fractional Black-Scholes equation and presented an interesting result. They demonstrate how effective and powerful the new approach is at locating both approximate and numerical solutions. However, to the best of our knowledge, the Black-Scholes PDE for the option pricing model using the ADM-Kamal method has not been studied in the above literature.

The key innovation and contribution of this study is the investigation of a combined approach for solving the Black-Scholes Fractional Partial Differential Equation (FPDE) for the Option Pricing Model using the Adomian Decomposition Method (ADM) and the Kamal Integral Transform (KIT).

The rest of the study is as follows. In Section 2, we briefly introduce the basic theories and theorems related to the modification and development of the ADM merging theorem with the Kamal Integral Transform. In Section 3, the combined theorem of the ADM and KIT to find a solution to the Black-Scholes FPDE for the option pricing model is discussed. Section 4 and 5 present a detailed description of the numerical experiments and concluding remarks, respectively.

## 2 Preliminaries

### 2.1 Kamal Integral Transform (KIT)

**Definition 2.1** [30] Based on the set of functions

$$S = \left\{ f(x) : \exists M, k_1, k_2 > 0, |f(x)| < M e^{\frac{|x|}{k_j}}, x \in (-1)^j \times [0, \infty) \right\},$$

the Kamal transformation of  $f$  to  $x$  is given as

$$\mathcal{G}[f(x)] = G(v) = \int_0^\infty f(x) e^{-\frac{x}{v}} dx = \lim_{b \rightarrow \infty} \int_0^b f(x) e^{-\frac{x}{v}} dx, \quad x \geq 0, k_1 \leq v \leq k_2,$$

where either the integral is unreasonably convergent or the limit value exists and is finite. The inverse transformation is given as

$$\mathcal{G}^{-1}[G(v)] = f(x) \cdot x \geq 0.$$

According to Definition 2.1, for  $f(x) = x^n$  with  $n$  being non negative integers and  $x \geq 0$ , the Kamal transformation of  $f$  is

$$\mathcal{G}[x^n] = n!v^{n+1}. \tag{4}$$

If  $\alpha \in \mathbb{R}$ , then equation (4) is rewritten as

$$\mathcal{G}[x^\alpha] = \Gamma(\alpha + 1)v^{\alpha+1}, \quad (5)$$

where  $\Gamma(x)$  denotes the gamma function. In addition, according to Definition 2.1, the Kamal transformation of the derivative of order  $n$  is re-written as

$$\mathcal{G}[f^{(n)}(x)] = \frac{G(v)}{v^n} - \sum_{k=0}^{n-1} \frac{f^{(k)}(0)}{v^{n-k-1}}.$$

**Definition 2.2** [31] The fundamental Mittag-Leffler function is represented by  $E_\alpha(z)$  for  $\alpha \in \mathbb{R}$ ,  $\text{Re}(\alpha) > 0$ , and  $\alpha \in \mathbb{C}$ , and is defined as

$$E_\alpha(z) = \sum_{k=0}^{\infty} \frac{z^k}{\Gamma(\alpha k + 1)}.$$

**Definition 2.3** [32] The Caputo fractional derivative (CFD) of  $f$  with respect to  $x$  and for order  $\alpha > 0$  is defined as

$${}^C D_x^\alpha f(x) = \frac{1}{\Gamma(n-\alpha)} \int_a^x (x-s)^{n-\alpha-1} f^{(n)}(s) ds, \quad n-1 < \alpha \leq n.$$

**Definition 2.4** [33] The Kamal transformation of the CFD is defined as

$$\mathcal{G} \left[ {}^C D_x^\alpha f(x) \right] = \frac{G(v)}{v^\alpha} - \sum_{k=0}^{n-1} \frac{f^{(k)}(0)}{v^{\alpha-k-1}}, \quad n-1 < \alpha \leq n.$$

## 2.2 The ADM-Kamal method

The fractional PDE is given as

$$\mathcal{G} D_t^\alpha w(x, t) + Nw(x, t) + Rw(x, t) = g(x, t). \quad (6)$$

The defined powerpoint is  $w(x, 0) = f(x)$ , where  $w$  is the function to be determined,  $g$  denotes the function that illustrates the homogeneity of the differential equation,  $R$  is a linear operator,  $N$  is a nonlinear operator, and  $D_t^\alpha$  is the CFD operator with  $0 < \alpha \leq 1$ , then the approximate solution of equation (6) is

$$\begin{aligned} w_0 &= f(x) + \mathcal{G}^{-1} [v^\alpha \mathcal{G} [g(x, t)]], \\ w_{n+1} &= -\mathcal{G}^{-1} [v^\alpha \mathcal{G} [A_n] + v^\alpha \mathcal{G} [Rw_n]], \quad n = 0, 1, 2, \dots, \end{aligned} \quad (7)$$

where

$$w = \lim_{k \rightarrow \infty} \sum_{n=0}^k w_n.$$

**Proof.** Equation (6) can be rewritten with  $D_t^\alpha w(x, t)$  as the subject,

$$D_t^\alpha w(x, t) = g(x, t) - Nw(x, t) - Rw(x, t). \quad (8)$$

Using the Kamal transformation in equation (8), we obtain

$$\mathcal{G}[D_t^\alpha w(x, t)] = G[g(x, t) - Nw(x, t) - Rw(x, t)],$$

where  $\alpha$  is the order of the CFD,  $n - 1 < \alpha \leq n, n \in \mathbb{Z}^+$ .

$$\frac{w(x, v)}{v^\alpha} - \sum_{k=0}^{n-1} \frac{w^{(k)}(x, 0)}{v^{\alpha-k-1}} = \mathcal{G}[g(x, t)] + \mathcal{G}[Nw(x, t)] + \mathcal{G}[Rw(x, t)].$$

For  $0 < \alpha \leq 1$  such that  $k = 0$ , it becomes

$$\begin{aligned} \frac{w(x, v)}{v^\alpha} - \frac{w(x, 0)}{v^{\alpha-1}} &= \mathcal{G}[g(x, t)] - \mathcal{G}[Nw(x)] + \mathcal{G}[Rw(x)], \\ w(x, v) - vw(x, 0) &= v^\alpha \mathcal{G}[g(x, t)] - v^\alpha \mathcal{G}[Nw(x, t)] + v^\alpha \mathcal{G}[Rw(x, t)], \\ w(x, v) &= vw(x, 0) + v^\alpha \mathcal{G}[g(x, t)] - v^\alpha \mathcal{G}[Nw(x, t)] - v^\alpha \mathcal{G}[Rw(x, t)]. \end{aligned} \tag{9}$$

We use the inverse Kamal transformation in equation (9) to obtain

$$w(x, t) = w(x, 0) + \mathcal{G}^{-1}[v^\alpha \mathcal{G}[g(x, t)]] - \mathcal{G}^{-1}[v^\alpha \mathcal{G}[Nw(x, t)]] - \mathcal{G}^{-1}[v^\alpha \mathcal{G}[Rw(x, t)]] \tag{10}$$

The ADM presumes that the function  $w$  can be broken down into an infinite series

$$w = \sum_{n=0}^{\infty} w_n, \tag{11}$$

where  $w_n$  is recursively determinable. Additionally, this approach presupposes that the infinite polynomial series may decompose the nonlinear operator  $Nw$ :

$$Nw = \sum_{n=0}^{\infty} A_n, \tag{12}$$

where  $A_n = A_n(w_0, w_1, w_2, \dots, w_n)$  is the defined Adomian polynomial (AP)

$$A_n(w_0, w_1, w_2, \dots, w_n) = \frac{1}{n!} \frac{d^n}{d\lambda^n} \left[ N \left( \sum_{k=0}^n \lambda^k w_k \right) \right]_{\lambda=0}; \quad n \geq 0.$$

With  $\lambda$  denoting a parameter, the AP  $A_n$  can be parsed as

$$\begin{aligned} A_0 &= \frac{1}{0!} \frac{d^0}{d\lambda^0} \left[ N \left( \sum_{k=0}^0 \lambda^k w_k \right) \right]_{\lambda=0} = N(w_0), \\ A_1 &= \frac{1}{1!} \frac{d^1}{d\lambda^1} \left[ N \left( \sum_{k=0}^1 \lambda^k w_k \right) \right]_{\lambda=0} = w_1 N'(w_0), \\ A_2 &= \frac{1}{2!} \frac{d^2}{d\lambda^2} \left[ N \left( \sum_{k=0}^2 \lambda^k w_k \right) \right]_{\lambda=0} = \frac{w_1^2}{2!} N''(w_0) + w_2 N'(w_0), \\ &\vdots \end{aligned}$$

We substitute the initial conditions, equations (11) and (12) into equation (10):

$$\sum_{n=0}^{\infty} w_n = f(x) + \mathcal{G}^{-1}[v^\alpha \mathcal{G}[g(x, t)]] - \mathcal{G}^{-1} \left[ v^\alpha \mathcal{G} \left[ \sum_{n=0}^{\infty} A_n \right] + v^\alpha \mathcal{G} \left[ R \sum_{n=0}^{\infty} w_n \right] \right]. \tag{13}$$

Describing both sides of (13) gives

$$\begin{aligned} w_0 &= f(x) + \mathcal{G}^{-1} [v^\alpha \mathcal{G} [g(x, t)]], \\ w_1 &= -\mathcal{G}^{-1} [v^\alpha \mathcal{G} [A_0] + v^\alpha \mathcal{G} [Rw_0]], \\ w_2 &= -\mathcal{G}^{-1} [v^\alpha \mathcal{G} [A_1] + v^\alpha \mathcal{G} [Rw_1]], \\ w_3 &= -\mathcal{G}^{-1} [v^\alpha \mathcal{G} [A_2] + v^\alpha \mathcal{G} [Rw_2]]. \\ &\vdots \end{aligned}$$

The iterative relation derived from the approximate solution to FPDE (6) is generally defined as

$$\begin{aligned} w_0 &= f(x) + \mathcal{G}^{-1} [v^\alpha \mathcal{G} [g(x, t)]], \\ w_{n+1} &= -\mathcal{G}^{-1} [v^\alpha \mathcal{G} [A_n] + v^\alpha \mathcal{G} [Rw_n]], n = 0, 1, 2, \dots, \end{aligned} \quad (14)$$

where

$$w = \lim_{k \rightarrow \infty} \sum_{n=0}^k w_n.$$

### 3 Mean Absolute Error (MAE)

The method that can be used to measure the accuracy of the model in this study is the Mean Absolute Error (MAE). The MAE value represents the average error/error/absolute error between the calculation results/estimated model and the actual value [34]. The MAE formula is defined as

$$MAE = \frac{1}{n} \sum_{i=1}^n |\hat{y}_i - y_i|, \quad (15)$$

where  $n$  is the number of data,  $\hat{y}_i$  is the approximate value, and  $y_i$  is the actual value.

### 4 Solution of the Black-Scholes FPDE for the Option Pricing Model Using the Combined ADM-Kamal Method

This study analyzed the performance of the Black-Scholes FPDE via the combined ADM-Kamal method. The Black-Scholes FPDE defined below follows from (3):

$$\frac{\partial^\alpha v(x, \tau)}{\partial \tau^\alpha} = \frac{\partial^2 v(x, \tau)}{\partial x^2} + (k-1) \frac{\partial v(x, \tau)}{\partial x} - kv(x, \tau), \quad (16)$$

where  $0 < \alpha \leq 1$  and  $v(x, 0) = \max\{e^x - 1, 0\}$  represents the initial condition.

Based on the defined algorithm of the Black-Scholes fractional partial differential equation with the combined ADM-Kamal method, equation (16) can be rewritten as

$$D_\tau^\alpha v(x, \tau) = Rv(x, \tau), \quad (17)$$

where  $Rv = \frac{\partial^2 v}{\partial x^2} + (k-1) \frac{\partial v}{\partial x} - kv$  is a linear operator.

Based on the solution in the form of a recursive relation in equation (14), the solution of equation (17) is

$$v_0 = \max \{e^x - 1, 0\},$$

$$v_{n+1} = \mathcal{G}^{-1} [v^\alpha \mathcal{G} [Rv_n]], \quad n = 0, 1, 2, \dots$$

If the iterative solution is explained, then based on equation (5) and the inverse Kamal transformation, we obtain

$$\begin{aligned} v_1 &= \mathcal{G}^{-1} [v^\alpha \mathcal{G} [Rv_0]] \\ &= \mathcal{G}^{-1} \left[ v^\alpha \mathcal{G} \left[ \frac{\partial^2 v_0}{\partial x^2} + (k - 1) \frac{\partial v_0}{\partial x} - kv_0 \right] \right] \\ &= \mathcal{G}^{-1} [v^\alpha \mathcal{G} [k \max \{e^x, 0\} - k \max \{e^x - 1, 0\}]] \\ &= \mathcal{G}^{-1} [v^{\alpha+1} (k \max \{e^x, 0\} - k \max \{e^x - 1, 0\})] \\ &= \frac{\tau^\alpha}{\Gamma(\alpha + 1)} (k \max \{e^x, 0\} - k \max \{e^x - 1, 0\}). \end{aligned}$$

If  $\frac{\partial v_1}{\partial x} = \frac{\tau^\alpha}{\Gamma(\alpha+1)} (k \max \{e^x, 0\} - k \max \{e^x, 0\}) = 0$ , we get

$$v_1 = \frac{\tau^{3\alpha}}{\Gamma(3\alpha + 1)} (k^3 \max \{e^x, 0\} - k^3 \max \{e^x - 1, 0\}).$$

Therefore, the approximation solution of the Black-Scholes fractional partial differential equation (16) is obtained as follows:

$$v(x, \tau) = \sum_{n=0}^{\infty} v_n = \max \{e^x - 1, 0\} E_\alpha(-k\tau^\alpha) + \max \{e^x, 0\} (1 - E_\alpha(-k\tau^\alpha)), \quad (18)$$

where  $E_\alpha(z)$  is a one-parameter Mittag-Leffler function. Based on Definition 2.2, for  $\alpha = 1$ , equation (18) can be written as

$$v(x, \tau) = \max \{e^x - 1, 0\} e^{-k\tau} + \max \{e^x, 0\} (1 - e^{-k\tau}). \quad (19)$$

It is obvious that the solution of (19) is similar to the approximate solution of the classical Black-Scholes PDE for order  $\alpha = 1$ , by using the Sumudu decomposition method. Furthermore, the Black-Scholes PDE defined in (3) has the following exact solution:

$$v(x, \tau) = e^x N(d_1) - e^{-k\tau} N(d_2), \quad (20)$$

where

$$d_1 = \frac{x}{\sqrt{2\tau}} + \frac{1}{2} (k + 1) \sqrt{2\tau}, \quad d_2 = d_1 - \sqrt{2\tau}, \quad k = \frac{2r}{\sigma^2},$$

and  $N(d)$  is the cumulative distribution function.

### 5 Numerical Simulation

This section investigates the solution by the Black-Scholes PDE approach based on the combined ADM-Kamal method. Table 1 shows the numerical comparison of the Black-Scholes PDE solution defined in equation (19) for  $\alpha = 1$  with the exact solution (equation (20)), for  $k = 0.75$ , and the magnitude of the error.

$x$	$\tau$	Approach Solution	Exact Solution	Error
-0.50	0.50	0.189669	0.082462	0.107207
-0.40	1.00	0.353683	0.353395	0.000288
-0.30	1.50	0.500310	0.539833	0.039523
-0.20	2.00	0.636047	0.688686	0.052639
-0.10	2.50	0.766076	0.819751	0.053675
0.00	3.00	0.894601	0.943932	0.049331
0.10	3.50	1.032731	1.068042	0.035311
0.20	4.00	1.171616	1.196726	0.025110
0.30	4.50	1.315641	1.333412	0.017771
0.40	5.00	1.468307	1.480838	0.012531
0.50	5.50	1.632558	1.641369	0.008811

**Table 1:** Comparison of the numerical solution of the Black-Scholes PDE with the exact solution.

The example of Table 1 with a caption is given below.

Based on the numerical simulations presented in Table 1, the results of the comparison of the Black-Scholes PDE solution with the exact solution using equation (15) is 3.66%.

Referring to equation (2), then we get

$$x = \ln \left( \frac{S}{E} \right) \tau = \frac{\sigma^2}{2} (T - t) v(x\tau) = \frac{C(S,t)}{E} k = \frac{2r}{\sigma^2},$$

where  $T$  denotes the time or maturity date,  $r$  is the risk-free interest rate,  $E$  is the exercise price,  $\sigma$  is the volatility of the asset price,  $t$  is the time, and  $S$  is the price of the asset. Based on (18), the price model for the call option  $C$  of fractional order is

$$C(S,t) = \max\{S - E, 0\} E_\alpha(\zeta) + \max\{S, 0\} (1 - E_\alpha(\zeta)), \quad (21)$$

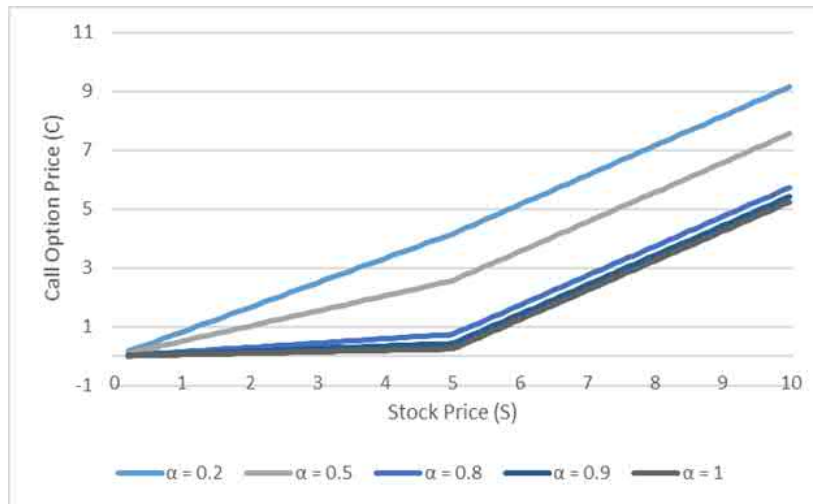
where  $\zeta = -\frac{2^{2-\alpha} r}{\sigma^2 - 2\alpha} (T - t)^\alpha$ . Next, the formula for the price of the put option  $P$  of fractional order, which is based on the put-call parity formula, is given as

$$P(S,t) = \max\{S - E, 0\} E_\alpha(\zeta) + \max\{S, 0\} (1 - E_\alpha(\zeta)) + Ee^{-r(T-t)} - S. \quad (22)$$

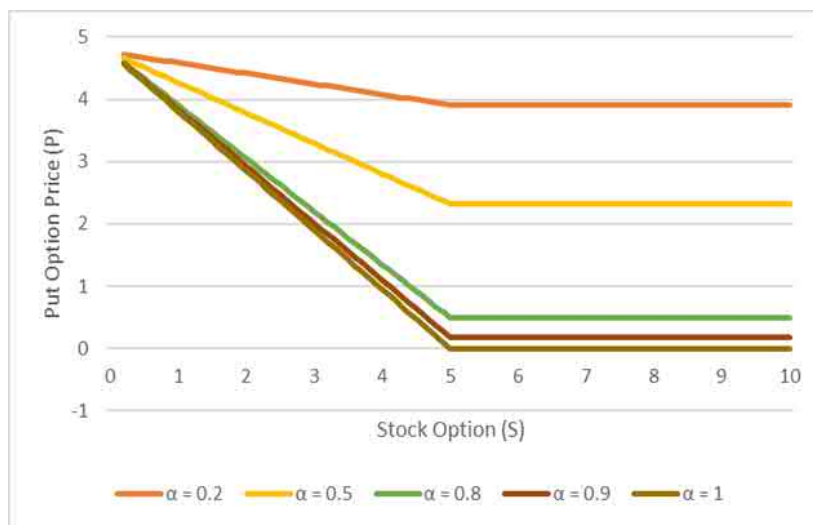
Suppose the stock price is represented by the price of asset  $S$  in this study. Figure 1 shows the call option price  $C(S,t)$  against the stock price  $S$  of the Black-Scholes partial differential equation solution based on the combined ADM-Kamal method, with dissimilar values of  $\alpha$ , where the exercise price is  $E = 5$  and the risk-free interest rate (RIR) is  $r = 5\%$  for a one-year option contract.

Figure 2 shows the put option price  $P(S,t)$  against the stock price variable  $S$  from the Black-Scholes PDE solution based on the combined ADM-Kamal method with dissimilar values of  $\alpha$ , where the exercise price is  $E = 5$  and the RIR is  $r = 5\%$  for a one-year contract.

We fix  $\alpha = \{0.2, 0.5, 0.8, 0.9, 1\}$ . In Fig. 1, an increase in  $\alpha$  value will lower the call option price. Meanwhile, in Fig.2, an increase in alpha value will lower the put option price. We have calculated the price of the call option  $C$  in equation (21) which is



**Figure 1:** The price  $C(S,t)$  with a fractional order of  $\alpha$  against the stock price  $S$ .



**Figure 2:** The price  $P(S,t)$  with a fractional order of  $\alpha$  against the stock price  $S$ .

simplified to

$$\begin{aligned}
 C(S,t) &= \max\{S - E, 0\}E_\alpha(\zeta) + \max\{S, 0\}(1 - E_\alpha(\zeta)) \\
 &= (S - E)E_\alpha(\zeta) + S(1 - E_\alpha(\zeta)) \\
 &= SE_\alpha(\zeta) - EE_\alpha(\zeta) + S - SE_\alpha(\zeta) \\
 &= S - EE_\alpha(\zeta).
 \end{aligned}
 \tag{23}$$

Meanwhile, for the put option price  $P$ , the equation (22) becomes

$$\begin{aligned}
 P(S,t) &= \max\{S - E, 0\}E_\alpha(\zeta) + \max\{S, 0\}(1 - E_\alpha(\zeta)) + Ee^{-r(T-t)} - S \\
 &= (S - E)E_\alpha(\zeta) + S(1 - E_\alpha(\zeta)) + Ee^{-r(T-t)} - S \\
 &= SE_\alpha(\zeta) - EE_\alpha(\zeta) + S - SE_\alpha(\zeta) + Ee^{-r(T-t)} - S \\
 &= E\left(e^{-r(T-t)} - E_\alpha(\zeta)\right).
 \end{aligned} \tag{24}$$

The price of  $P(S,t)$  for the stock price is higher than the exercise price ( $S > E$ ) and is not affected by the stock price  $S$ . However, it is only affected by the exercise price  $E$ ,  $e^{-r(T-t)}$  and  $\zeta$  is constant. Also, if  $S > E$ , then the price of the put option tends to be constant, regardless of the stock price.

To calculate the price of the call option  $C$ , if the share price is less than or equal to the exercise price ( $S \leq E$ ), we obtained

$$C(S,t) = \max\{S - E, 0\}E_\alpha(\zeta) + \max\{S, 0\}(1 - E_\alpha(\zeta)) = S(1 - E_\alpha(\zeta)). \tag{25}$$

The call option price for the stock price is less than or equal to the exercise price ( $S \leq E$ ) and is not affected by the exercise price  $E$ , but only influenced by the stock prices  $S$  and  $\zeta$  is constant.

Meanwhile, we get

$$\begin{aligned}
 P(S,t) &= \max\{S - E, 0\}E_\alpha(\zeta) + \max\{S, 0\}(1 - E_\alpha(\zeta)) + Ee^{-r(T-t)} - S \\
 &= S(1 - E_\alpha(\zeta)) + Ee^{-r(T-t)} - S \\
 &= S - SE_\alpha(\zeta) + Ee^{-r(T-t)} - S \\
 &= Ee^{-r(T-t)} - SE_\alpha(\zeta).
 \end{aligned} \tag{26}$$

Then, with using Definition 2.2, for  $\alpha = 1$ , equations (21) and (22) become

$$C(S,t) = \max\{S - E, 0\}e^{-r(T-t)} + \max\{S, 0\}\left(1 - e^{-r(T-t)}\right), \tag{27}$$

and

$$C(S,t) = SN(d_1) - Ee^{-r(T-t)}N(d_2). \tag{28}$$

Based on equations (27) and (28), it can be seen that the determination of the price of buy and sell options, respectively, using the Black-Scholes model with a fractional order for  $\alpha = 1$  is not affected by the stock price volatility because there is no parameter. Equations (27) and (28) are equivalent to the formula for the call and put option prices obtained from the results of the classical Black-Scholes equation (not fractional order) via the method of the Adomian-Laplace decomposition [35].

Based on equation (20), thus obtained the classical Black-Scholes model (CBLM) for the call option price is as follows:

$$P(S,t) = \max\{S - E, 0\}e^{-r(T-t)} + \max\{S, 0\}\left(1 - e^{-r(T-t)}\right) + Ee^{-r(T-t)} - S. \tag{29}$$

$$d_1 = \frac{\ln\left(\frac{S}{E}\right) + \left(r + \frac{\sigma^2}{2}\right)(T-t)}{\sigma\sqrt{T-t}}, d_2 = d_1 - \sigma\sqrt{T-t}.$$

Furthermore, we use the put-call parity formula, which is  $S + P - C = Ee^{-r(T-t)}$ , and the identity formula for the cumulative distribution function for the normal distribution, which is  $N(d) + N(-d) = 1$ . So, the CBLM is obtained for the put option price as follows:

$$P(S,t) = Ee^{-r(T-t)}N(-d_2) - SN(-d_1), \tag{30}$$

where  $\sigma$  is the volatility of the stock price,  $r$  is the risk-free interest rate,  $E$  is the exercise price,  $S$  is the stock price, and  $T$  is the expiration date of the option contract.

Figure 3 shows the  $C(S,t)$  against the stock price  $S$  of the Black-Scholes model with a fractional order for  $\alpha = 1$  (see equation (27)) compared to the classical Black-Scholes model (see equation (29)), where the exercise price  $E = 5$  and the interest rate  $r = 5\%$  for a one-year option contract.

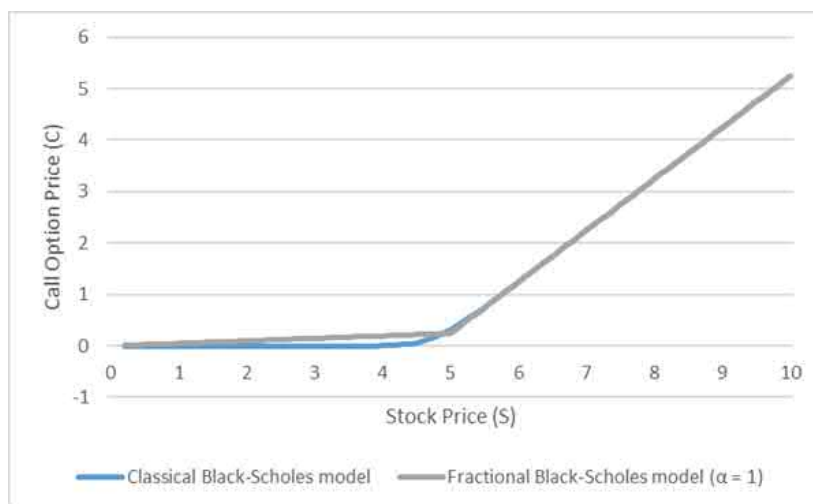


**Figure 3:** Comparison of the fractional order Black-Scholes model for  $\alpha = 1$  with the classical Black-Scholes model for call option prices over a one-year period.

Furthermore, Figure 4 shows the  $P(S,t)$  against the stock price  $S$  of the Black-Scholes model with a fractional order for  $\alpha = 1$  (see equation (28)) compared to the classical Black-Scholes model (see equation (30)), where the exercise price  $E = 5$  and the interest rate  $r = 5\%$  for a one-year option contract.

Based on the numerical simulation presented in Figure 3, the comparison of the fractional Black-Scholes model for  $\alpha = 1$  with the classical Black-Scholes model for call options prices over a one-year period is 7.80%. Meanwhile, in Figure 4, the comparison of the Black-Scholes model with a fractional order for  $\alpha = 1$  with the CBSM for put option prices over a one-year period is 7.80%.

For the stock price higher than the exercise price ( $S > E$ ), the Black-Scholes model has a fractional order with  $\alpha = 1$  and the calculation of the call option price  $C$  in

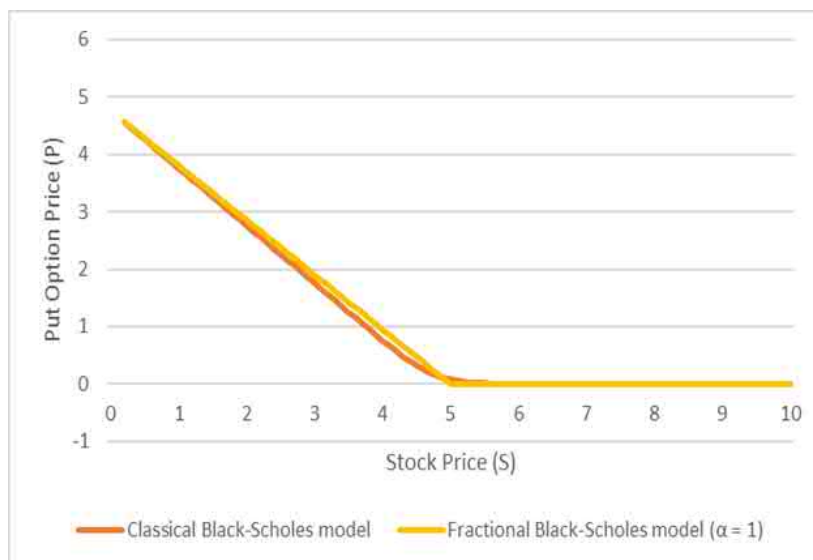


**Figure 4:** Comparison of the fractional order Black-Scholes model for  $\alpha = 1$  with the classic Black-Scholes model for put option prices over a one-year period.

equation (27) can be simplified to

$$\begin{aligned}
 C(S,t) &= \max\{S - E, 0\}e^{-r(T-t)} + \max\{S, 0\} \left(1 - e^{-r(T-t)}\right) \\
 &= (S - E)e^{-r(T-t)} + S \left(1 - e^{-r(T-t)}\right) \\
 &= Se^{-r(T-t)} - Ee^{-r(T-t)} + S - Se^{-r(T-t)} \\
 &= S - Ee^{-r(T-t)}.
 \end{aligned} \tag{31}$$

Meanwhile, for the put option price  $P$ , equation (28) becomes

$$\begin{aligned}
 P(S,t) &= \max\{S - E, 0\}e^{-r(T-t)} + \max\{S, 0\} \left(1 - e^{-r(T-t)}\right) + Ee^{-r(T-t)} - S \\
 &= (S - E)e^{-r(T-t)} + S \left(1 - e^{-r(T-t)}\right) + Ee^{-r(T-t)} - S \\
 &= Se^{-r(T-t)} - Ee^{-r(T-t)} + S - Se^{-r(T-t)} + Ee^{-r(T-t)} - S \\
 &= 0.
 \end{aligned} \tag{32}$$

If the stock price is higher than the exercise price ( $S > E$ ), then the put price  $P$  is equal to 0. This is in accordance with the illustration of the numerical simulation in Figure 4. For the stock price less than or equal to the exercise price ( $S \leq E$ ) and the Black-Scholes model of fractional order with  $\alpha = 1$ , the calculation of the call option price can be simplified to

$$C(S,t) = \max\{S - E, 0\}e^{-r(T-t)} + \max\{S, 0\} \left(1 - e^{-r(T-t)}\right) = S \left(1 - e^{-r(T-t)}\right). \tag{33}$$

The call option price for the stock price less than or equal to the exercise price ( $S \leq E$ ) is not affected by the exercise price  $E$ , only influenced by the stock price  $S$  and  $e^{-r(T-t)}$  which are constant.

Meanwhile, we get

$$\begin{aligned} P(S,t) &= \max\{S - E, 0\}e^{-r(T-t)} + \max\{S, 0\} \left(1 - e^{-r(T-t)}\right) + Ee^{-r(T-t)} - S \\ &= S \left(1 - e^{-r(T-t)}\right) + Ee^{-r(T-t)} - S \\ &= (E - S)e^{-r(T-t)}. \end{aligned} \quad (34)$$

The price of put options for the stock prices less than or equal to the exercise price ( $S \leq E$ ) is affected by the difference between the exercise price and the stock price ( $E - S$ ) and  $e^{-r(T-t)}$  which is constant.

Next, suppose  $T = t$ , the option transaction is exercised at maturity, thus equations (27) and (28) become

$$C(S, T) = \max\{S - E, 0\}, \quad (35)$$

and

$$P(S, T) = \max\{S - E, 0\} + E - S. \quad (36)$$

Equations (35) and (36) are equivalent to the payoff obtained from buying call and put options without taking into account the premium.

## 6 Conclusion

The main finding of this study is the investigation of a combined approach for solving the Black-Scholes Fractional Partial Differential Equation (FPDE) for the Option Pricing Model using the Adomian Decomposition Method (ADM) and the Kamal Integral Transform (KIT). In conclusion, the ADM-Kamal method is a very effective and powerful way to obtain both approximate and numerical solutions.

## Acknowledgment

The authors would like to thank the Rector of Universitas Padjadjaran for the financial support through Research of Universitas Padjadjaran 2023.

## References

- [1] L. Zeng. Analysing the high-tech industry with a multivariable grey forecasting model based on fractional order accumulation. *Kybernetes* **48** (6) (2018) 1158–1174.
- [2] A. Jegatheesh and C. A. Kumar. Novel fuzzy fractional order PID controller for nonlinear interacting coupled spherical tank system for level process. *Microprocessors and Microsystems* **72** (102948) (2002).
- [3] B. Guo, A. Raza, K. Al-Khaled, S. U. Khan, S. Farid, Y. Wang, and S. Saleem. Fractional-order simulations for heat and mass transfer analysis confined by elliptic inclined plate with slip effects: A comparative fractional analysis. *Case Studies in Thermal Engineering* **28** (101359) (2021).
- [4] N. HariPriya, P. Kavitha, S. Srinivasan, and J. Belikov. Evolutionary optimisation-based fractional order controller for web transport systems in process industries. *International Journal of Advanced Intelligence Paradigms* **12** (3-4) (2019) 317–330.

- [5] A. Sambas, S. Vaidyanathan, X. Zhang, I. Koyuncu, T. Bonny, M. Tuna, I. M. Sulaiman, and P. Kumam. A Novel 3D Chaotic System with Line Equilibrium: Multistability, Integral Sliding Mode Control, Electronic Circuit, FPGA Implementation and Its Image Encryption. *IEEE Access* **10** (2022) 68057–68074.
- [6] A. Sambas, S. Vaidyanathan, E. Tlelo-Cuautle, B. Abd-El-Atty, A. A. Abd El-Latif, O. Guillen-Fernandez, Sukono, H. Yuyun, G. Gundara. A 3-D multi-stable system with a peanut-shaped equilibrium curve: Circuit design, FPGA realization, and an application to image encryption. *IEEE Access* **8** (2022) 137116–137132.
- [7] N. Nikdel, M. Badamchizadeh, V. Azimirad, and M. A. Nazari. Fractional-order adaptive backstepping control of robotic ma-nipulators in the presence of model uncertainties and external disturbances. *IEEE Transactions on Industrial Eelctronics* **63** (10) (2016) 6249–6256.
- [8] A. Morsli, A. Tlemcani, and H. Nouri. Control of a Shunt Active Power Filter by the Synchronous Referential Method Connected with a Photovoltaic Solar Energy. *Nonlinear Dynamics and Systems Theory* **22** (4) (2022) 424–431.
- [9] Y. Hu, X. Ma, W. Li, W. Wu, and D. Tu. Forecasting manufacturing industrial natural gas consumption of China using a novel time-delayed fractional grey model with multiple fractional order. *Computational and Applied Mathematics* **39** (4) (2020) 1–30.
- [10] A. Sambas, S. Vaidyanathan, T. Bonny, S. Zhang, T. Hidayat, G. Gundara, and M. Mamat. Mathematical model and FPGA realiza-tion of a multi-stable chaotic dynamical system with a closed butterfly-like curve of equilibrium points. *Applied Sciences* **11** (2) (2021) 788.
- [11] M. labid, and N. Hamri. Chaos Synchronization between Fractional-Order Lesser Date Moth Chaotic System and Integer-Order Chaotic System via Active Control. *Nonlinear Dynamics and Systems Theory* **2** (4) (2022) 407–413.
- [12] H. Delavari and H. Heydarinejad. Adaptive fractional order Backstepping sliding mode controller design for a magnetic levita-tion system. *Modares Mechanical Engineering* **17** (3) (2017) 187–195.
- [13] D. Dong and M. Deng. GPU Based Modelling and Analysis for Parallel Fractional Order Derivative Model of the Spiral-Plate Heat Exchanger. *Axioms* **10** (4) (2021) 344.
- [14] Y. Xie, Z. Wang, nad B. Meng. Stability and bifurcation of a delayed time-fractional order business cycle model with a general liquidity preference function and investment function. *Mathematics* **7** (9) (2019) 846.
- [15] J. Ma and W. Ren. Complexity and Hopf bifurcation analysis on a kind of fractional-order IS-LM macroeconomic system. *In-ternational Journal of Bifurcation and Chaos* **26** (11) (2016) 1650181.
- [16] Sukono, A. Sambas, S. He, H. Liu, S. Vaidyanathan, Y. Hidayat, and J. Saputra. Dynamical analysis and adaptive fuzzy control for the fractional-order financial risk chaotic system. *Advances in Difference Equations* **2020** (674) (2020).
- [17] B. Subartini, S. Vaidyanathan, A. Sambas, and S. Zhang. Multistability in the Finance Chaotic System, Its Bifurcation Analysis and Global Chaos Synchronization via Integral Sliding Mode Control. *IAENG International Journal of Applied Mathematics* **51** (4) (2021) 995–1002.
- [18] M. D. Johansyah, A. K. Supriatna, E. Rusyaman, and J. Saputra. Solving the Economic Growth Acceleration Model with Memory Effects: An Application of Combined Theorem of Adomian Decomposition Methods and Kashuri–Fundo Transformation Methods. *Symmetry* **14** (2) (2022) 192.
- [19] M. D. Johansyah, A. K. Supriatna, E. Rusyaman, and J. Saputra. The Existence and Uniqueness of Riccati Fractional Differential Equation Solution and Its Approximation Applied to an Economic Growth Model. *Mathematics* **10** (17) (2022) 3029.

- [20] P. Veerasha and D. Kumar. Analysis and dynamics of the Ivancevic option pricing model with a novel fractional calculus approach. *Waves in Random and Complex Media* (2022) 1-18, 2022.
- [21] F. Black and M. Scholes. The pricing of options and corporate liabilities. *Journal of political economy* **81** (3) (1973) 637–654.
- [22] V. Gulkac. The homotopy perturbation method for the Black–Scholes equation. *Journal of Statistical Computation and Simulation* **80** (12) (2010) 1349–1354.
- [23] R. Company, E. Navarro, J.R. Pintos, and E. Ponsoda. Numerical solution of linear and nonlinear Black-Scholes option pricing equations. *Computers & Mathematics with Applications* **56** (3) (2008) 813-821.
- [24] L. Song and W. Wang. Solution of the fractional Black-Scholes option pricing model by finite difference method. *Abstract and applied analysis* **2013** (194286) (2013).
- [25] S. Wang. A novel fitted finite volume method for the Black–Scholes equation governing option pricing. *IMA Journal of Numerical Analysis* **24** (4) (2004) 699-720.
- [26] S. O. Edeki, O. O. Ugbebor, and E. A. Owoloko. Analytical solutions of the Black–Scholes pricing model for European option valuation via a projected differential transformation method. *Entropy* **17** (11) (2015) 7510–7521.
- [27] X. J. He and S. Lin. A fractional Black-Scholes model with stochastic volatility and European option pricing. *Expert Systems with Applications* **178** (114983) (2021).
- [28] R. Mohammadi. Quintic B-spline collocation approach for solving generalized Black–Scholes equation governing option pricing. *Computers & Mathematics with Applications* **69** (8) (2015) 777–797.
- [29] A. A. Elbeleze, A. Kilicman, and B. M. Taib. Homotopy perturbation method for fractional Black-Scholes European option pricing equations using Sumudu transform. *Mathematical problems in engineering* **2013** (524852) (2013).
- [30] A. Kamal and H. Sedeeq. The new integral transform Kamal Transform. *Advances in Theoretical and Applied Mathematics* **11** (4) (2016) 451–458.
- [31] L. Debnath. A brief historical introduction to fractional calculus. *International Journal of Mathematical Education in Science and Technology* **35** (4) (2004) 487–501.
- [32] J. D. Ramírez and A. S. Vatsala. Generalized monotone iterative technique for Caputo fractional differential equation with periodic boundary condition via initial value problem. *International Journal of Differential Equations* **2012** (842813) (2012).
- [33] M. A. Hussein. A Review on Integral Transforms of Fractional Integral and Derivative. *International Academic Journal of Science and Engineering* **9** (2022) 52–56.
- [34] T. Chai and R.R. Draxler. Root mean square error (RMSE) or mean absolute error (MAE)?—Arguments against avoiding RMSE in the literature. *Geoscientific model development* **7** (3) (2014) 1247–1250.
- [35] I. Sumiati, E. Rusyaman, Sukono. Black-Scholes Equation Solution Using Laplace-Adomian Decomposition Method. *IAENG International Journal of Computer Science* **46** (4) (2019) 1–6.



# A Novel Adaptive Method Based on New Minorant-Majorant Functions Without Line Search for Semidefinite Optimization

S. Leulmi<sup>1\*</sup> and A. Leulmi<sup>2</sup>

<sup>1</sup> *Department of Mathematics, 20 August 1955, Skikda, Algeria.*

<sup>2</sup> *Ferhat Abbas University of Setif-1, Algeria.*

Received: April 1, 2023; Revised: June 25, 2023

**Abstract:** A novel robust adaptive method, to solve a semidefinite programming (SDP) problem, is proposed in this study. We are interested in computation of the direction by Newton's method and of the displacement step using minorant-majorant functions instead of line search methods in order to reduce the computation cost. Our new approach is even more beneficial than classical line search methods. We created a MATLAB implementation and ran numerical tests on various sizable instances to validate it. The numerical data gained demonstrate the correctness and effectiveness of our strategy, and are presented in the last section of this paper.

**Keywords:** *semidefinite optimization, interior point methods, perturbations minorant-majorant functions, general perturbation schemes, line search.*

**Mathematics Subject Classification (2010):** 90C22, 90C05, 90C51, 70K60, 93C73.

## 1 Introduction

In the last twenty years, Semidefinite Programming (SDP) has evolved as the most exciting and active research area in optimization. Combinatorial optimization, control theory, and conventional convex constrained optimization are only a few of the many disciplines in which SDP has applications. SDP problems arise in several areas of applications such as economic, social, public planning and nonlinear dynamics and systems (see [2, 18]). Most of these applications can often be solved pretty efficiently both in theory and in reality since SDP is solvable through interior-point methods.

---

\* Corresponding author: <mailto:leulsou@yahoo.fr>

Interior point methods were developed in the sixties by Dikin and Fiacco–McCormick [7], to solve nonlinear mathematical programs with large dimension.

In order to solve the SDP problems, several algorithms have been proposed. Nesterov and Nemirovski [16] and Alizadeh [1] are the researchers who developed interior-point methods (IPMs) for SDP.

To solve SDP, a number of approaches have been put forth, including projective IPMs and their variants [10, 14], central trajectory methods [19], logarithmic barrier methods [5].

The determination and calculation of the displacement step provide an obstacle to establishing an iteration. Unfortunately, computing the displacement step is expensive and difficult in the case of semidefinite problems (particularly when using line search methods [12]).

In this paper, we are interested in solving SDP using a barrier logarithmic method that is simple and effective and is based on new approximate functions (new minorant and new majorant functions). These approximate functions allow the computation of the displacement step easily and quickly, and are more efficient than classical line searches.

We focus on the following SDP problem:

$$\begin{cases} \min b^T x \\ \sum_{i=1}^m x_i A_i - C \in S_n^+, \\ x \in \mathbb{R}^m, \end{cases} \quad (1)$$

where  $b \in \mathbb{R}^m$ , the matrices  $C, A_i$ , with  $i = 1, \dots, m$ , are the given symmetrical matrices and  $S_n^+$  designs the cone of the symmetrical semidefinite positive  $n \times n$  matrix.

The problem (1) is the dual of the following SDP problem:

$$\begin{cases} \max \langle C, Y \rangle \\ \langle A_i, Y \rangle = b_i, \forall i = 1, \dots, m, \\ Y \in S_n^+. \end{cases} \quad (2)$$

Recall that  $\langle \cdot, \cdot \rangle$  corresponds to an inner product on the space of  $n \times n$  matrices, where the trace of the matrix  $(C^T Y)$  is denoted by  $\langle C, Y \rangle$ .

Their feasible sets involving a non polyhedral convex cone, of positive semidefinite matrices, are called linear semidefinite programs. A priori, one of the advantages of the problem (1) with respect to its dual problem (2) is that the variable of the objective function is a vector instead of being a matrix in the problem (2). Furthermore, under certain convenient hypothesis, the resolution of the problem (1) is equivalent to that of the problem (2) in the sense that the optimal solution of one of the two problems can be reduced directly from the other through the application of the theorem on complementary slackness, see for instance [1, 8, 15].

The problem (1) is approximated by the following perturbed problem  $(SDP)_\eta$  :

$$\begin{cases} \min f_\eta(x) \\ x \in \mathbb{R}^m \end{cases} \quad (SDP)_\eta$$

with the penalty parameter  $\eta > 0$  and  $f_\eta : \mathbb{R}^m \rightarrow ]-\infty, +\infty]$  being the barrier function defined by

$$f_\eta(x) = \begin{cases} b^T x + n\eta \ln \eta - \eta \ln[\det(\sum_{i=1}^m x_i A_i - C)] & \text{if } x \in \widehat{X}, \\ +\infty & \text{if not.} \end{cases}$$

The problem  $(SDP)_\eta$  can be solved via a classical Newton descent method.

The difficulty in line search is the presence of the determinant in the definition of the logarithmic barrier function which leads to a very high cost in the classical exact or approximate procedures of line search. In our approach, instead of minimizing  $f_\eta$ , along the descent direction at a current point  $x$ , we propose the minorant  $\check{G}$  and majorant  $\tilde{G}$  functions for which the optimal solution of the displacement step  $\alpha$  is obtained explicitly.

Let us minimize the function  $G$  so that

$$\begin{aligned} \frac{1}{\eta}[f_\eta(x + \alpha d) - f_\eta(x)] &= G(\alpha) \geq \check{G}(\alpha), \quad \forall \alpha > 0, \\ \frac{1}{\eta}[f_\eta(x + \alpha d) - f_\eta(x)] &= G(\alpha) \leq \tilde{G}(\alpha), \quad \forall \alpha > 0, \end{aligned}$$

with  $G(0) = \check{G}(0) = 0$ ,  $G'(0) = \check{G}'(0) < 0$  and  $G(0) = \tilde{G}(0) = 0$ ,  $G'(0) = \tilde{G}'(0) < 0$ .

The criterion  $G'''(0) = \check{G}'''(0)$  and  $G'''(0) = \tilde{G}'''(0)$  guarantees that the approximations  $\check{G}$  and  $\tilde{G}$  of  $G$  are of the highest quality.

This novel strategy's key idea is to present a unique method for computing the displacement step based on minorant-majorant functions. In contrast to the conventional methods of line search, we then achieve an explicit approximation that reduces the objective and is both inexpensive and reliable.

The main advantage of  $(SDP)_\eta$  resides in the strict convexity of its objective function and convexity of its feasible domain. As a result, the prerequisites for optimality are both necessary and sufficient. This encourages theoretical and numerical research of the problem.

Six sections make up the remainder of this paper. In Section 2, we briefly recall some results in linear semidefinite programming and give some preliminary results. The convergence findings of the perturbed problem into the initial one are presented in Section 3. In Section 4, we provide the solution of the associated perturbed problem and the important crucial result of the paper by introducing new approximate functions (minorant and majorant functions). The effectiveness of the approximations as compared to classical line-searches is illustrated by numerical tests in Section 5. Section 6 contains some concluding remarks.

## 2 Background and Preliminary Results

This section provides the necessary background for the upcoming development. In Subsection 2.1, we review some results in linear semidefinite programming. In Subsection 2.2, we review some statistical inequalities.

### 2.1 Backdrop and brief information on linear semidefinite programming

In what follows, we denote by

1.  $X = \{x \in \mathbb{R}^m : \sum_{i=1}^m x_i A_i - C \in S_n^+\}$  the set of feasible solutions of (1).
2.  $\hat{X} = \{x \in \mathbb{R}^m : \sum_{i=1}^m x_i A_i - C \in \text{int}(S_n^+)\}$  the set of strictly feasible solutions of (1).
3.  $F = \{Y \in S_n^+ : \langle A_i, Y \rangle = b_i, \forall i = 1, \dots, m\}$  the set of feasible solutions of (2).

4.  $\widehat{F} = \{Y \in F : Y \in \text{int}(S_n^+)\}$  the set of strictly feasible solutions of (2).

Here,  $\text{int}(S_n^+)$  is the set of the symmetrical definite positive  $n \times n$  matrices. Let us state the following necessary assumptions.

- (A1) The system of equations  $\langle A_i, Y \rangle = b_i, i = 1, \dots, m$  is of rank  $m$ .
- (A2) The sets  $\widehat{X}$  and  $\widehat{F}$  are non empty.

We know that (see [1, 3])

1. The sets of optimal solutions of problems (2) and (1) are non empty convex and compact.
2. If  $\bar{x}$  is an optimal solution of (1), then  $\bar{Y}$  is an optimal solution of (2) if and only if  $\bar{Y} \in F$  and  $\left(\sum_{i=1}^m \bar{x}_i A_i - C\right) \bar{Y} = 0$ .
3. If  $\bar{Y}$  is an optimal solution of (2), then  $\bar{x}$  is an optimal solution of (1) if and only if  $\bar{x} \in X$  and  $\left(\sum_{i=1}^m \bar{x}_i A_i - C\right) \bar{Y} = 0$ .

According to assumptions (A1) and (A2), the solution of problem (1) permits to give the solution of problem (2) and vice-versa.

### 2.2 Preliminary inequalities

The following result is due to H. Wolkowicz et al. [20], see also J. P. Crouzeix et al. [6] for additional results.

**Proposition 2.1** [20]

$$\begin{aligned} \bar{x} - \sigma_x \sqrt{n-1} &\leq \min_i x_i \leq \bar{x} - \frac{\sigma_x}{\sqrt{n-1}}, \\ \bar{x} + \frac{\sigma_x}{\sqrt{n-1}} &\leq \max_i x_i \leq \bar{x} + \sigma_x \sqrt{n-1}. \end{aligned}$$

Let us recall that B. Merikhi et al. [5] proposed some useful inequalities related to the maximum and minimum of  $x_i > 0$  for any  $i = 1, \dots, n$ .

$$n \ln(\bar{x} - \sigma_x \sqrt{n-1}) \leq A \leq \sum_{i=1}^n \ln(x_i) \leq B \leq n \ln(\bar{x}) \tag{7}$$

with

$$\begin{aligned} A &= (n-1) \ln\left(\bar{x} + \frac{\sigma_x}{\sqrt{n-1}}\right) + \ln(\bar{x} - \sigma_x \sqrt{n-1}), \\ B &= \ln(\bar{x} + \sigma_x \sqrt{n-1}) + (n-1) \ln\left(\bar{x} - \frac{\sigma_x}{\sqrt{n-1}}\right) \end{aligned}$$

so that  $\bar{x}$  and  $\sigma_x$  are respectively, the mean and the standard deviation of a statistical series  $\{x_1, x_2, \dots, x_n\}$  of  $n$  real numbers. These quantities are defined as follows:

$$\bar{x} = \frac{1}{n} \sum_{i=1}^n x_i \quad \text{and} \quad \sigma_x^2 = \frac{1}{n} \sum_{i=1}^n x_i^2 - \bar{x}^2 = \frac{1}{n} \sum_{i=1}^n (x_i - \bar{x})^2.$$

The main advantage of  $(SDP)_\eta$  resides in the strict convexity of its objective function and its feasible domain. Consequently, the conditions of optimality are necessary and sufficient. This fosters theoretical and numerical studies of the problem.

Before this, it is necessary to show that  $(SDP)_\eta$  has at least an optimal solution.

### 3 Theoretical Aspects of Perturbed Problem

#### 3.1 Existence of solution of the perturbed problem

For  $x \in \widehat{X}$ , let us introduce the symmetrical positive definite matrix  $B(x)$  of rank  $m$ , and the lower triangular matrix  $L(x)$  such that

$$B(x) = \sum_{i=1}^m x_i A_i - C = L(x)L^T(x),$$

and let us define, for  $i, j = 1, \dots, m$ ,

$$\begin{aligned} \widehat{A}_i(x) &= [L(x)]^{-1} A_i [L^T(x)]^{-1}, \\ b_i(x) &= \text{trace}(\widehat{A}_i(x)) = \text{trace}(A_i B^{-1}(x)), \\ \Delta_{ij}(x) &= \text{trace}(B^{-1}(x) A_i B^{-1}(x) A_j) = \text{trace}(\widehat{A}_i(x) \widehat{A}_j(x)). \end{aligned}$$

Thus,  $b(x) = (b_i(x))_{i=1, \dots, m}$  is a vector of  $\mathbb{R}^m$  and  $\Delta(x) = (\Delta_{ij}(x))_{i, j=1, \dots, m}$  is a symmetrical matrix of rank  $m$ .

The previous notation will be used in the expressions of the gradient and the Hessian  $H$  of  $f_\eta$ . To show that problem  $(SDP)_\eta$  has a solution, it is sufficient to show that  $f_\eta$  is inf-compact.

**Theorem 3.1** [5] *The function  $f_\eta$  is twice continuously differentiable on  $\widehat{X}$ . Actually, for all  $x \in \widehat{X}$ , we have*

- (a)  $\nabla f_\eta(x) = b - \eta b(x)$ .
- (b)  $H = \nabla^2 f_\eta(x) = \eta \Delta(x)$ .
- (c) *The matrix  $\Delta(x)$  is positive definite.*

Since  $f_\eta$  is strictly convex,  $(SDP)_\eta$  has at most one optimal solution.

For the existence of solution of the perturbed problem, firstly, we start with the following definition.

**Definition 3.1** Let  $f$  be a function defined from  $\mathbb{R}^m$  to  $\mathbb{R} \cup \{\infty\}$ ,  $f$  is called inf-compact if for all  $\eta > 0$ , the set  $S_\eta(f) = \{x \in \mathbb{R}^m : f(x) \leq \eta\}$  is compact, which implies its cone of recession is reduced to zero.

As the function  $f_\eta$  takes the value  $+\infty$  on the boundary of  $X$  and is differentiable on  $\widehat{X}$ , then it is lower semi-continuous. In order to prove that  $(SDP)_\eta$  has one optimal solution, it suffices to prove that the recession cone of  $f_\eta$

$$S_0((f_\eta)_\infty) = \{d \in \mathbb{R}^m, (f_\eta)_\infty(d) \leq 0\}$$

is reduced to zero, i.e.,  $d = 0$  if  $(f_\eta)_\infty(d) \leq 0$ , where  $(f_\eta)_\infty$  is defined for  $x \in \widehat{X}$  as

$$(f_\eta)_\infty(d) = \lim_{\alpha \rightarrow +\infty} \left[ \xi(\alpha) = \frac{f_\eta(x + \alpha d) - f_\eta(x)}{\alpha} \right].$$

This leads to the following proposition.

**Proposition 3.1** [5] *If  $b^T d \leq 0$  and  $\sum_{i=1}^m d_i A_i \in \widehat{X}$ , then  $d = 0$ .*

### 3.2 Uniqueness of the solution of the perturbed problem

As  $f_\eta$  is inf-compact and strictly convex, therefore the problem  $(SDP)_\eta$  admits a unique optimal solution. We denote by  $x(\eta)$  or  $x_\eta$  the unique optimal solution of  $(SDP)_\eta$ .

### 3.3 Convergence of perturbed problem to (1)

**Proposition 3.2** [5] *For  $\eta > 0$ , let  $x_\eta$  be an optimal solution of the problem  $(SDP)_\eta$ , then there exists  $x \in X$  being an optimal solution of (1) such that*

$$\lim_{\eta \rightarrow 0} x_\eta = x.$$

**Remark 3.1** We know that if one of the problems (1) and (2) has an optimal solution, and the values of their objective functions are equal and finite, the other problem has an optimal solution.

## 4 The Numerical Aspects of Perturbed Problem

### 4.1 Newton descent direction

With the presence of the barrier function, the problem  $(SDP)_\eta$  can be considered as the one without constraints. So, one can solve it by a classical slope method. As  $f_\eta$  takes the  $+\infty$  value on the boundary of  $X$ , then the iterates  $x$  are in  $\widehat{X}$ . Thus, the new proposed method is an interior point method.

Let  $x \in \widehat{X}$  be the actual iterate. As a slope direction in  $x$ , let us take Newton's direction  $d$  as a solution of the linear system

$$\nabla^2 f_\eta(x)d = -\nabla f_\eta(x).$$

By virtue of Theorem 1, the precedent linear system is equivalent to the system

$$\Delta(x)d = b(x) - \frac{1}{\eta}b, \tag{3}$$

where  $b(x)$  and  $\Delta(x)$  are defined in Subsection 3.1.

The matrix  $\Delta(x)$  being symmetrical, positive definite, the linear system (3) can be effectively solved through the Cholesky decomposition.

Evidently, one can admit  $\nabla f(x) \neq 0$  (otherwise, the optimum is reached). It follows that  $d \neq 0$ . The direction  $d$  being calculated, we search  $\bar{\alpha} > 0$  giving a significant decrease to  $f_\eta$  over the semi-line  $x + \alpha d$ ,  $\alpha > 0$ , with the conservation of the positive definiteness of the matrix  $B(x + \bar{\alpha}d)$ . Then, the next iterate will be taken equal to  $x + \bar{\alpha}d$ . Thus, we can consider the function

$$\begin{aligned} G(\alpha) &= \frac{1}{\eta}[f_\eta(x + \alpha d) - f_\eta(x)], \quad x + \alpha d \in \widehat{X}, \\ G(\alpha) &= \frac{1}{\eta}b^T d\alpha - \ln \det(B(x + \alpha d)) + \ln \det(B(x)). \end{aligned}$$

Since  $\nabla^2[f_\eta(x)]d = -\nabla f_\eta(x)$ , we have

$$d^T \nabla^2 f_\eta(x) d = -d^T \nabla f_\eta(x) = d^T b(x) - \eta d^T b.$$

To simplify the notations, we consider

$$B = B(x) = \sum_{i=1}^m x_i A_i - C \text{ and } H = \sum_{i=1}^m d_i A_i,$$

$B$  being symmetrical and positive definite, there exists a lower triangular matrix  $L$  such that  $B = LL^T$ .

Next, let us put  $E = L^{-1}H(L^{-1})^T$ , since  $d \neq 0$ , the assumption (A1) implies that  $H \neq 0$  and then  $E \neq 0$ .

There are two main techniques used for computing the displacement step  $\alpha_k$ .

**1) Line search methods** such as the Goldstein-Armijo method, Wolfe method, Fibonacci method, etc. These methods are based on the minimization of the one-dimensional function

$$\varphi(\alpha) = \min_{\alpha > 0} f_\eta(x + \alpha d).$$

Unfortunately, they are very delicate and time consuming.

**2) The approximate function (majorant and minorant function) method** is a sophisticated technique introduced by Cruzeix and Merikhi [5] to solve a positive semidefinite programming problem. The goal of this technique consists in approximating the function  $G(\alpha)$  defined by

$$G(\alpha) = \frac{1}{\eta} [f_\eta(x + \alpha d) - f_\eta(x)].$$

Contrarily to the line search method, the approximate function is simple, and one can easily compute its minimum. This allows the computation of the displacement step without complications and in a short time.

In the following proposition, we give a simple form of the function  $G(\alpha)$ .

**Proposition 4.1** [5] *With this notation, for any  $\alpha > 0$  such that  $I + \alpha E$  is positive definite,*

$$G(\alpha) = \alpha[\text{trace}(E) - \text{trace}(E^2)] - \ln \det(I + \alpha E). \quad (4)$$

*Let us denote by  $\lambda_i$  the eigenvalues of the symmetric matrix  $E$ , then the function  $G$  can be written as follows:*

$$G(\alpha) = \sum_{i=1}^n [\alpha(\lambda_i - \lambda_i^2) - \ln(1 + \alpha\lambda_i)], \quad \alpha \in [0, \hat{\alpha}[, \quad (5)$$

with

$$\hat{\alpha} = \sup[\alpha : 1 + \alpha\lambda_i > 0 \text{ for all } i] = \sup[\alpha : x + \alpha d \in \hat{X}]. \quad (6)$$

Let us observe that  $\hat{\alpha} = +\infty$  if  $E$  is positive semidefinite, and  $0 < \hat{\alpha} < \infty$  otherwise. It is clear that  $G$  is convex on  $[0, \hat{\alpha}[$ ,  $G(0) = 0$  and

$$0 < \sum_i \lambda_i^2 = G''(0) = -G'(0).$$

Besides,  $G(\alpha) \rightarrow +\infty$  when  $\alpha \rightarrow \hat{\alpha}$ . It follows that there exists a unique point  $\alpha_{opt}$  such that  $G'(\alpha_{opt}) = 0$ , where  $G$  reaches its minimum at this point.

Unfortunately, there is no an explicit formula that gives  $\alpha_{opt}$ , and the resolution of the equation  $G'(\alpha_{opt}) = 0$  through iterative methods needs at each iteration the computation of  $G$  and  $G'$ . These computations are too expensive because the expression of  $G$  in (4) contains the determinant which is difficult to calculate and the expression of (5) necessitates the knowledge of the eigenvalues of  $E$ . It is a numerical problem of large size. These difficulties make us look for other new alternatives approaches. Once  $E$  is calculated, it is easy to calculate the following quantities:

$$trace(E) = \sum_i e_{ii} = \sum_i \lambda_i \quad \text{and} \quad trace(E^2) = \sum_{i,j} e_{ij}^2 = \sum_i \lambda_i^2.$$

Based on this proposition, we give, in the following section, new notions of non expensive approximate functions for  $G$  that offer some variable displacement steps to every iteration with a simple technique. We prove the efficiency of one of them by numerical experiments that we will present at the end of this work.

Now, we give the crucial result of the paper.

#### 4.2 New minorant and majorant functions of G

Let us go back to the equations (5) and (6), denote by  $\bar{\lambda}$  and  $\sigma_\lambda$ , respectively, the mean and the standard deviations of  $\lambda_i$ , and by  $\|\lambda\|$  the Euclidean norm of the vector  $\lambda$ . So,

$$\|\lambda\|^2 = n(\bar{\lambda}^2 + \sigma_\lambda^2) = G''(0) = -G'(0),$$

and

$$G(\alpha) = n\bar{\lambda}\alpha - \|\lambda\|^2\alpha - \sum_{i=1}^n \ln(1 + \alpha\lambda_i). \tag{8}$$

The problem consists in looking for  $\bar{\alpha} \in ]0, \hat{\alpha}[$  with  $\hat{\alpha} = \min_{\lambda_i < 0} \left\{ \frac{-1}{\lambda_i} \right\}$  to give a significant decrease of the convex function  $G$ . Let us insist that the best natural choice  $\bar{\alpha} = \alpha_{opt}$ , where  $G'(\alpha_{opt}) = 0$ , presents numerical complications. However, one can find approximately  $\bar{\alpha}$ , but this procedure necessitates, also, too many computations of  $G$  and  $G'$ . However, if we use a line search, it becomes convenient to know the superior born  $\check{\alpha}$  of the  $G$  domain, which is numerically difficult to solve. Consequently, we will take the upper borne of  $\tilde{\alpha}$  given in Proposition 2.1.

$$\begin{aligned} \check{\alpha} &= \sup[\alpha : 1 + \alpha\gamma > 0] \text{ with } \gamma = \bar{\lambda} + \sigma_\lambda\sqrt{n-1}, \\ \tilde{\alpha} &= \sup[\alpha : 1 + \alpha\beta > 0] \text{ with } \beta = \bar{\lambda} + \frac{\sigma_\lambda}{\sqrt{n-1}}. \end{aligned}$$

This strategy consists in minimizing a minorant and majorant approximation  $\check{G}$  and  $\tilde{G}$  of  $G$  instead of minimizing  $G$  over  $[0, \hat{\alpha}[$ . To be efficient, this minorant and majorant approximation needs to be simple and sufficiently near  $G$ . In our case, it requires

$$\begin{aligned} 0 &= \check{G}'(0), \quad \|\lambda\|^2 = \check{G}''(0) = -\check{G}'(0), \\ 0 &= \tilde{G}'(0), \quad \|\lambda\|^2 = \tilde{G}''(0) = -\tilde{G}'(0). \end{aligned}$$

The following lemma introduces two new approximate functions for  $G$ .

**Lemma 4.1** For all  $\alpha \in [0, \hat{\alpha}[ \cap ]0, \check{\alpha}[$ , we have

$$\check{G}_{Min}(\alpha) \leq G(\alpha),$$

and for all  $\alpha \in [0, \hat{\alpha}[ \cap ]0, \tilde{\alpha}[$ , we have

$$G(\alpha) \leq \tilde{G}_{Maj}(\alpha),$$

where

$$\check{G}_{Min}(\alpha) = \frac{\|\lambda\|^2}{\gamma} \alpha - q \ln \left( 1 + \frac{\|\lambda\|^2}{\gamma} \alpha \right), \quad \forall \alpha \geq 0, \quad 0 < q < 1,$$

and

$$\tilde{G}_{Maj}(\alpha) = \frac{\|\lambda\|^2}{\beta} \alpha - p \ln \left( 1 + \frac{\|\lambda\|^2}{\beta} \alpha \right), \quad \forall \alpha \geq 0, \quad 0 < p < 1.$$

**Proof.** 1. We start by proving that  $\check{G}_{Min}(\alpha) \leq G(\alpha)$ .

We have  $G(\alpha) = n\bar{\lambda}\alpha - \|\lambda\|^2\alpha - \sum_{i=1}^n \ln(1 + \alpha\lambda_i)$ . Then we put

$$H(\alpha) = G(\alpha) - \check{G}_{Min}(\alpha).$$

Then  $H(0) = H'(0) = 0$  and we have, for all  $\alpha > 0$ ,

$$H''(\alpha) = \sum_{i=1}^n \frac{\lambda_i^2}{(1 + \alpha\lambda_i)^2} - \frac{\lambda_i^2}{\left(1 + \alpha \frac{\|\lambda\|^2}{\gamma}\right)^2} \geq 0.$$

Because  $|\lambda_i| \leq \|\lambda\|$  and  $\gamma \leq \|\lambda\|$ , it gives  $H(\alpha) \geq 0, \forall \alpha \geq 0$ .

So  $\check{G}_{Min}(\alpha) \leq G(\alpha)$ .

2. Now we prove that  $G(\alpha) \leq \tilde{G}_{Maj}(\alpha)$ . We put:  $K(\alpha) = \tilde{G}_{Maj}(\alpha) - G(\alpha)$ . Then  $K(0) = K'(0) = 0$  and we have, for all  $\alpha > 0$ ,

$$K''(\alpha) = \frac{\|\lambda\|^4}{(\beta + \alpha\|\lambda\|^2)^2} + \sum_{i=1}^n \frac{\lambda_i^2}{(1 + \alpha\lambda_i)^2} \geq 0.$$

This gives  $K(\alpha) \geq 0, \forall \alpha \geq 0$ . So  $G(\alpha) \leq \tilde{G}_{Maj}(\alpha)$ .

We deduce that the functions  $\check{G}_{Min}$  and  $\tilde{G}_{Maj}$  reach their minimum at one unique point:

$$\bar{\alpha}_{Min} = (q-1) \frac{\gamma^2}{\|\lambda\|^2}, \quad \bar{\alpha}_{Maj} = (p-1) \frac{\beta^2}{\|\lambda\|^2}.$$

## 5 Description of the Algorithm and Numerical Results

In this section, we present the algorithm of our approach to obtain an optimal solution  $\bar{x}$  of the problem (1) and some numerical results to demonstrate the performance of our methods.

### 5.1 The algorithm

#### Begin algorithm

##### Initialization

We have to decide on the strategy of the displacement step.  $\varepsilon > 0$  is a given precision,  $\eta > 0$ ,  $\rho > 0$  and  $\sigma \in ]0, 1[$  are fixed parameters. Start with  $x^k \in \widehat{X}$  and  $k = 0$ .

##### Iteration

1. Take  $B = B(x^k) = \sum_{i=1}^m x_i^k A_i - C$  and  $L$  such that  $B = LL^T$ .
2. Compute
 
$$\begin{cases} \widehat{A}_i(x^k) = [L(x^k)]^{-1} A_i [L^T(x^k)]^{-1}, & b(x^k) = \text{trace}(\widehat{A}_i(x^k)), \\ \Delta_{ij}(x^k) = \text{trace}(\widehat{A}_i(x^k) \widehat{A}_j(x^k)), & H = \eta \Delta(x^k). \end{cases}$$
3. Solve the linear system  $Hd = \eta b(x) - b$ .
4. Calculate  $E = L^{-1}H(L^{-1})^T$ ,  $\text{trace}(E)$  and  $\text{trace}(E^2)$ .
5. Take the new iterate  $x^{k+1} = x^k + \bar{\alpha}d$  such that  $\bar{\alpha}$  is obtained by the use of the displacement step strategy of  $\check{G}_i$ ,  $i = 1, \dots, 3$ .
6. If  $n\eta > \varepsilon$ , do  $x^k = x^{k+1}$ ,  $\eta = \sigma\eta$  and go to (1).
7. If  $|b^T x^{k+1} - b^T x^k| > n\rho\eta$ , do  $x^k = x^{k+1}$  and go to (1).
8. Take  $k = k + 1$ .
9. **Stop:**  $x^{k+1}$  is an approximate solution of the problem (1).

#### End algorithm

We know that the optimal solution of  $(SDP)_\eta$  is an approximation of the solution of problem (1). The closer  $\eta$  is to zero, the better the approximation. Unfortunately, when  $\eta$  approaches zero; the problem  $(SDP)_\eta$  becomes ill-conditioned. For this reason, we use at the beginning of the iteration the values of  $\eta$  that are not near to zero, and verify  $n\eta < \varepsilon$ . We can explain the interpretation of the update  $\eta$  as follows: if  $x(\eta)$  is an exact solution of  $(SDP)_\eta$ , so  $b^T x(\eta) \in [m(0), m(0) + n\eta]$ . It is then not necessary to keep on the calculus of the iterates when  $|b^T x^{k+1} - b^T x^k| \leq n\rho\eta$ .

The displacement step  $\bar{\alpha}$  will be determined by the classical line search of Armijo-Goldstein-Price type or by one of three following strategies St  $i$ , by minimizing the majorant function  $\check{G}$  and the minorant function  $\check{G}$ .

In the next subsection, we present comparative numerical tests to prove the effectiveness of our approach over the line search method.

### 5.2 Numerical tests

The following examples are taken from the literature, see for instance [4, 5, 9], and implemented in MATLAB. We have taken  $\varepsilon = 1.0e - 004$ ,  $\sigma = 0.125$  and two values of  $\rho$ ,  $\rho = 1$  or  $\rho = 2$ .

In the table of results,  $(\text{exp } (m, n))$  represents the size of the example, (Itrat) represents the number of iterations necessary to obtain an optimal solution, (Time) represents the time of computation in seconds (s), (LS) represents the classical line search of the Armijo-Goldstein method and (St Maj) and (St Min) represent the strategies which use the minorant functions  $\check{G}$  and the majorant function  $\check{G}$ , respectively.

### 5.2.1 Examples with fixed size

In the following examples,  $\text{diag}(x)$  is the  $n \times n$  diagonal matrix with the components of  $x$  as the diagonal entries.

**Example 1:**  $m = 2, n = 3,$

$$C = \begin{pmatrix} 1 & -1 & 1 \\ -1 & 2 & -2 \\ 1 & -2 & 2 \end{pmatrix}, A_1 = \begin{pmatrix} 1 & -1 & 1 \\ -1 & 0 & 0 \\ 1 & 0 & 0 \end{pmatrix}, A_2 = \begin{pmatrix} 1 & 0 & 0 \\ 0 & 1 & 0 \\ 0 & 0 & 1 \end{pmatrix}, b = (0, 1)^t.$$

**Example 2:**  $m = 3, n = 5,$

$$C = \begin{pmatrix} -4 & 0 & 0 & 0 & 0 \\ 0 & -5 & 0 & 0 & 0 \\ 0 & 0 & 0 & 0 & 0 \\ 0 & 0 & 0 & 0 & 0 \\ 0 & 0 & 0 & 0 & 0 \end{pmatrix}, A_1 = \begin{pmatrix} 2 & 0 & 0 & 0 & 0 \\ 0 & 1 & 0 & 0 & 0 \\ 0 & 0 & 1 & 0 & 0 \\ 0 & 0 & 0 & 0 & 0 \\ 0 & 0 & 0 & 0 & 0 \end{pmatrix}$$

$$A_2 = \begin{pmatrix} 1 & 0 & 0 & 0 & 0 \\ 0 & 2 & 0 & 0 & 0 \\ 0 & 0 & 0 & 0 & 0 \\ 0 & 0 & 0 & 1 & 0 \\ 0 & 0 & 0 & 0 & 0 \end{pmatrix}, A_3 = \begin{pmatrix} 0 & 0 & 0 & 0 & 0 \\ 0 & 1 & 0 & 0 & 0 \\ 0 & 0 & 0 & 0 & 0 \\ 0 & 0 & 0 & 0 & 0 \\ 0 & 0 & 0 & 0 & 1 \end{pmatrix}, b = (8, 7, 3)^t.$$

**Example 3:**  $m = 3, n = 6,$

$$C = \begin{pmatrix} 3 & 0 & 0 & 0 & 0 & 0 \\ 0 & -1 & 0 & 0 & 0 & 0 \\ 0 & 0 & 1 & 0 & 0 & 0 \\ 0 & 0 & 0 & 0 & 0 & 0 \\ 0 & 0 & 0 & 0 & 0 & 0 \\ 0 & 0 & 0 & 0 & 0 & 0 \end{pmatrix}, A_1 = \begin{pmatrix} 2 & 0 & 0 & 0 & 0 & 0 \\ 0 & 1 & 0 & 0 & 0 & 0 \\ 0 & 0 & 0 & 0 & 0 & 0 \\ 0 & 0 & 0 & -1 & 0 & 0 \\ 0 & 0 & 0 & 0 & 0 & 0 \\ 0 & 0 & 0 & 0 & 0 & 0 \end{pmatrix}$$

$$A_2 = \begin{pmatrix} 0 & 0 & 0 & 0 & 0 & 0 \\ 0 & 0 & 0 & 0 & 0 & 0 \\ 0 & 0 & 1 & 0 & 0 & 0 \\ 0 & 0 & 0 & 0 & 0 & 0 \\ 0 & 0 & 0 & 0 & 1 & 0 \\ 0 & 0 & 0 & 0 & 0 & -1 \end{pmatrix}, A_3 = \begin{pmatrix} 1 & 0 & 0 & 0 & 0 & 0 \\ 0 & 1 & 0 & 0 & 0 & 0 \\ 0 & 0 & 1 & 0 & 0 & 0 \\ 0 & 0 & 0 & 1 & 0 & 0 \\ 0 & 0 & 0 & 0 & 1 & 0 \\ 0 & 0 & 0 & 0 & 0 & 1 \end{pmatrix}, b = (0, 0, 1)^t.$$

**Example 4:**  $m = 6, n = 12,$

$$C = \text{diag}(-4, -5, -1, -3, 5, -8, 0, 0, 0, 0, 0, 0)^t,$$

$$A_1 = \text{diag}(1, 0, -4, 3, 1, 1, 1, 0, 0, 0, 0, 0)^t,$$

$$A_2 = \text{diag}(5, 3, 1, 0, -1, 3, 0, 1, 0, 0, 0, 0)^t, A_3 = \text{diag}(4, 5, -3, 3, -4, 1, 0, 0, 1, 0, 0, 0)^t,$$

$$A_4 = \text{diag}(0, -1, 0, 2, , 1, -5, 0, 0, 0, 1, 0, 0)^t, A_5 = \text{diag}(-2, 1, 1, 1, 2, 2, 0, 0, 0, 0, 1, 0)^t,$$

$$A_6 = \text{diag}(2, -3, 2, -1, 4, 5, 0, 0, 0, 0, 0, 1)^t, b = (1, 4, 4, 5, 7, 5)^t.$$

The obtained results are given in the following table.

exp ( $m, n$ )	St Min		St Maj		LS	
	Itrat	Time	Itrat	Time	Itrat	Time
exp 1(2, 3)	4	0.032	3	0.024	5	0.25
exp 2(3, 5)	5	0.056	2	0.0022	7	0.36
exp 3(3, 6)	5	0.094	4	0.023	6	0.36
exp 5(6, 12)	3	0.0016	1	0.0002	3	0.087

5.2.2 Example with variable size

Example 1: (Example Cube)

$n = 2m$ ,  $C$  is the  $n \times n$  identity matrix,  $b = (2, \dots, 2)^T \in \mathbb{R}^m$ ,  $a \in \mathbb{R}$ , and the entries of the  $n \times n$  matrix  $A_k$ ,  $k = 1, \dots, m$ , are given by

$$A_k[i, j] = \begin{cases} 1 & \text{if } i = j = k & \text{or } i = j = k + m, \\ a^2 & \text{if } i = j = k + 1 & \text{or } i = j = k + m + 1, \\ -a & \text{if } i = k, j = k + 1 & \text{or } i = k + m, j = k + m + 1, \\ -a & \text{if } i = k + 1, j = k & \text{or } i = k + m + 1, j = k + m, \\ 0 & \text{otherwise.} \end{cases}$$

Test:  $a = 0$  and  $C = -I$ .

The following table resumes the obtained results.

Size $(m, n)$	St Min		St Maj		LS	
	Itrat	Time	Itrat	Time	Itrat	Time
(50, 100)	2	102	1	65	dvg	
(100, 200)	3	402	2	214	dvg	
(200, 400)	3	798	2	685	dvg	

dvg means that the algorithm does not terminate within a finite time.

**Commentary.** We notice that the two strategies converge to the optimal solution. These tests show clearly that our two strategies offer an optimal solution of (1) and (2) in a reasonable time and with a small number of iterations. We conclude the proposed method is more effective than the line search, and it can improve the results obtained by the line search method. When the instances get larger, this is especially true. Additionally, the reduction in time is substantial because it is clear that the suggested technique takes at least twice as long as the line searches method to arrive at the best answer.

6 Conclusion

In order to solve a linear semidefinite problem, a logarithmic barrier technique based on novel majorant and minorant functions is presented in this study. These two novel approximations provide displacement steps more quickly, cheaply, and easily than the line search. The effectiveness of the majorant and minorant function methodology in comparison to the line search method is demonstrated by numerical data. Our important result is applicable and very important in different problems of nonlinear dynamics in practice. As always, we arrived to problem of optimization after we solve these problems, then we choose our approach for solving it. The idea of introducing our new majorant and minorant functions appears to be a topic worth exploring in the future in the nonlinear dynamics problems and other problems.

Acknowledgements

The authors would like to thank the anonymous referees for their useful comments and suggestions, which helped improve the presentation of this paper.

## References

- [1] F. Alizadeh, J.P. Haberly and M.L. Overton. Primal-dual interior-point methods for semidefinite programming, convergence rates, stability and numerical results. *SIAM Journal on Optimization* **8** (1998) 746–768.
- [2] M. Baddi, M. Chqondi and Y. Akdim, Exponential and Strong Stabilization for Inhomogeneous Semilinear Control Systems by Decomposition Method. *Nonlinear Dynamics and Systems Theory* **23** (1) (2023) 1–13.
- [3] D. Benterki, J. P. Crouzeix and B. Merikhi. A numerical implementation of an interior point method for semidefinite programming. *Pesquisa Operacional Journal* **23** (2003). 49–59.
- [4] D. Benterki, J. P. Crouzeix and B. Merikhi. A numerical feasible interior point method for linear semidefinite programs. *RAIRO Oper. Res.* **41** (2007) 49–59.
- [5] J.P. Crouzeix and B. Merikhi. A logarithm barrier method for semidefinite programming. *RAIRO-Oper. Res.* **42** (2008) 123–139.
- [6] J. P. Crouzeix and A. Seeger. New bounds for the extreme values of a finite sample of real numbers. *Journal of Mathematical Analysis and Applications* **197** (1996) 411–426.
- [7] A. V. Fiacco and G.P. McCormick. *Nonlinear Programming: Sequential Unconstrained Minimization Techniques*. John Wiley and Sons, New York, 1968.
- [8] J. Ji, F. A. Potra and R. Sheng. On the local convergence of a predictor-corrector method for semidefinite programming. *SIAM Journal on Optimization* **10** (1999) 195–210.
- [9] S. Kettab and D. Benterki. A relaxed logarithmic barrier method for semidefinite programming. *RAIRO-Oper. Res.* **49** (2015) 555–568.
- [10] T. Kim-Chuan. Some new search directions for primal-dual interior point methods in semidefinite programming. *SIAM Journal on Optimization* **11** (1) (2000) 223–242.
- [11] A. Leulmi. Etude d’une méthode barrière logarithmique via minorants fonctions pour la programmation semi-définie. Thèse de doctorat, Université de Biskra (2018).
- [12] A. Leulmi, B. Merikhi and D. Benterki. Study of a Logarithmic Barrier Approach for Linear Semidefinite Programming. *Journal of Siberian Federal University. Mathematics & Physics* **11** (3) (2018) 1–13.
- [13] A. Leulmi and S. Leulmi. Logarithmic Barrier Method via Minorant Function for Linear Programming. *J. Sib. Fed. Univ. Math. Phys.* **12** (2) (2019) 191–201.
- [14] B. Merikhi. Extension de quelques méthodes de points intérieurs pour la programmation semi-définie, Thèse de Doctorat, Département de Mathématiques, Université Ferhat Abbas, Sétif-1 (2007).
- [15] R. D. C. Monteiro. Primal-dual path-following algorithms for semidefinite programming. *SIAM Journal on Optimization* **7** (1997) 663–678.
- [16] Y. E. Nesterov and A. Nemirovski. Optimization over positive semidefinite matrices: Mathematical background and user’s manual, Technical report. Central economic and mathematical institute, USSR academy of science, Moscow, USSR, 1990.
- [17] R. T. Rockafellar. *Convex Analysis*. Princeton University Press, New Jerzy, 1970.
- [18] S. A. Surulere, M. Y. Shatalov, A. C. Mkolesia and I. Fedotov. Dynamics of Nonlinear Longitudinal Vibrations in a 1D Nano-Scale Continuum Described by the Generalized Morse Potential. *Nonlinear Dynamics and Systems Theory* **21** (2) (2021) 202–215.
- [19] I. Touil, D. Benterki and A Yassine. A feasible primal–dual interior point method for linear semidefinite programming. *Journal of Computational and Applied Mathematics* **312** (2017) 216–230.
- [20] H. Wolkowicz and G.P.H. Styan. Bounds for eigenvalues using traces. *Linear Algebra and Appl.* **29** (1980) 471–506.



## Electronic Nose for Classifying Civet Coffee and Non-Civet Coffee

D. B. Magfira<sup>1</sup>, R. Sarno<sup>2</sup>, F. A. Susanto<sup>1</sup>, T. Herlambang<sup>1</sup>,  
K. Oktafianto<sup>3</sup>, W. Hartawan<sup>4</sup> and I. W. Farid<sup>5\*</sup>

<sup>1</sup> *Information System Department, Universitas Nahdlatul Ulama Surabaya, Indonesia.*

<sup>2</sup> *Department of Informatics, Institute of Teknologi Sepuluh Nopember, Indonesia.*

<sup>3</sup> *Department of Mathematics, University of PGRI Ronggolawe, Indonesia.*

<sup>4</sup> *Department of Computer Science, University of Pat Petulai, Indonesia.*

<sup>5</sup> *Department of Electrical Automation Engineering, Vocational Faculty,  
Institute of Teknologi Sepuluh Nopember, Surabaya, Indonesia.*

Received: December 23, 2022; Revised: July 26, 2023

**Abstract:** Several Electronic Nose (E-nose) studies on coffee classification have been conducted. The E-nose uses gas sensors to detect the aroma of coffee and generate signals. Then the signals are classified using machine learning algorithms. In this study, the E-nose used five gas sensors to classify civet coffee and non-civet coffee, and the machine learning algorithms used were SVM, KNN and Decision Tree. The coffee variant used was Arabica coffee with the types of civet coffee (kopi luwak) and non-civet coffee (kopi non-luwak) originating from Aceh, Arjuno Malang, Bengkulu. In this study, the mixture of civet coffee and non-luwak coffee was made with a percentage of 100: 0, 90:10, 10:90, 80:20, 20:80, 75:25, 25:75, 50:50. The accuracy of the classification of Aceh civet coffee (LA) and Aceh non-civet coffee (NLA) was 90% (SVM), 100% (KNN), 100% (Decision Tree). The accuracy of the classification of Arjuno civet coffee (LAR) and Arjuno non-civet coffee (NLAR) was 100% (SVM, KNN, Decision Tree). The accuracy of the classification of Bengkulu civet coffee (LB) and Bengkulu non-civet (NLB) was 45% (SVM), 100% (KNN, Decision Tree). And the accuracy of coffee mixture classification (Aceh civet and Aceh non-civet) was 90% (SVM), 93.75% (KNN), and 95% (Decision Tree). The accuracy level obtained was affected by the age of coffee storage, the data collection process when detecting the coffee aroma, and the number of class attributes used.

**Keywords:** *E-nose; SVM; KNN; decision tree; civet coffee; non-civet coffee.*

**Mathematics Subject Classification (2010):** 62H30, 68W40, 68Q17.

---

\* Corresponding author: <mailto:wahyu@ee.its.ac.id>

## 1 Introduction

Coffee is a plant that produces fruit that can be extracted into several types of products, one of the famous and easy-to-find coffee products are beverages. Coffee beans produced from coffee cherries go through several stages of processing [1]. In Indonesia, there are two variants of coffee commonly found, that is, arabica coffee and robusta coffee, and there are also two types of coffee called civet coffee resulted from the civet digestive process. Coffee beans that have gone through the civet digestion process can reduce their acid level so that the coffee beans produced become the best quality coffee [2]. In the process of odor stimulation, the gas-stimulating molecules are small or few in number. In this process, more decisive is not the amount of all gas entering through the nose but the number of gas molecules per unit time that touch odor sensitive cells in the nasal cavity [3]. Smells are usually produced from very low concentrations. The arising of the aroma of food and drink is caused by the formation of volatile compounds. The aroma that is released by every food and drink varies [4]. In addition, different cooking methods will cause different aromas. Likewise, coffee has a distinctive smell after passing through the roasting process [5].

Based on the raw material of each coffee cultivar, civet coffee has different chemical characteristics from the others. The chemical compounds contained in coffee beans greatly influence the taste and aroma of steeping coffee [6]. Therefore, the differences in chemical characteristics make the taste of Arabica civet coffee better than the taste of robusta civet coffee [7]. The coffee drink generally smells less when its temperature decreases because volatile substances will evaporate at high coffee temperatures. The sharp aroma of coffee can be smelled because coffee has polyphenol compounds [8]. The air containing volatile substances from a food will flow turbulently through the crevices of the nasal cavity. The gas molecules in the inhaled air stimulate and touch odor sensitive cells in the nasal cavity. The aroma of coffee can be detected by measuring the gas contained in it. The electronic nose technology can be used to detect the aroma present in coffee with the help of digital data from signaling that appears through the Arduino screen [9].

Classification research for the introduction of the coffee aroma is needed, especially in the introduction of civet coffee and non-civet coffee. This is followed by the increasing demand for the best arabica civet coffee from Indonesia, in meeting domestic and foreign market needs. With the high demand for arabica civet coffee, it is very susceptible to fraud committed by businessmen who expect greater profits, whereas the price of civet coffee is higher than the price of non-civet coffee. In this paper, the authors conducted a study of the types of civet arabica coffee and non-civet arabica coffee from three coffee-producing regions in Indonesia, namely, Aceh coffee, Malang coffee (Arjuno), Bengkulu coffee, the three types of coffee from these regions have not previously been studied simultaneously with arabica civet coffee and arabica non-civet coffee samples from Aceh, Malang (Arjuno coffee) and Bengkulu. This research detects coffee aroma with a series of gas sensors called the electronic nose, the E-nose circuit consists of five MQ-type gas sensors, they are MQ2, MQ3, MQ4, MQ7 and MQ135, from the aroma detection data shown in the displayed signal by the sensor via a monitor screen in the form of a digital signal. The data obtained from the detection of coffee aroma will be processed in main data to find information from the results of coffee aroma detection using the machine learning algorithm for data to be classified, and analyzed based on the accuracy produced so that to find the authenticity of arabica civet coffee and arabica non-civet coffee from

the coffee samples used [10], [11], [12].

## 2 Research Method

The research aims to design an electronic nose used to detect the aroma of coffee. The variants used are arabica coffee with civet coffee and non-civet coffee originating from the three best coffee-producing regions in Indonesia: Aceh, Arjuno and Bengkulu. The aroma of coffee is detected with an electronic nose which generates digital data. The detected digital data are processed and tested in the classification process by applying machine learning classification algorithms by using Weka software.

### 2.1 Electronic nose design

The electronic nose circuit is designed with five MQ-type gas sensors, Arduino, a USB cable, a small fan and one tightly closed container. Table 1 shows the sensitivity of each sensor used in the study [13].

Sensor	Sensitivity to
MQ 2	Hydrogen, Methane, Alcohol, Propane, Butane
MQ 3	Alcohol, Methane, Benzine, Hexane, LPG, Carbon Monoxide
MQ 4	Methane, Hydrogen, Carbon Monoxide, Alcohol, Smoke
MQ 7	$CO$ (Carbon Monoxide)
MQ 135	Air Quality ( $SnO_2$ , Ammonia, Gasoline vapor, Sulfide, and other harmful gases)

**Table 1:** Types and sensitivity of sensors.

These five sensors can detect some of the same gases and what distinguishes them is the sensitivity level of each sensor to the gas, which can be detected based on sensor technical data [14]. In order to detect the aroma in coffee, all sensors are arranged in a circuit called the Electronic nose [15].

#### 2.1.1 Electronic nose (E-nose)

The electronic nose (E-nose) is an instrument used to detect odors or aromas [16]. This system is built of an array of gas sensors known as the electronic olfactory system because the Electronic nose has the ability to imitate the work of the human sense of smell [17]. The output of the Electronic nose system is a signal forming patterns that represent each scent so that it is applicable for identification, comparison, quantification and classification based on the aroma [18], [19].

## 2.2 Coffee

Coffee is one of the largest plantation commodities in Indonesia, spread in the highlands. Coffee plants growing in the highlands produce the best quality coffee [20]. The regions producing the best quality coffee being in great demand on the international market and by domestic consumers include Gayo Arabica coffee from Aceh, Arjuno Arabica coffee from Malang and Kepahiang Arabica coffee from Bengkulu. The Gayo Highlands, situated at an altitude of 1200 meters above sea level, make coffee plants grow well, with

the cool natural conditions of the Gayo Highlands giving an impact on the quality of the aroma and taste of the coffee produced [21]. Kepahiang is one of the districts in Bengkulu province with the majority of the population being coffee farmers. The coffee plantations in Kepahiang, situated at an altitude of 900 to 1300 meters above sea level, were originally planted with Robusta coffees only. With the increasing demand for Arabica coffee in the international market, farmers in Bengkulu were getting convinced to plant Arabica coffee, among them were those farmers in Kepahiang district. Currently, Arabica coffee in Kepahiang is very popular in the international market, especially on the European continent [22]. The foot of Mount Arjuna in Malang Regency, East Java, situated at an altitude of 900 to 1500 meters above sea level, is an ideal site for coffee plantations. The coffee produced on the slopes of Mount Arjuno in Karangploso sub-district-Malang Regency often wins the national and even international coffee competitions. Arabica coffee from the slopes of Mount Arjuno has a soft and fragrant taste due to the effect of volcanic soil and forest vegetation which is a heterogeneous forest. In addition, another very influential factor is the smell of sulfur from Mount Wilerang adjacent to Mount Arjuno so that different aromas and tastes give characteristics to Arjuno Arabica coffee [23].

### 2.2.1 Civet coffee and non-civet

Kopi luwak (civet coffee) is one of the typical Indonesian coffee products produced from the feces of a civet animal (*Paradoxurus hermaphroditus*) after the animal consumes ripe coffee cherries [24]. The luwak (civet) selects coffee cherries with an optimum maturity level based on taste and aroma, eats them by peeling the outer skin, then swallows the seeds and mucus. In the civet's digestive system, the coffee beans undergo a natural fermentation process at an optimal temperature level with the help of microbes and enzymes present in the civet's digestion. The fermentation process provides changes in the chemical composition of the coffee beans, which can improve the quality of the taste of Luwak coffee to be different from ordinary coffee so that Luwak coffee has a specific and special taste and aroma. The improvement in the taste quality of Luwak coffee is caused by the low protein content and high fat content compared to ordinary coffee. Low protein content can reduce bitter taste, while high fat content can increase body weight [25].

### 2.2.2 Data mining

Data mining is a process that uses statistical, mathematical, artificial intelligence, and machine learning techniques to extract and identify useful information and related knowledge from various databases [26]. The data mining process is done by applying a classification machine learning algorithm in recognizing information from a data [27]. The machine learning algorithms applied in this research are Support Vector Machine (SVM), k-nearest neighbor (KNN) and Decision Tree.

### 2.2.3 Support vector machine (SVM)

This method uses a two-step classification process. First, a kernel function transforms low-dimensional features into high-dimensional features [28]. Such transformation transforms non-linearly separable data into linearly separable data of higher dimensions. There are various kinds of kernels to use such as the Polynomial and Radial Basis Function

(RBF). The second step is to construct the maximum margin of the hyperplane to determine the decision limit for each class. The concept of maximum separation prevents misclassification of outliers, thus making the SVM a high-accuracy classification method [29]. In classifying the data, the data are divided into two types, that is, the training data and the test data, the training data set is labeled as  $T = \{(x_i, l_i), i = 1, 2, \dots, L\}$  with  $x_i \in R^P$  and  $l_i \in \{-1, 1\}$ , and the test data as  $f(x) = \text{sign} \sum_{i=1}^L a_i \cdot l_i \cdot K(x_i, x) + b$ , where  $a_i$  is the Lagrange multiplier,  $b$  is the limit value,  $K$  is the kernel function, so the SVM is a subset of the training data with  $a_i > 0$  [30].

#### 2.2.4 K-nearest neighbor (KNN)

The K-Nearest Neighbor (KNN) is a classification algorithm that will determine the label (class) of a test data based on many classes from the closest distance to  $k$  in the training data group [31]. The value of  $k$  used is 3 and 5 to be used in applying the KNN method, while the distance calculation uses the Euclidean Distance method [32]. The KNN will classify the test image into the class with the highest number of members [33]. The working principle of KNN is to find the shortest distance between the data to be evaluated and its  $k$ -closest neighbors in the training data [34]. The following is the equation for calculating the distance to the nearest neighbor:  $D = \sqrt{(x_1 - y_1)^2 + (x_2 - y_2)^2}$  with  $x$  being the sample data,  $y$  being the test data, and  $D$  being the distance.

#### 2.2.5 Decision tree (C4.5)

This algorithm has the input in the form of training samples and test samples [35], [36]. The training samples are in the form of sample data to be used to build a tree that has been tested for its credibility, while the test samples are data fields to be used later as parameters in classifying data [37]. In general, the C4.5 algorithm builds a decision tree following the steps as below: 1. Select an attribute as a root. 2. Create a branch for each value. 3. Divide cases in branches. 4. Repeat the process for each branch until all cases in the branch have the same class. Select the root attribute based on the highest gain value of the existing attributes. To calculate the gain, use the formula  $\text{Gain}(S, A) = \text{Entropy}(S) - \sum_{i=1}^N \frac{|S_i|}{|S|} \text{Entropy}(S_i)$ , where  $S$  is the set of cases,  $A$  is the attribute,  $N$  is the number of partitions of the attribute  $A$ ,  $(S_i)$  is the number of cases in the  $i$ -th partition, and  $|S_r|$  is the number of cases in  $S$ .

#### 2.2.6 Confusion matrix

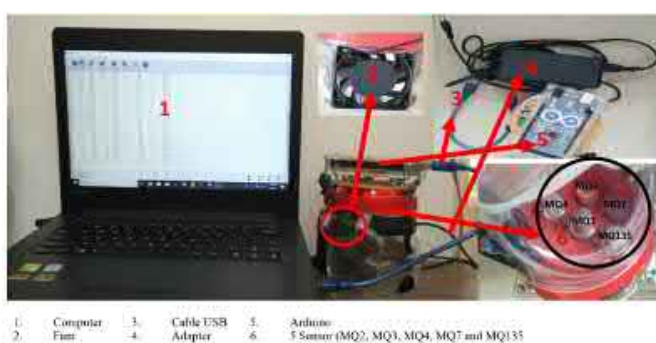
The confusion matrix is the most common way to show classification results, especially in multiclass data, to present it in the form of a confusion matrix also known as a contingency table [38]. For instance,  $x_{r,c}$  of the confusion matrix  $C \in N^{l \times l}$  with  $r$  indicating the prediction class and  $c$  indicating the correct prediction results, and those outside the diagonal being the wrong prediction results. Table 2 shows the form of the matrix to be built in displaying the classification results [39].

### 3 Results and Analysis

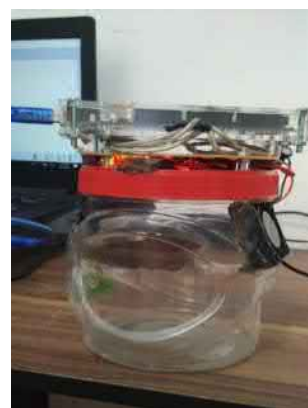
This research aimed to design an Electronic nose and to perform the process of analyzing data from coffee aroma detection results by applying machine learning algorithms for recognizing and finding information from the data resulted from the detection of the

Prediction (r)	Original (c)			
	Class 1	Class 2	...	Class n
Class 1	$X_{11}$	$X_{12}$	...	$X_{1n}$
Class 2	$X_{21}$	$X_{22}$	...	$X_{2n}$
Class n	$X_{n1}$	$X_{n2}$	...	$X_{nn}$

**Table 2:** Confusion Matrix.



(a) Detailed Hardware Design.



(b) Finished Design

**Figure 1:** Design of the Electronic Nose.

aromas of the civet coffee and non-civet coffee originating from three coffee-producing regions in Indonesia: Aceh, Arjuno Malang and Bengkulu.

### 3.1 Hardware design of electronic nose

Five gas sensors (MQ2, MQ3, MQ4, MQ7 and MQ 135) were assembled into one above the Printed Circuit Board (PCB) and connected to the Arduino device so as to be able to read the aroma detection of coffee.

The hardware designed to detect the aroma of civet coffee and non-civet coffee is called the Electronic nose. The Electronic nose was connected to a computer and run on the Arduino IDE software, and it displayed the results of the coffee aroma detection on the cooltrem screen. The results of the coffee aroma detection displayed on the cooltrem screen can be seen in Figure 2.

Each line in Figure 2 displays the value of the detection results from the MQ2, MQ3, MQ4, MQ7, and MQ135 sensors every 2 seconds. The data collection in each experiment was done for 15 minutes.

The experiment conducted in this study was to detect the aroma of Arabica coffee variants with civet and non-civet coffee types from the best three coffee-producing areas: Aceh, Arjuno Malang, Bengkulu. This study was also conducted for an experimental mixture of Aceh civet coffee with Aceh non-civet coffee. The Aceh coffee mixture is divided into eight mixtures with the percentage of each mixture shown in Table 3. The experiments on each type of mixture, Aceh civet coffee with Aceh non-civet coffee, Arjuno civet coffee with Arjuno non-civet coffee, Bengkulu civet coffee with Bengkulu non-civet

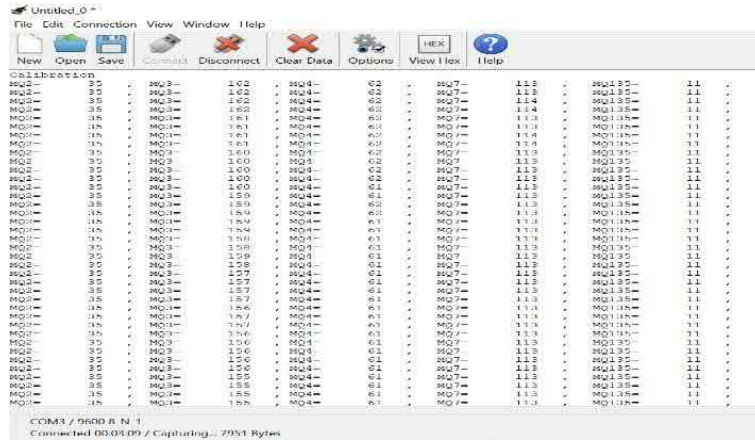


Figure 2: Digital data display of coffee aroma detection results.

No.	Aceh Civet	Aceh Non-civet	Class
1	100%	0%	L100NL0
2	90%	10%	L90NL10
3	10%	90%	L10NL90
4	80%	20%	L80NL20
5	20%	80%	L20NL80
6	75%	25%	L75NL25
7	25%	75%	L25NL75
8	50%	50%	L50NL50

Table 3: Percentage of Aceh Coffee Mixture.

coffee, and coffee mixture (Aceh civet with Aceh non-civet), are conducted as many as 50 times of data collection using the Electronic nose. One-time data collection is carried out for 15 minutes at room temperature. The coffee used as an experimental material is ground coffee with an ideal grinding level, from coarse to medium, with a coffee weight of 15 grams per data collection. The output of the coffee aroma detection produces a digital value from each sensor and is displayed on the cooltrem screen (Figure 2). To classify the coffee aroma detection data, the digital data will go through the process of calculating the average value and standard deviation. The calculations are made in each column based on the sensor name contained in the Electronic nose circuit. The calculation of the average value and standard deviation is made for all aroma detection results in each data sampling. The data from the calculation of the average value and standard deviation of each sensor can be seen in Figure 3, Figure 4, Figure 5, and Figure 6.

Figure 3 displays the results of calculating the average value and standard deviation of each sensor from the detection of Aceh Arabica coffee aroma. The Aceh Arabica coffee data are divided into two classes: Aceh civet (LA) and Aceh non-civet (NLA). Each class has 50 data, with the data range of 1-50 for the Aceh civet class (LA) and of 51-100 data for the Aceh non-civet class (NLA). Aceh Arabica coffee has 10 attributes: avrMQ2, avrMQ3, avrMQ4, avrMQ7, avrMQ135, stdMQ2, stdMQ3, stdMQ4, stdMQ7,

No	Class	avrMQ2	avrMQ3	avrMQ4	avrMQ7	avrMQ135	stdMQ2	stdMQ3	stdMQ4	stdMQ7	stdMQ135
1	LA	50.87755	99.14286	84.40816	175.5102	15.28571	0.917687	1.355262	0.924019	1.51351	0.494872
2	LA	54.72	108.12	91.86	186	15.94	1.990377	0.886341	5.321691	8.270429	0.732393
...	...	...	...	...	...	...	...	...	...	...	...
50	LA	51.2	107.2	87.42	177.2	15.96	1.296148	1.232883	3.826696	1.865476	0.824864
51	NLA	32.41	55.04333	42.49333	87.03	8.516667	1.114406	0.813299	0.499956	0.801519	0.499722
...	...	...	...	...	...	...	...	...	...	...	...
100	NLA	32.49	56.49	49.46333	99.53	10	0.4999	0.4999	0.498654	0.499099	0

Figure 3: Data of Aceh Arabica Coffee Aroma : Civet and Non-Civet.

stdMQ135. The attributes in the aroma data of Aceh Arabica coffee are the values from the calculation results of the average and standard deviation of five sensors in the Electronic nose circuit.

No	Class	avrMQ2	avrMQ3	avrMQ4	avrMQ7	avrMQ135	stdMQ2	stdMQ3	stdMQ4	stdMQ7	stdMQ135
1	LAR	29.87667	77.75	43.13333	90.39	9.006667	0.338805	3.778117	0.418994	0.760197	0.081377
2	LAR	31.00667	66.62667	45.54333	93.34667	9.5	0.553735	1.230429	1.004053	1.59786	0.5
...	...	...	...	...	...	...	...	...	...	...	...
50	LAR	29.49333	76.01667	45.06	92.66667	10.00333	0.499956	1.438653	1.369818	1.958457	0.806219
51	NLAR	30.47667	50.54667	43.49667	90.53667	10.95	0.499455	0.497817	0.499989	0.498654	0.232737
...	...	...	...	...	...	...	...	...	...	...	...
100	NLAR	30.44667	50.50333	43.48667	90.55333	159.5	0.497147	0.499989	0.499822	0.497147	86.60206

Figure 4: Data of Arjuno Arabica Coffee Aroma: Civet and Non-Civet.

The data of Arjuno civet Arabica coffee in Figure 4 has 2 classes and 10 class attributes. Each class has 50 data, 1-50 data for the Arjuno civet class (LAR) and 51-100 data for the Arjuno non-civet class (LAR). There are 10 attributes in Arjuno Arabica coffee aroma data, that is, avrMQ2, avrMQ3, avrMQ4, avrMQ7, avrMQ135, stdMQ2, stdMQ3, stdMQ4, stdMQ7, stdMQ135. These attributes are the results of the calculation of the average and standard deviation of five sensors in the Electronic nose circuit.

No	Class	avrMQ2	avrMQ3	avrMQ4	avrMQ7	avrMQ135	stdMQ2	stdMQ3	stdMQ4	stdMQ7	stdMQ135
1	LB	32.20667	90.33333	50.35667	112.88	9.776667	0.733	5.148031	1.917322	3.351457	0.41648
2	LB	47.11667	127.7767	108.2867	248.7133	16.98	0.754799	2.051046	1.031741	1.269313	0.14
...	...	...	...	...	...	...	...	...	...	...	...
50	LB	50.17667	106.3833	113.9667	204.2233	20.32	1.11001	2.820707	2.283029	3.415668	0.507543
51	NLB	41.53667	121.49	94.44	180.9833	13.52	0.498654	0.4999	0.496387	0.84245	0.4996
...	...	...	...	...	...	...	...	...	...	...	...
100	NLB	41.51333	121.52	94.44667	180.9933	13.49667	0.499822	0.4996	0.497147	0.808263	0.499989

Figure 5: Data of Bengkulu Arabica Coffee Aroma : Civet and Non-Civet.

Figure 5 displays the data of Bengkulu Arabica coffee aroma, divided into two classes, that is, Bengkulu civet (LB) and Bengkulu non-civet (NLB). Each class has 50 data with the order range of the data as in the table: 1-50 for the Bengkulu civet (LB) class and 51-100 for the Bengkulu non-civet class (NLB). There are 10 data attributes for each class: avrMQ2, avrMQ3, avrMQ4, avrMQ7, avrMQ135, stdMQ2, stdMQ3, stdMQ4, stdMQ7, stdMQ135. The class attributes are the result of the calculation of the average and standard deviation of five sensors in the Electronic nose circuit.

The coffee mixture of Aceh civet coffee and non-civet Aceh coffee, divided into eight mixture classes, has a total of 400 data. There are 50 data for each coffee mixture class.

No	Class	avrMQ2	avrMQ3	avrMQ4	avrMQ7	avrMQ135	StdMQ2	stdMQ3	stdMQ4	stdMQ7	stdMQ135
1	LA100NLA0	50.9	99.14	84.44	175.56	15.3	0.921954	1.34179	0.941488	1.512085	0.5
50	LA100NLA0	51.2	107.2	87.42	177.2	15.86	1.296148	1.232883	3.826696	1.865476	0.824864
51	LA90NLA10	67.34	87.91	125.64	197.73	10.37333	6.381567	3.662681	12.32114	14.81431	0.50394
100	LA90NLA10	67.34	87.91	125.64	197.73	10.37333	6.381567	3.662681	12.32114	14.81431	0.50394
101	LA10NLA90	39.7833	79.49	72.1466	163.51	8.673333	0.695022	2.787454	1.251062	2.385351	0.468994
150	LA10NLA90	54.1166	75.4866	105.916	187.056	9.956667	1.393935	0.499822	1.403468	0.836733	0.203606
151	LA80NLA20	48.13	83.1353	84.9333	148.696	7.46	1.089235	3.618907	2.532559	5.339339	0.498397
200	LA80NLA20	60.8233	79.7	114.113	186.103	9.95	0.803402	0.493288	0.860517	0.687499	0.217945
201	LA20NLA80	51.39	92.69	93.056	188.093	10.96667	0.48775	2.694544	0.812479	0.494593	0.179505
250	LA20NLA80	55.5266	95.5566	98.4566	198.093	10.45667	0.567998	0.535527	0.498119	2.037471	0.498119
251	LA75NLA25	67.8495	90.1170	128.337	211.645	10.99666	1.218897	2.032267	2.660804	2.623805	0.057735
300	LA75NLA25	59.5866	92.2666	116.39	200.07	9.993333	3.416015	2.833529	7.666675	11.41279	0.804128
301	LA25NLA75	55.5233	91.58	105.916	194.303	9.993333	0.550263	3.812733	1.209568	0.937011	0.081377
350	LA25NLA75	59.01	82.5866	122.026	210.933	10.98333	0.806164	1.087423	0.820135	0.825967	0.151841
351	LA50NLA50	47.9933	84.5566	88.5966	205.82	11	0.081377	2.499358	0.808696	1.381159	0
400	LA50NLA50	51.42	88.9833	97.8	219.2	11.49333	1.607358	2.050135	3.1241	4.693968	0.499956

Figure 6: Data of Aceh Arabica Coffee Aroma for 8 Mixtures of Civet and Non-Civet Coffee.

The data are: for the LA100NLA class, the order range is 1-50; for the LA90NLA10 class, the order range is 51-100; for the LA10NLA90 class, the order range is 101-150; for the LA80NLA20 class, the order range is 151-200, for the LA20NLA80 class, the order range is 201-250; for the LA75NLA25 class, the order range is 251-300; for the LA25NLA75 class, the order range is 301-350; and for the LA50NLA50 class, the order range is 350-400. Each class has 10 class attributes, that is, avrMQ2, avrMQ3, avrMQ4, avrMQ7, avrMQ135, StdMQ2, stdMQ3, stdMQ4, stdMQ7, stdMQ135. The class attribute is the result of the calculation of the average and standard deviation of five sensors in the Electronic nose circuit. The aroma data from each type of the regional coffee and coffee mixture were tested in the classification process by the SVM, KNN, and Decision Tree algorithms. The tests were done based on the attribute values existing in each class. The test data in the classification process were divided into two types, that is, the training data and the test data. The percentage distribution of the training data and the test data is 80% of the training data and 20% of the test data from the total data entered. The results of the tests carried out on the data for each regional coffee aroma (Aceh, Arjuno, Bengkulu) and coffee mixture (Aceh civet coffee with Aceh non-civet coffee) are shown in the tables below.

Prediction	Target						
	SVM			KNN		Decision Tree	
		LA	NLA	LA	NLA	LA	NLA
	LA	10	1	11	0	11	0
NLA	1	8	0	9	0	9	

Table 4: Confusion Matrix of Aceh Arabika Coffee.

The classification results on testing the aroma data of Aceh civet coffee (LA) with Aceh non-civet coffee (NLA) by the SVM classification algorithm are: 10 data classified according to the prediction class and target class and 1 data classified in Aceh non-civet target class (NLA) based on the prediction of the Aceh civet class (LA). The Aceh non-

civet prediction class (NLA) classified 1 data in the target class of Aceh civet (LA) and 8 data in the target class of Aceh non-civet (NLA). The results of the classification by the SVM algorithm based on the prediction of the same class and target class have an accuracy of 90%. The classification results on testing the aroma data of Aceh civet coffee (LA) with Aceh non-civet coffee (NLA) by the KNN and Decision Tree algorithms are: 11 data classified in the same prediction class and target class in the Aceh civet class (LA). The classification according to the prediction of the Aceh non-civet class (NLA) indicates 9 data in the Aceh non-civet target class (NLA). The classification results displayed in the confusion matrix of the KNN and Decision Tree algorithms represent the data classified in each prediction class and target class having the same amount of data. The results of the classification by the KNN and Decision Tree algorithms show the same accuracy in each algorithm, which is 100%.

Prediction	Target						
	SVM			KNN		Decision Tree	
		LAR	NLAR	LAR	NLAR	LAR	NLAR
	LAR	11	0	11	0	11	0
NLAR	0	9	0	9	0	9	

**Table 5:** Confusion Matrix of Arjuno Arabica Coffee.

The results of the classification of Arjuno civet coffee aroma data (LAR) with Arjuno non-civet coffee (NLAR) by the SVM, KNN, and Decision Tree algorithms represent the amount of data classified by each algorithm, having the same amount, 11 data classified in the Arjuno civet target class (LAR) from the Arjuno civet prediction class (LAR), in the Arjuno non-civet prediction class (NLAR), 9 data classified in the Arjuno non-civet target class, so the accuracy of these three algorithms is the same, that is, 100%.

Prediction	Target						
	SVM			KNN		Decision Tree	
		LB	NLB	LB	NLB	LB	NLB
	LB	0	11	11	0	11	0
NLB	0	9	0	9	0	9	

**Table 6:** Confusion Matrix of Bengkulu Arabica Coffee.

The classification results on testing the Bengkulu civet coffee aroma data with Bengkulu non-civet coffee by the SVM algorithm show 11 data classified in the Bengkulu non-civet target class (NLB) from the Bengkulu civet prediction class (LB). The classified data from the prediction of the Bengkulu non-civet class with the target of the Bengkulu non-civet class indicate there are 9 data. In the Bengkulu civet prediction class (LB) with the same target class, there is no data classified in the Bengkulu civet class (LB), so the accuracy of the SVM algorithm is only 45%. Based on the confusion matrix of the classification results by the SVM algorithm, it shows that the test data entered in the classification process do not meet the right target class, this greatly affects the accuracy obtained from the classification results by the SVM algorithm. The results of testing data on the aroma of the Bengkulu civet coffee (LB) with the Bengkulu non-civet coffee (NLB) by the KNN and Decision Tree algorithms show the same amount of classified data, 11 data classified in the Bengkulu civet target class (LB) from the Bengkulu civet

prediction class (LB), in the Bengkulu non-civet prediction class (NLB), 9 data classified, 9 in the Bengkulu non-civet target class (NLB). Thus, the KNN and Decision Tree algorithms show the same accuracy of 100%.

The classification results for the Aceh coffee mixture with 8 mixture classes and 10 class attributes, tested by the machine learning algorithms are as shown in the following table. The results of the Aceh coffee mixture classification (Aceh civet coffee and Aceh

	Target								
	LA100NLA0	LA90NLA10	LA10NLA90	LA80NLA20	LA20NLA80	LA75NLA25	LA25NLA75	LA50NLA50	
Prediction	LA100NLA0	13	0	0	0	0	0	0	0
LA90NLA10	0	7	0	2	0	1	0	0	0
LA10NLA90	0	0	5	0	0	1	0	0	0
LA80NLA20	0	0	3	8	0	0	0	0	0
LA20NLA80	0	0	0	0	12	0	0	0	0
LA75NLA25	0	0	0	0	0	11	0	0	0
LA25NLA75	0	0	0	0	0	1	9	0	0
LA50NLA50	0	0	0	0	0	0	0	0	7

Figure 7: Confusion Matrix of the Aceh Coffee Mixture by the SVM Algorithm.

non-civet coffee) show an accuracy of 90% by the SVM algorithm. The data tested were 80 data, and the classification results are presented in the form of a matrix (Table 4). The matrix formed based on the classification results shows the predicted distribution of data in each class. The data for the coffee mixture of the LA100NLA0 prediction class classified 13 data in the target class. In the prediction class of LA90NLA10 there are 7 data classified according to the target class, 2 data classified in the target class of LA80NLA20 and 1 data classified in the target class of LA75NLA25. In the prediction class of LA10NLA90 there are 5 data classified according to the target class and 1 data classified in the target class of LA75NLA25. In the prediction class of LA80NLA20, there are 8 data classified according to the target class and 3 data classified in the target class of LA10NLA90. In the LA20NLA80 class there are 12 data classified with the right target class. In the LA75NLA25 class there are 11 data classified with the same target class. In the LA25NLA75 class there are 9 data classified according to the target class and 1 incoming data classified in the LA75NLA25 class. The LA50NLA50 class is classified according to the target class of 7 data. In the LA90NLA10 class classification, there are 2 data that fall into the LA80NLA20 target class and 1 data into the LA75NLA25 target class, meaning that the detection data among the coffee aromas from three types of mixtures have similarities in some of the data when detecting the coffee aroma. The similarity in the aroma detection data makes the data predictable in classes that are not in accordance with the target class. The mixture of 90% of Aceh civet coffee and 10% of Aceh non-civet coffee and that of 90% of Aceh civet coffee and 20% of Aceh non-luwak coffee have a similar aroma detected by the Electronic nose. The number of data samples used for each class can help minimize the occurrence of target class errors during the classification process.

The results of the coffee mixture classification by using the KNN algorithm are observed. For the prediction class of LA100NLA0, there are 13 data classified, predicted in accordance with the target class, and for the prediction class of LA90NLA10, there are 7 data classified matching the prediction with the target of the same class, 2 data in the target class of LA80NLA20 and 1 data in the target class of LA75NLA25. As predicted in accordance with the target class, 2 data are classified correctly, 2 data are classified into LA80NLA20 and 1 data is classified into LA75NLA25. LA10NLA90 is classified

	Target								
	LA100NLA0	LA90NLA0	LA10NLA90	LA80NLA20	LA20NLA80	LA75NLA25	LA25NLA75	LA50NLA50	
Prediction	LA100NLA0	13	0	0	0	0	0	0	0
LA90NLA0	0	7	0	2	0	1	0	0	
LA10NLA90	0	0	6	0	0	0	0	0	
LA80NLA20	0	0	0	11	0	0	0	0	
LA20NLA80	0	0	0	0	12	0	0	0	
LA75NLA25	0	0	0	0	1	10	0	0	
LA25NLA75	0	0	0	0	1	0	9	0	
LA50NLA50	0	0	0	0	0	0	0	7	

Figure 8: Confusion Matrix of Aceh Coffee Mixture by the KNN Algorithm.

as 6 data correctly. 11 data are classified in LA80NLA20. 12 data are classified in the LA20NLA80 class. The LA75NLA25 class is classified as 10 data predicted correctly and 1 data included in the class of LA20NLA80. For LA25NLA75, there are 11 data classified correctly in accordance with the class, and 1 data is classified in LA20NLA80. LA50NLA50 has correctly predicted 7 data in accordance with its prediction class, then the accuracy of the classification by the KNN algorithm is 93.75% of the test input data amounting to 80 data.

	Target								
	LA100NLA0	LA90NLA0	LA10NLA90	LA80NLA20	LA20NLA80	LA75NLA25	LA25NLA75	LA50NLA50	
Prediction	LA100NLA0	13	0	0	0	0	0	0	0
LA90NLA0	0	8	0	2	0	0	0	0	
LA10NLA90	0	0	6	0	0	0	0	0	
LA80NLA20	0	0	0	11	0	0	0	0	
LA20NLA80	0	0	0	0	12	0	0	0	
LA75NLA25	0	0	0	0	0	11	0	0	
LA25NLA75	0	0	0	0	0	2	8	0	
LA50NLA50	0	0	0	0	0	0	0	7	

Figure 9: Confusion Matrix of Aceh Coffee Mixture by the Decision Tree Algorithm.

The classification by the Decision Tree algorithm indicates LA100NLA0 classified as 13 data, LA90NLA10 predicted 8 data in accordance with the prediction class, 2 data predicted in the LA80NLA20 class. For LA10NLA90, 6 data are correctly predicted in the right class. 11 data are predicted in the LA80NLA20 class. 12 data are classified in the LA20NLA80 class. For the LA75NLA25 class, 11 data predicted are classified in accordance with the class. For the LA25NLA75 class, 8 data are classified in the right class and 2 data fall into the incorrect prediction in the LA75NLA25 class. And for the LA50NLA50 class, 7 data are classified as correct so that from all the correct class predictions, an accuracy of 95% is obtained.

After testing the aroma data of the civet and non-civet arabica coffee from each region (Aceh, Arjuno, Bengkulu) and of the coffee mixture (Aceh civet and Aceh non-civet), it is suggested that the data can be effectively classified by using the machine learning algorithms: SVM, KNN, and Decision Tree. During the research, the researcher observed that in detecting the coffee aroma, it is more effective if the coffee used is ground coffee with a medium-sized grinding level, thereby, to maximize the aroma detection stage because at the time of data collection, the coffee aroma lifted by a fan to the lip of the sensor does not leave coffee powder making it easier for further data collection, and with this medium size the aroma released by the coffee can be smelled well so that it is detected optimally. The storage age of coffee, especially ground coffee, greatly affects the level of

aroma contained in the coffee. The longer the ground coffee is stored, the less the aroma contained in the coffee, thus reducing the taste of the coffee. During the collection of the data on the aroma of the civet coffee and non-civet coffee from three coffee producing regions (Aceh, Arjuno Malang, Bengkulu) and Aceh coffee mixture (Aceh civet and Aceh non-civet), the room temperature greatly affected the data produced. The time used to collect coffee aroma data also affects the final results of the data to be used, the longer the data collection process, the better data provided for classification. In data classifying, the data used greatly affects the resulting accuracy value, the more attributes used in the classification process, the higher accuracy value gained. The accuracy of the classification results greatly affected the number of class attributes used, it is suggested to also use the calculated values of min, max, mean, range, kurtosis and skewness.

#### 4 Conclusion

In this research, an Electronic nose (E-nose) was developed with five MQ gas sensors (MQ2, MQ3, MQ4, MQ7 and MQ135) which can detect the aroma of each coffee variant. The results of the aroma detection were shown by sensor signals displayed in digital data. For the digital data resulted from each sensor, the average and standard deviations were calculated. The result of calculating the average and standard deviation of the detection results of each sensor was named the class attribute. The classification by using the SVM, KNN, and Decision Tree algorithms was based on the average value and standard deviation of each coffee variant. The classification results showed an accuracy of above 90% for all the variants of coffee mixtures, and there was still 1 variant having an accuracy of below 50%, that is, the classification of Bengkulu civet coffee with Bengkulu non-civet coffee. As seen from the average of all accuracy produced, the classification of the civet coffee with the non-civet was effectively done with the data resulted from the aroma detection carried out by the Electronic nose. In classifying data, the data used greatly affected the resulting accuracy, the more attributes used in the classification process, the higher accuracy value gained.

#### Acknowledgment

The authors would like to thank: Institute of Technology Sepuluh Nopember, Sekar Gayo coffee Bener Meriah - Aceh, Apresio Kopi Malang, Permata Sari Kepahiang Farmers Group - Bengkulu, who have supported the author in conducting this research. This research was supported by LPPM - Nahdlatul Ulama Surabaya of University (UNUSA). Constructive criticism and suggestions from readers are highly expected, to improve research and research achievements.

#### References

- [1] M. I. Sofyan and T. E. Sebayang. Investigation of Coffee Export Dynamics in Indonesia. *Jurnal Bisma Unesa* **11** (1) (2018) 67–76.
- [2] S. A. W. Kristanti and R. Sutamih. Tingkat Kematangan Biji Kopi Arabika (Coffee arabica L) dalam Menghasilkan Kadar Kafein. *Sain Natural* **9** (1) (2019) 22–28.
- [3] D. R. Wijaya, R. Samo and E. Zulaika. Sensor Array Optimization for Mobile Electronic Nose: Wavelet Transform and Filter Based Feature Selection Approach. *International Review on Computers and Software (I.RE.CO.S.)* **11** (8) (2016) 659–671.

- [4] D. R. Wijaya, R. Samo and E. Zulaika. Information Quality Ratio as a novel metric for mother wavelet selection. *Elsevier, Chemometrics and Intelligent Laboratory Systems* **160** (2017) 59–71.
- [5] D. Giacalone, T. D. Kreuzfeldt, N. Yang, C. Liu and I. Fisk. Common roasting defects in coffee: Aroma composition, sensory characterization and consumer perception. *Elsevier* (2018) 1–12.
- [6] J. Towaha and B. T. Eka. Kopi Luwak Budidaya Sebagai Diversifikasi Produk Yang Mempunyai Citarasa Khas. *SIRINOV* **3** (1) (2015) 19–30.
- [7] E. Wahyuni, A. Karim and A. Anhar. Analysis of Taste Quality of Organic Arabica Coffee in Several Altitudes and Processing Techniques in Gayo Highlands. *Jurnal Manajemen Sumberdaya Lahan* **2** (3) (2013) 261–269.
- [8] A. T. Toci and M. V. Z. Boldrin. Coffee Beverages and Their Aroma Compounds. *Natural and Artificial Flavoring Agents and Food Dyes, Elsevier* (2018) 379–423.
- [9] K. C. Hsu, T. H. Fang, Y. J. Hsiao and P. C. Wu. Response and Characteristics of TiO<sub>2</sub>/Perovskite Heterojunctions for CO Gas Sensors. *Journal of Alloys and Compounds* **1** (1) (2019) 2–39.
- [10] R. Radi, S. Ciptohadijoyo, W. S. Litananda, M. Rivai and M. H. Purnomo. *Electronic Nose Based on Partition Column Integrated With Gas Sensor for fruit Identification and Classification*. Yogyakarta, Indonesia, 2016.
- [11] U. Jumhawan, S. Prama Putri, Y. T. Bamba and E. F. Application of gas chromatography/flame ionization detector-based metabolite fingerprinting for authentication of Asian palm civet coffee (Kopi Luwak). *Journal of Bioscience and Bioengineering* **20** (20) (2015) 1–7.
- [12] V. Vapnik. *Support Vector Networks*. Kluwer Academic Publishers, Boston. Manufactured in The Netherlands (1995) 273–297.
- [13] F. R. Rozak. *Flowing System Design of Indirect Elektronik Nose to Tea Aroma Dedection*. Universitas Gadjah Mada, Yogyakarta, Indonesia, 2015.
- [14] S. S. Izza, R. Sarno and J. Siswantoro. Estimating Gas Concentration using Artificial Neural Network for Electronic Nose. In: *Elsevier, 4th Information Systems International Conference (ISICO 2017)* Bali, Indonesia, 2017.
- [15] H. Hanwei. Technical Data MQ135, MQ4, MQ7, MQ2 and MQ3 Gas Sensor. <http://www.hwsensor.com>. Hanwei Electronics Group Corporation, 1998.
- [16] D. W. Rahman, R. Sarno and E. Zulaika. Gas Concentration Analysis of Resistive Gas Sensor Array. *International Symposium on Electronics and Smart Devices (ISESD)* (2017) 337–342.
- [17] D. B. Magfira and R. Sarno. Classification Of Arabika and Robusta Coffee Using Elektronik Nose. In: *ICOI ACT* Yogyakarta, Indonesia, 2018.
- [18] S. Baskara, D. Lelono and T. W. Widodo. Pengembangan Hidung Elektronik untuk Klasifikasi Mutu Minyak Goreng dengan Metode Principal Component Analysis. *IJEIS* **6** (2) (2016) 221–230.
- [19] R. Sarno and D. W. Rahman. Recent Development in Electronic Nose Data Processing for Beef Quality Assessment. *Telkomnika* **17** (1) (2019) 337–348.
- [20] F. Chamim. <https://mlgcoffee.com/2014/09/19/definisi-kopi-dan-sejarah-penyebaran-kopi-di-dunia/>. 27 February 2014. [Online]. [Accessed 2019].
- [21] Y. W. Teniro, Z. Zulfan and H. Husaini. Perkembangan Pengolahan Kopi Arabika Gayo Mulai Dari Panen Hingga Pasca Panen Di Kampung Simpang Teritit Tahun 2010-2017. *Jurnal Ilmiah Mahasiswa (JIM) Pendidikan Sejarah FKIP Unsyiah* **3** (3) (2018) 52–63.

- [22] D. Listyati, B. Sudjarmoko and A. M. Hasibua. Farming Analysis and Marketing Chain of Robusta Coffee in Bengkulu. *Journal of Industrial and Beverage Crops* **4** (3) (2017) 145–154.
- [23] T. Ada. <https://www.timesindonesia.co.id/read/187708/20181028/000141/kopi-arabika-arjuno-kopi-unggulan-dari-malang/>. 29 April 2019. [Online]. [Accessed 2019].
- [24] M. F. Marcone. Composition and properties of Indonesian palm civet coffee (Kopi Luwak) and Ethiopian civet coffee. *Elsevier Canada*, 2004.
- [25] R. Rubiyono and J. Towaha. The Effect of Fermentation on Flavor Quality of Probiotic Civet Coffee. *RISTI* **4** (2) (2013) 175–182.
- [26] T. Herlambang, H. Nurhadi, A. Muhith, A. Suryowinoto, and K. Oktafianto. Estimation of Forefinger Motion with Multi-DOF Using Advanced Kalman Filter. *Nonlinear Dynamics and Systems Theory*. **23** (1) (2023) 24–33.
- [27] A. Lukman and M. Marwana. Machine Learning Multi Klasifikasi Citra Digital. *Konfrensi Nasional Ilmu Komputer (KONIK)* Makassar, 2014.
- [28] M. Jupri and R. Sarno. Taxpayer Compliance Classification Using C4.5, SVM, KNN, Naive Bayes and MLP. *ICOIATC* Yogyakarta, 2017.
- [29] R. Sarno, J. A. Ridoean and D. Sunaryono. Classification of Music Mood Using MPEG-7 Audio Features and SVM with Confidence Interval. *International Journal on Artificial Intelligence Tools, World Scientific Publishing Company* **27** (5) (2018) 1–18.
- [30] K. Oktafianto, A. Z. Arifin, E. F. Kurniawati, T. Herlambang and F. Yudianto. Tsunami Wave Simulation in the Presence of a Barrier. *Nonlinear Dynamics and Systems Theory*. **23** (1) (2023) 69–78.
- [31] J. Gou, H. Ma, W. Ou, S. Zeng and Y. Rao. A Generalized Mean Distance-Based K-Nearest Neighbor Classifier. *ELSEVIER, Expert Systems with Applications* **115** (1) (2018) 356–372.
- [32] K. Zhao and C. Huang. Air Combat Situation Assessment for UAV Based on Improved Decision Tree. *Chinese Control And Decision Conference (CCDC)* Shenyang, China, 2018.
- [33] J. Gou, W. Qiu, Z. Yi and X. Shen. Locality Constrained Representation-Based K-Nearest Neighbor Classification. *Knowledge-Based Systems* **167** (1) (2019) 38–52.
- [34] A. Utku, I. D. Alper and M. A. Akcayol. Decision Tree Based Android Malware Detection System. *Signal Processing and Communications Applications Conference (SIU)* Izmir, Turkey, 2018.
- [35] H. Elaidi, Y. Elhaddar, Z. Benabbou and H. Abbar. An Idea of a Clustering Algorithm using Support Vector Machines Based on Binary Decision Tree. *International Conference on Intelligent Systems and Computer Vision (ISCV)* Fez, Maroko, 2018.
- [36] M. Y. Anshori, I. H. Santoso, T. Herlambang, K. Oktafianto and P. Katias. Forecasting of Occupied Rooms in the Hotel Using Linear Support Vector Machine. *Nonlinear Dynamics and Systems Theory*. **23** (2) (2023) 129–140.
- [37] E. S. Sankari and D. Manimegalai. Predicting Membrane Protein Types Using Various Decision Tree Classifiers Based on Various Modes of General PseAAC for Imbalanced Datasets. *Journal of Theoretical Biology* **435** (12) (2018) 208–217.
- [38] A. Luque, A. Carrasco, A. Martin and A. H. Las. The Impact of Class Imbalance in Classification Performance Metrics Based on the Binary Confusion Matrix. *Pattern Recognition* **91** (6) (2019) 216–231.
- [39] S. Ruuska, W. Hamalainen, S. Kajava and M. Mughal. Evaluation of the Confusion Matrix Method in the Validation of an Automated System for Measuring Feeding Behaviour of Cattle. *Behavioural Processes* **148** (4) (2018) 56–62.



# Global Existence for the 3-D Generalized Micropolar Fluid System in Critical Fourier-Besov Spaces with Variable Exponent

F. Ouidirne, H. Srhiri, C. Allalou\* and M. Oukessou

*LMACS Laboratory, FST of Beni-Mellal, Sultan Moulay Slimane University, Morocco.*

Received: February 27, 2023; Revised: May 26, 2023

**Abstract:** In this work, we study the 3-D generalized Cauchy problem of the incompressible micropolar fluid system (GMFS) in the critical variable exponent Fourier-Besov space  $\mathcal{FB}_{p(\cdot),q}^{4-\frac{3}{p(\cdot)}-2\alpha}$ . We establish the global well-posedness result with the initial data belonging to  $\mathcal{FB}_{p(\cdot),q}^{4-\frac{3}{p(\cdot)}-2\alpha}$ , where  $p = p(\cdot)$  is a bounded function satisfying  $p \in [2, \frac{6}{5-4\alpha}]$ ,  $\alpha \in (\frac{1}{2}, 1]$  and  $q \in [1, \frac{3}{2\alpha-1}]$ .

**Keywords:** *global existence; 3-D generalized micropolar fluid system; variable Fourier-Besov space.*

**Mathematics Subject Classification (2010):** 35B65,35Q35,70K20,76D03.

## 1 Introduction and Statement of Main Result

We investigate the generalized incompressible micropolar system in the whole space  $\mathbb{R}^3$ ,

$$\begin{cases} \partial_t u + (\chi + \nu)(-\Delta)^{\alpha_1} u + u \cdot \nabla u + \nabla \pi - 2\chi \nabla \times w = 0, & \text{in } \mathbb{R}^3 \times \mathbb{R}^+, \\ \partial_t w + \mu(-\Delta)^{\alpha_2} w + u \cdot \nabla w + 4\chi w - \kappa \nabla \operatorname{div} w - 2\chi \nabla \times u = 0, & \text{in } \mathbb{R}^3 \times \mathbb{R}^+, \\ \operatorname{div} u = 0, & \text{in } \mathbb{R}^3 \times \mathbb{R}^+, \\ (u, w)|_{t=0} = (u_0, w_0), & \text{in } \mathbb{R}^3. \end{cases} \quad (1)$$

The unknowns are  $u = u(x, t)$ ,  $w = w(x, t)$  and  $\pi = \pi(x, t)$  representing, respectively, the linear velocity field, the micro-rotation velocity field and the pressure field of the fluid. The nonnegative constants  $\kappa, \mu, \nu$  and  $\chi$  represent the viscosity coefficients, which determine fluid physical characteristics and  $\alpha_1, \alpha_2 \in (\frac{1}{2}, 1]$  are two positive constants.  $u_0$  and  $w_0$  represent the initial velocities and we assume that  $\operatorname{div} u_0 = 0$ . Recall that

\* Corresponding author: <mailto:chakir.allalou@yahoo.fr>

the Riesz potential operator  $(-\Delta)^k$  is defined as usual through the Fourier transform as  $\mathcal{F}[(-\Delta)^k f](\xi) := |\xi|^{2k} \mathcal{F}[f](\xi)$ , where  $\mathcal{F}[f](\xi) := \hat{f}(\xi) = \frac{1}{(2\pi)^{3/2}} \int_{\mathbb{R}^3} e^{-ix\xi} f(x) dx$ . Without loss of generality, throughout this paper, we only consider the situation with  $\kappa = \mu = 1$  and  $\chi = \nu = 1/2$ .

Notice that if  $\alpha_1 = \alpha_2 = 1$ , then system (1) reduces to the standard micropolar fluid system

$$\begin{cases} \partial_t u - (\chi + \nu)\Delta u + u \cdot \nabla u + \nabla \pi - 2\chi \nabla \times w = 0, & \text{in } \mathbb{R}^3 \times \mathbb{R}^+, \\ \partial_t w - \mu \Delta w + u \cdot \nabla w + 4\chi w - \kappa \nabla \operatorname{div} w - 2\chi \nabla \times u = 0, & \text{in } \mathbb{R}^3 \times \mathbb{R}^+, \\ \operatorname{div} u = 0, & \text{in } \mathbb{R}^3 \times \mathbb{R}^+, \\ (u, w)|_{t=0} = (u_0, w_0), & \text{in } \mathbb{R}^3, \end{cases} \quad (2)$$

which was created by A.C. Eringen [9] in 1996. It is an essential modification to the classical Navier-Stokes equations in order to better characterize the motion of real-world fluids made up of rigid but randomly oriented particles (such as blood) by investigating the effect of micro-rotation of particles suspended in a viscous medium.

There is a lot of literature devoted to the mathematical theory of the micropolar fluid system. The first result on the existence and uniqueness of solutions of the standard micropolar fluid system was obtained by Galdi and Rionero in [10]. Chen and Miao [5] proved the global existence for the problem (2) with small initial data in the Besov spaces  $\dot{B}_{p,q}^{-1+\frac{3}{p}}$  when  $p \in [1, 6)$  and  $q = \infty$ . Inspired by the work of Cannone and Karch [6] on the incompressible Navier-Stokes equations, V.-Roa and Ferreira [8] showed the existence of the solution for the generalized micropolar fluid system in the pseudo-measure space  $PM^\tau$  which is defined by

$$PM^\tau = \left\{ f \in \mathcal{S}'(\mathbb{R}^n) : \hat{f} \in L^1_{loc}(\mathbb{R}^n), \|f\|_{PM^\tau} = \operatorname{ess\,sup}_{x \in \mathbb{R}^n} |\xi|^\tau |\hat{f}(\xi)| < \infty \right\}.$$

Our main result can be stated as follows.

**Theorem 1.1** *Let  $\frac{1}{2} < \alpha = \min(\alpha_1, \alpha_2) = \alpha_1 \leq 1$ ,  $p(\cdot) \in C^{\log}(\mathbb{R}^n) \cap \mathcal{P}(\mathbb{R}^n)$  such that  $2 \leq p(\cdot) \leq \frac{6}{5-4\alpha}$ ,  $1 \leq \rho < \infty$  and  $1 \leq q < \frac{3}{2\alpha-1}$ . Then there exists a small  $\varepsilon_0$  such that for any  $(u_0, w_0) \in \mathcal{FB}_{p(\cdot),q}^{4-2\alpha-\frac{3}{p(\cdot)}}$  satisfying  $\nabla \cdot u_0 = 0$  with  $\|(u_0, w_0)\|_{\mathcal{FB}_{p(\cdot),q}^{4-2\alpha-\frac{3}{p(\cdot)}}} < \varepsilon_0$ , the problem (1) admits a unique global mild solution  $(u, w)$  in*

$$\mathcal{L}^\rho([0, \infty), \mathcal{FB}_{p(\cdot),q}^{4-2\alpha-\frac{3}{p(\cdot)}+\frac{2\alpha}{\rho}}) \cap \mathcal{L}^\rho([0, \infty), \mathcal{FB}_{2,q}^{\frac{2\alpha}{\rho}+\frac{5}{2}-2\alpha}) \cap \mathcal{L}^\infty([0, \infty), \mathcal{FB}_{2,q}^{\frac{5}{2}-2\alpha}),$$

such that

$$\begin{aligned} \|(u, w)\|_{\mathcal{L}^\rho([0, \infty), \mathcal{FB}_{p(\cdot),q}^{4-2\alpha-\frac{3}{p(\cdot)}+\frac{2\alpha}{\rho}}) \cap \mathcal{L}^\rho([0, \infty), \mathcal{FB}_{2,q}^{\frac{2\alpha}{\rho}+\frac{5}{2}-2\alpha}) \cap \mathcal{L}^\infty([0, \infty), \mathcal{FB}_{2,q}^{\frac{5}{2}-2\alpha})} \\ \leq \|(u_0, w_0)\|_{\mathcal{FB}_{p(\cdot),q}^{4-2\alpha-\frac{3}{p(\cdot)}}}. \end{aligned}$$

**Remark 1.1** Notice that the result of Theorem 1.1 is correct only if the bounded function  $p \neq 1$ , and then the case  $(p, \alpha) = (1, 1)$ , which corresponds to  $\mathcal{FB}_{1,q}^{-1}$ , is not included. It is proved in [13] that if  $(p, \alpha) = (1, 1)$ , then the standard micropolar fluid system (SMFS) is well-posed in  $\mathcal{FB}_{1,q}^{-1}$ , where  $1 \leq q \leq 2$ , and ill-posed in these spaces for  $2 < q \leq \infty$ , which means that the space  $\mathcal{FB}_{1,q}^{-1}$  is optimal. Furthermore, our result

is a generalization of the works [4, 12] in which the authors proved that the problem (1) is globally well-posed in the Fourier-Besov spaces  $\mathcal{FB}_{p,q}^{4-\frac{3}{p}-2\alpha}$  for  $\alpha \in (\frac{1}{2}, 1]$ ,  $1 < p \leq \infty$ ,  $1 \leq q \leq \infty$  and the initial data being small. The aim of this work is to establish this result in the case of variable exponent.

Throughout the paper, we denote  $\alpha = \min(\alpha_1, \alpha_2)$ . Let  $X, Y$  be the Banach spaces. We use  $(a, b) \in X$  to denote  $(a, b) \in X \times X$ ,  $\|(a, b)\|_X$  to denote  $\|(a, b)\|_{X \times X}$  and we denote  $\|\cdot\|_{X \cap Y} = \|\cdot\|_X + \|\cdot\|_Y$ . The notation  $a \lesssim b$  means that there exists a positive constant  $C$  such that  $a \leq Cb$ .

## 2 Preliminaries

In this section, we review the Littlewood-Paley theory and some of the used function spaces and the related properties, we state the micropolar semigroup and the notion of mild solutions for the system (1), we recall the Banach fixed point theorem which we will apply for proving the existence of a unique mild solution and we present the definition of the Chemin-Lerner type homogeneous Fourier-Besov spaces.

### 2.1 Littlewood-Paley theory and Fourier-Besov spaces with variable exponent

Let us present some basic properties of the Littlewood-Paley theory and Fourier-Besov spaces with variable exponent.

Let  $\theta \in \mathcal{S}(\mathbb{R}^n)$  be a radial positive function such that  $0 \leq \theta \leq 1$ ,  $\text{supp}(\theta) \subset \{\xi \in \mathbb{R}^n : \frac{3}{4} \leq |\xi| \leq \frac{8}{3}\}$  and

$$\sum_{j \in \mathbb{Z}} \theta(2^{-j}\xi) = 1, \quad \text{for all } \xi \neq 0.$$

Put

$$\theta_j(\xi) = \theta(2^{-j}\xi), \quad \varphi_j(\xi) = \sum_{k \leq j-1} \theta_k(\xi)$$

and

$$g(x) = \mathcal{F}^{-1}\theta(x), \quad h(x) = \mathcal{F}^{-1}\varphi(x).$$

Now, we present some frequency localization operators

$$\Delta_j u := \mathcal{F}^{-1}(\theta_j \mathcal{F}(u)) = 2^{nj} \int_{\mathbb{R}^n} g(2^j y) u(x - y) dy,$$

$$S_j u := \sum_{k \leq j-1} \Delta_k f = \mathcal{F}^{-1}(\varphi_j \mathcal{F}(u)) = 2^{nj} \int_{\mathbb{R}^n} h(2^j y) u(x - y) dy,$$

where  $\Delta_j = S_j - S_{j-1}$  is a frequency projection to the annulus  $\{|\xi| \sim 2^j\}$  and  $S_j$  is a frequency to the ball  $\{|\xi| \lesssim 2^j\}$ .

By using the definition of  $\Delta_j$  and  $S_j$ , we easily prove that

$$\begin{aligned} \Delta_j \Delta_k f &= 0, & \text{if } |j - k| \geq 2, \\ \Delta_j (S_{k-1} f \Delta_k f) &= 0, & \text{if } |j - k| \geq 5. \end{aligned}$$

The following Bony para-product decomposition will be applied around the paper:

$$uv = \dot{T}_u v + \dot{T}_v u + R(u, v),$$

where  $\dot{T}_u v = \sum_{j \in \mathbb{Z}} \dot{S}_{j-1} u \dot{\Delta}_j v$ ,  $\dot{R}(u, v) = \sum_{j \in \mathbb{Z}} \dot{\Delta}_j u \tilde{\Delta}_j v$  and  $\tilde{\Delta}_j v = \sum_{|j'-j| \leq 1} \dot{\Delta}_{j'} v$ .

We define the variable exponent Lebesgue spaces  $L^{p(\cdot)}$ .

**Definition 2.1** ([2]) Let  $\mathcal{P}(\mathbb{R}^n)$  denote the set of all measurable functions  $p(\cdot) : \mathbb{R}^n \rightarrow (0, \infty)$  such that

$$0 < p_- = \operatorname{ess\,inf}_{x \in \mathbb{R}^n} p(x), \operatorname{ess\,sup}_{x \in \mathbb{R}^n} p(x) = p_+ < \infty.$$

The variable exponent Lebesgue space is defined by

$$L^{p(\cdot)}(\mathbb{R}^n) = \left\{ f : \mathbb{R}^n \rightarrow \mathbb{R} \text{ is measurable, } \int_{\mathbb{R}^n} |f(x)|^{p(x)} dx < \infty \right\}$$

equipped with the Luxemburg-Nakano norm

$$\|f\|_{L^{p(\cdot)}} = \inf \left\{ \delta > 0 : \int_{\mathbb{R}^n} \left( \frac{|f(x)|}{\delta} \right)^{p(x)} dx \leq 1 \right\}.$$

The space  $L^{p(\cdot)}(\mathbb{R}^n)$  is a Banach space.

Since the  $L^{p(\cdot)}$  does not have the same desired properties as  $L^p(\mathbb{R}^n)$ , we propose the following standard conditions to prove that the Hardy-Littlewood maximal operator  $M$  is bounded on  $L^{p(\cdot)}(\mathbb{R}^n)$ :

**i)** We say that  $p : \mathbb{R}^n \rightarrow \mathbb{R}$  is locally log-Hölder continuous,  $p \in C_{loc}^{log}(\mathbb{R}^n)$ , if there exists a constant  $c_{log} > 0$  with

$$|p(x) - p(y)| \leq \frac{c_{log}}{\log \left( e + \frac{1}{|x-y|} \right)} \quad \text{for all } x, y \in \mathbb{R}^n \text{ and } x \neq y.$$

**ii)** We say that  $p$  is globally log-Hölder continuous,  $p \in C^{log}(\mathbb{R}^n)$ , if  $p \in C_{loc}^{log}(\mathbb{R}^n)$  and there exist a  $p_\infty \in \mathbb{R}$  and a constant  $c_\infty > 0$  with

$$|p(x) - p_\infty| \leq \frac{c_\infty}{\log(e + |x|)} \quad \text{for all } x \in \mathbb{R}^n.$$

**iii)** We write  $p \in \mathcal{P}^{log}(\mathbb{R}^n)$  if  $0 < p^- \leq p(x) \leq p^+ \leq \infty$  with  $1/p \in C^{log}(\mathbb{R}^n)$ .

Let  $p, q \in \mathcal{P}(\mathbb{R}^n)$ , we denote by  $\ell^{q(\cdot)}(L^{p(\cdot)})$  the space consisting of all sequences  $\{h_i\}_i$  of measurable functions on  $\mathbb{R}^n$  such that

$$\varrho_{\ell^{q(\cdot)}(L^{p(\cdot)})}((h_i)_i) := \sum_{i \geq 0} \inf \left\{ \delta_i > 0 \mid \varrho_{p(\cdot)} \left( h_i / \delta_i^{\frac{1}{q(\cdot)}} \right) \leq 1 \right\}$$

with the convention  $\delta^{1/\infty} = 1$ . Also, the norm is defined as usual:

$$\| (h_i)_i \|_{\ell^{q(\cdot)}(L^{p(\cdot)})} := \inf \left\{ \lambda > 0 \mid \varrho_{\ell^{q(\cdot)}(L^{p(\cdot)})} \left( \frac{1}{\lambda} (h_i)_i \right) \leq 1 \right\}.$$

If  $q^+ < \infty$ , then

$$\mathcal{Q}_{\ell^{q(\cdot)}(L^{p(\cdot)})}((h_i)_i) = \sum_{i \geq 0} \| |h_i|^{q(\cdot)} \|_{\frac{p(\cdot)}{q(\cdot)}}.$$

Then we define the variable exponent homogeneous Fourier-Besov space  $\mathcal{F}\dot{\mathcal{B}}_{p(\cdot),q(\cdot)}^{s(\cdot)}$ .

**Definition 2.2** ([3]) Let  $s(\cdot) \in C^{log}(\mathbb{R}^n)$  and  $p(\cdot), q(\cdot) \in \mathcal{P}(\mathbb{R}^n) \cap C^{log}(\mathbb{R}^n)$  with  $0 < p_- \leq p(\cdot) \leq \infty$ . The homogeneous Fourier-Besov space with variable exponent  $\mathcal{F}\dot{\mathcal{B}}_{p(\cdot),q(\cdot)}^{s(\cdot)}$  is defined by the set of all  $f \in \mathcal{Z}'(\mathbb{R}^n)$  such that

$$\|f\|_{\mathcal{F}\dot{\mathcal{B}}_{p(\cdot),q(\cdot)}^{s(\cdot)}} := \|\{2^{js(\cdot)}\theta_j \hat{f}\}_{j \geq 0}\|_{\ell^{q(\cdot)}(L^{p(\cdot)})} < \infty.$$

The space  $\mathcal{Z}'(\mathbb{R}^n)$  is the dual space of

$$\mathcal{Z}(\mathbb{R}^n) = \{f \in \mathcal{S}(\mathbb{R}^n) : (D^\alpha f)(0) = 0, \forall \alpha \text{ multi-index}\}.$$

Next proposition describes some useful assertions we use in this work related to  $L^{p(\cdot)}$  spaces and Besov spaces with variable exponent.

**Proposition 2.1** ([7]). (1) (Hölder inequality) Let  $p_1(\cdot), p_2(\cdot) \in \mathcal{P}(\mathbb{R}^n)$ , and define  $p \in \mathcal{P}(\mathbb{R}^n)$  by  $\frac{1}{p(x)} = \frac{1}{p_1(x)} + \frac{1}{p_2(x)}$ . Then there exists a constant  $C$  depending only on  $p_-$  and  $p_+$  such that

$$\|fg\|_{L^{p(\cdot)}} \leq C \|f\|_{L^{p_1(\cdot)}} \|g\|_{L^{p_2(\cdot)}}$$

holds for every  $f \in L^{p_1(\cdot)}$  and  $g \in L^{p_2(\cdot)}$ .

(2) ([2]) Let  $p_0(\cdot), p_1(\cdot), q(\cdot) \in \mathcal{P}(\mathbb{R}^n)$ , and  $s_0(\cdot), s_1(\cdot) \in L^\infty \cap C^{log}(\mathbb{R}^n)$  with  $s_0(\cdot) \geq s_1(\cdot)$ . If  $\frac{1}{q_0(\cdot)}, \frac{1}{q_1(\cdot)}$  and  $s_0(x) - \frac{n}{p_0(x)} = s_1(x) - \frac{n}{p_1(x)}$  are locally log-Hölder continuous, then

$$\dot{\mathcal{B}}_{p_0(\cdot),q(\cdot)}^{s_0(\cdot)} \hookrightarrow \dot{\mathcal{B}}_{p_1(\cdot),q(\cdot)}^{s_1(\cdot)}.$$

The following result deals with the product of two functions in the Chemin-Lerner space.

**Proposition 2.2** ([1]). Let  $s > 0, 1 \leq \gamma, \rho, \rho_1, \rho_2, p, q, r \leq \infty$  such that  $\frac{1}{\rho} = \frac{1}{\rho_1} + \frac{1}{\rho_2}$  and  $\frac{1}{\gamma} = \frac{1}{r} + \frac{1}{p}$ . Then we have

$$\|ab\|_{\mathcal{L}^\rho \dot{B}_{\gamma,q}^s} \lesssim \|a\|_{\mathcal{L}^{\rho_1} \dot{B}_{\gamma,q}^s} \|b\|_{\mathcal{L}^{\rho_2} L^r} + \|b\|_{\mathcal{L}^{\rho_1} \dot{B}_{\gamma,q}^s} \|a\|_{\mathcal{L}^{\rho_2} L^r}.$$

## 2.2 Fractional micropolar semigroup and mild solutions

The following system is the corresponding linear system of (1):

$$\begin{cases} \partial_t u + (-\Delta)^{\alpha_1} u - \nabla \times w = 0, \\ \partial_t w + (-\Delta)^{\alpha_2} w + 2w - \nabla \operatorname{div} w - \nabla \times u = 0, \\ \operatorname{div} u = 0, \\ (u, w)|_{t=0} = (u_0, w_0). \end{cases} \tag{3}$$

The solution operator of the above problem is denoted by the notation  $G(t)$ , i.e., for specified initial data  $(u_0, w_0)$  in suitable function space, if we denote by

$(u, w)^T = G(t)(u_0, w_0)^T$  the unique solution of the problem (3), then

$$(\widehat{G(t)f})(\xi) = e^{-A(\xi)t} \hat{f}(\xi) \quad \text{for } f(x) = (f_1(x), f_2(x))^T,$$

where

$$A(\xi) = \begin{bmatrix} |\xi|^{2\alpha_1} I & \mathcal{B}(\xi) \\ \mathcal{B}(\xi) & (|\xi|^{2\alpha_2} + 2) I + \mathcal{C}(\xi) \end{bmatrix}$$

with

$$\mathcal{B}(\xi) = i \begin{bmatrix} 0 & \xi_3 & -\xi_2 \\ -\xi_3 & 0 & \xi_1 \\ \xi_2 & -\xi_1 & 0 \end{bmatrix} \quad \text{and } \mathcal{C}(\xi) = \begin{bmatrix} \xi_1^2 & \xi_1 \xi_2 & \xi_1 \xi_3 \\ \xi_1 \xi_2 & \xi_2^2 & \xi_2 \xi_3 \\ \xi_1 \xi_3 & \xi_2 \xi_3 & \xi_3^2 \end{bmatrix}.$$

Moreover, by applying the Leray projection  $\mathbf{P}$  to both sides of the first equations of (1), one can eliminate the pressure  $\pi$  and we get

$$\begin{cases} \partial_t u + (-\Delta)^{\alpha_1} u + \mathbf{P}(u \cdot \nabla u) - \nabla \times w = 0, \\ \partial_t w + (-\Delta)^{\alpha_2} w + u \cdot \nabla w + 2w - \nabla \operatorname{div} w - \nabla \times u = 0, \\ \operatorname{div} u = 0, \\ (u, w)|_{t=0} = (u_0, w_0), \end{cases} \tag{4}$$

where  $\mathbf{P} = I + \nabla(-\Delta)^{-1} \operatorname{div}$  is the  $3 \times 3$  matrix pseudo-differential operator in  $\mathbb{R}^3$  with the symbol  $(\delta_{ij} - \frac{\xi_i \xi_j}{|\xi|^2})_{i,j=1}^3$ . We denote

$$U(x, t) = \begin{pmatrix} u(x, t) \\ w(x, t) \end{pmatrix}, \quad U_0 = \begin{pmatrix} u(x, 0) \\ w(x, 0) \end{pmatrix} = \begin{pmatrix} u_0 \\ w_0 \end{pmatrix},$$

$$U_i(x, t) = \begin{pmatrix} u_i(x, t) \\ w_i(x, t) \end{pmatrix}, \quad i = 1, 2,$$

and

$$U_1 \tilde{\otimes} U_2 = \begin{pmatrix} u_1 \otimes u_2 \\ u_1 \otimes w_2 \end{pmatrix}, \quad \tilde{\mathbf{P}} \nabla \cdot (U_1 \tilde{\otimes} U_2) = \begin{pmatrix} \mathbf{P} \nabla \cdot (u_1 \otimes u_2) \\ \nabla \cdot (u_1 \otimes w_2) \end{pmatrix}.$$

Solving system (4) can be reduced to finding a solution  $U$  to the following integral equations:

$$U(t) = G(t)U_0 - \int_0^t G(t - \tau) \tilde{\mathbf{P}} \nabla \cdot (U \otimes U)(\tau) d\tau. \tag{5}$$

A solution of (5) is called a mild solution of (1). Now, we present a property of the semigroup  $G(\cdot)$ .

**Lemma 2.1** ([8]) *Let  $\frac{1}{2} < \alpha \leq 1$ . Then for  $|\xi| \neq 0$  and  $t \geq 0$ , there exists  $C = C(\alpha_1, \alpha_2) > 0$  (independent of  $\xi$ ) such that*

$$|e^{-tA(\xi)}| \leq \begin{cases} e^{-|\xi|^{\alpha_1 t}} & \text{if } |\xi| \leq 1, \\ e^{-C|\xi|^{\alpha_2 t}} & \text{if } |\xi| > 1. \end{cases} \tag{6}$$

In particular, if  $\alpha = \alpha_1$ , then

$$\|e^{-tA(\xi)}\| \leq e^{-|\xi|^{2\alpha t}} \quad \text{for all } |\xi| > 0. \tag{7}$$

**2.3 Banach fixed point theorem and Chemin-Lerner type homogeneous Fourier-Besov spaces**

We recall an existence and uniqueness result for an abstract operator equation in a Banach space, which will be used to prove the main result.

**Lemma 2.2** ([13]) *Let  $E$  be a Banach space with the norm  $\|\cdot\|$  and  $B : E \rightarrow E$  be a bilinear operator such that for any  $x_1, x_2 \in E$ ,  $\|B(x_1, x_2)\| \leq \eta\|x_1\|\|x_2\|$ , then for any  $y \in E$  such that  $\|y\| < \frac{1}{4\eta}$ , the equation  $x = y + B(x, x)$  has a solution  $x \in E$ . In particular, the solution is such that  $\|x\| \leq 2\|y\|$  and it is the only one such that  $\|x\| < \frac{1}{2\eta}$ .*

Let us observe that if  $y = G(t)U_0$  and

$$B(U, U) = - \int_0^t G(t - \tau) \tilde{\mathbf{P}}\nabla \cdot (U \otimes U)(\tau) d\tau,$$

then the integral equation (5) has the form  $U = y + B(U, U)$  required in Lemma 2.2.

Now, we give the definition of the Chemin-Lerner type homogeneous Fourier-Besov spaces with variable exponent.

**Definition 2.3** ([11]) Let  $s(\cdot) \in C^{log}(\mathbb{R}^n)$ ,  $p(\cdot), q(\cdot) \in \mathcal{P}(\mathbb{R}^n) \cap C^{log}(\mathbb{R}^n)$ ,  $T \in [0, \infty)$  and  $1 \leq q, \rho \leq \infty$ . We define the Chemin-Lerner type homogeneous Fourier-Besov space with variable exponent  $\mathcal{L}^\rho([0, T]; \mathcal{F}\dot{\mathcal{B}}_{p(\cdot), q}^{s(\cdot)})$  by

$$\mathcal{L}^\rho([0, T]; \mathcal{F}\dot{\mathcal{B}}_{p(\cdot), q}^{s(\cdot)}) = \left\{ g \in \mathcal{Z}'(\mathbb{R}^n); \|g\|_{\mathcal{L}^\rho([0, T]; \mathcal{F}\dot{\mathcal{B}}_{p(\cdot), q}^{s(\cdot)})} < \infty \right\}$$

with the norm

$$\|g\|_{\mathcal{L}^\rho([0, T]; \mathcal{F}\dot{\mathcal{B}}_{p(\cdot), q}^{s(\cdot)})} = \left( \sum_{j \in \mathbb{Z}} \|2^{js(\cdot)} \theta_j \hat{g}\|_{L^\rho([0, T]; L^{p(\cdot)})}^q \right)^{\frac{1}{q}}.$$

**3 A Priori Estimates**

Thanks to Lemma 2.2, the key to the proof of Theorem 1.1 is to make a priori estimates for (1). In the lemma given below, we prove the linear estimate for equation (5).

**Lemma 3.1 (Linear estimate)** *Let  $\frac{1}{2} < \alpha = \alpha_1 \leq 1$ ,  $1 \leq \rho, q \leq +\infty$  and  $p(\cdot), p_1(\cdot) \in \mathcal{P}(\mathbb{R}^n)$  such that  $p_1(\cdot) \leq p(\cdot)$ . Assume that  $U_0 \in \mathcal{F}\dot{\mathcal{B}}_{p(\cdot), q}^{4-2\alpha-\frac{3}{p(\cdot)}}$  and  $\rho_1 \in [\rho, +\infty]$ , then the following inequality holds:*

$$\|G(t)U_0\|_{\mathcal{L}_T^{\rho_1} \mathcal{F}\dot{\mathcal{B}}_{p_1(\cdot), q}^{4-2\alpha+\frac{2\alpha}{\rho_1}-\frac{3}{p_1(\cdot)}}} \lesssim \|U_0\|_{\mathcal{F}\dot{\mathcal{B}}_{p(\cdot), q}^{4-2\alpha-\frac{3}{p(\cdot)}}}.$$

**Proof.** Thanks to Hölder’s inequality, Lemma 2.1 and the hypothesis  $p_1(\cdot) \leq p(\cdot)$ , we have

$$\begin{aligned} \|G(t)U_0\|_{\mathcal{L}^{\rho_1}([0,\infty), \mathcal{FB}_{p_1(\cdot),q}^{4-2\alpha-\frac{3}{p_1(\cdot)}+\frac{2\alpha}{\rho_1}})} &\leq \| \|2^j(4-2\alpha-\frac{3}{p_1(\cdot)}+\frac{2\alpha}{\rho_1})\theta_j e^{-\mathcal{A}(\xi)t}\widehat{U}_0\|_{L^{\rho_1}([0,\infty), L^{p_1(\cdot)})}\|_{\ell^q} \\ &\leq \| \sum_{k=0;\pm 1} \|2^{j(4-2\alpha-\frac{3}{p(\cdot)})}\theta_j \widehat{U}_0\|_{L^{p(\cdot)}} \|2^{j(\frac{2\alpha}{\rho_1}+\frac{3}{p_1(\cdot)}-\frac{3}{p(\cdot)})}\theta_{j+k} e^{-t|\cdot|^{2\alpha}}\|_{L^{\rho_1}([0,\infty), L^{\frac{p(\cdot)p_1(\cdot)}{p(\cdot)-p_1(\cdot)}})} \|_{\ell^q} \\ &\lesssim \|U_0\|_{\mathcal{FB}_{p(\cdot),q}^{4-2\alpha-\frac{3}{p(\cdot)}}}. \end{aligned}$$

Consequently, one obtains

$$\|G(t)U_0\|_{\mathcal{L}^{\rho_1}([0,\infty), \mathcal{FB}_{p_1(\cdot),q}^{4-2\alpha-\frac{3}{p_1(\cdot)}+\frac{2\alpha}{\rho_1}})} \lesssim \|U_0\|_{\mathcal{FB}_{p(\cdot),q}^{4-2\alpha-\frac{3}{p(\cdot)}}}. \tag{8}$$

For the bilinear estimate, we have the following lemma.

**Lemma 3.2 (Bilinear estimate)** *Let  $\frac{1}{2} < \alpha = \alpha_1 \leq 1$ ,  $p_1 \in \mathcal{P}(\mathbb{R}^n)$  such that  $p_1(\cdot) \leq \frac{6}{5-4\alpha}$ ,  $1 \leq \rho \leq \infty$  and  $\rho_1 \in [\rho, \infty]$ . Then we have the following inequality:*

$$\begin{aligned} &\| \int_0^t G(t-\tau)\widetilde{\mathbf{P}}\nabla \cdot (U_1 \otimes U_2)(\tau)d\tau \|_{\mathcal{L}^{\rho_1}([0,\infty), \mathcal{FB}_{p_1(\cdot),q}^{4-2\alpha-\frac{3}{p_1(\cdot)}+\frac{2\alpha}{\rho_1}})} \\ &\lesssim \|U_1\|_{\mathcal{L}^\rho([0,\infty), \mathcal{FB}_{2,q}^{\frac{5}{2}-2\alpha+\frac{2\alpha}{\rho}})} \|U_2\|_{\mathcal{L}^\infty([0,\infty), \mathcal{FB}_{2,q}^{\frac{5}{2}-2\alpha})} \\ &\quad \times \|U_2\|_{\mathcal{L}^\rho([0,\infty), \mathcal{FB}_{2,q}^{\frac{5}{2}-2\alpha+\frac{2\alpha}{\rho}})} \|U_1\|_{\mathcal{L}^\infty([0,\infty), \mathcal{FB}_{2,q}^{\frac{5}{2}-2\alpha})}. \end{aligned}$$

**Proof.** Thanks to Hölder’s inequality, Hausdorff-Young’s inequality, and Young’s inequality, we have

$$\begin{aligned} &\| \int_0^t G(t-\tau)\widetilde{\mathbf{P}}\nabla \cdot (U_1 \otimes U_2)(\tau)d\tau \|_{\mathcal{L}^{\rho_1}([0,\infty), \mathcal{FB}_{p_1(\cdot),q}^{4-2\alpha-\frac{3}{p_1(\cdot)}+\frac{2\alpha}{\rho_1}})} \\ &\lesssim \| \| \int_0^t 2^j(4-2\alpha-\frac{3}{p_1(\cdot)}+\frac{2\alpha}{\rho_1})\theta_j e^{-(t-\tau)\mathcal{A}(\xi)} \operatorname{div}(\widehat{U_1 \otimes U_2}) d\tau \|_{L^{\rho_1}([0,\infty), L^{p_1(\cdot)})}\|_{\ell^q} \\ &\lesssim \| \| \int_0^t 2^j(4-2\alpha-\frac{3}{p_1(\cdot)}+\frac{2\alpha}{\rho_1})\theta_j e^{-(t-\tau)|\cdot|^{2\alpha}} \operatorname{div}(\widehat{U_1 \otimes U_2}) d\tau \|_{L^{\rho_1}([0,\infty), L^{p_1(\cdot)})}\|_{\ell^q} \\ &\lesssim \| \| \int_0^t \|2^j(5-2\alpha-\frac{3}{p_1(\cdot)}+\frac{2\alpha}{\rho_1})\theta_j e^{-(t-\tau)|\cdot|^{2\alpha}}\|_{L^{\frac{6p_1(\cdot)}{6-(5-4\alpha)p_1(\cdot)}}} \| \widehat{U_1 \otimes U_2} \|_{L^{\frac{6}{5-4\alpha}}} d\tau \|_{L^{\rho_1}([0,\infty))}\|_{\ell^q} \\ &\lesssim \| \|2^j(\frac{2\alpha}{\rho}+\frac{5}{2}-2\alpha)\|_{L^{\frac{6}{4\alpha+1}}} \| \dot{\Delta}_j(U_1 \otimes U_2) \|_{L^\rho([0,\infty))}\|_{\ell^q}. \end{aligned}$$

Consequently, by using Proposition 2.2, we obtain the result

$$\begin{aligned} &B(U_1 \otimes U_2)\|_{\mathcal{L}^{\rho_1}([0,\infty), \mathcal{FB}_{p_1(\cdot),q}^{4-2\alpha-\frac{3}{p_1(\cdot)}+\frac{2\alpha}{\rho_1}})} \lesssim \|U_1 \otimes U_2\|_{\mathcal{L}^\rho([0,\infty), \mathcal{B}_{\frac{6}{4\alpha+1},q}^{\frac{2\alpha}{\rho}+\frac{5}{2}-2\alpha})} \\ &\lesssim \|U_1\|_{\mathcal{L}^\rho([0,\infty), \mathcal{FB}_{2,q}^{\frac{5}{2}-2\alpha+\frac{2\alpha}{\rho}})} \|U_2\|_{\mathcal{L}^\infty([0,\infty), \mathcal{FB}_{2,q}^{\frac{5}{2}-2\alpha})} \\ &\quad + \|U_2\|_{\mathcal{L}^\rho([0,\infty), \mathcal{FB}_{2,q}^{\frac{5}{2}-2\alpha+\frac{2\alpha}{\rho}})} \|U_1\|_{\mathcal{L}^\infty([0,\infty), \mathcal{FB}_{2,q}^{\frac{5}{2}-2\alpha})}. \end{aligned}$$

**4 Proof of Theorem 1.1**

In the following, we consider the Banach space

$$\mathcal{E} = \mathcal{L}^\rho([0, \infty), \mathcal{FB}_{p(\cdot),q}^{4-2\alpha-\frac{3}{p(\cdot)}+\frac{2\alpha}{\rho}}(\mathbb{R}^3)) \cap \mathcal{L}^\rho([0, \infty), \mathcal{FB}_{2,q}^{\frac{5}{2}-2\alpha+\frac{2\alpha}{\rho}}(\mathbb{R}^3)) \\ \cap \mathcal{L}^\infty([0, \infty), \mathcal{FB}_{2,q}^{\frac{5}{2}-2\alpha}(\mathbb{R}^3)),$$

and define mappings as  $\Theta(U) = G(t)U_0 + B(U, U)$ . Then, to solve (1), it suffices to find the fixed point of the mapping  $\theta$ . First, from Lemma 3.1, we have

$$\|G(t)U_0\|_{\mathcal{E}} \leq C_1 \|U_0\|_{\mathcal{FB}_{p(\cdot),q}^{4-2\alpha-\frac{3}{p(\cdot)}}}. \tag{9}$$

By Lemma 3.2, we obtain

$$\|B(U_1 \otimes U_2)\|_{\mathcal{L}^\rho([0,\infty), \mathcal{FB}_{p(\cdot),q}^{4-2\alpha-\frac{3}{p(\cdot)}+\frac{2\alpha}{\rho}})} \lesssim \|U_1\|_{\mathcal{L}^\rho([0,\infty), \mathcal{FB}_{2,q}^{\frac{5}{2}-2\alpha+\frac{2\alpha}{\rho}})} \|U_2\|_{\mathcal{L}^\infty([0,\infty), \mathcal{FB}_{2,q}^{\frac{5}{2}-2\alpha})} \\ + \|U_2\|_{\mathcal{L}^\rho([0,\infty), \mathcal{FB}_{2,q}^{\frac{5}{2}-2\alpha+\frac{2\alpha}{\rho}})} \|U_1\|_{\mathcal{L}^\infty([0,\infty), \mathcal{FB}_{2,q}^{\frac{5}{2}-2\alpha})}, \\ \|B(U_1 \otimes U_2)\|_{\mathcal{L}^\infty([0,\infty), \mathcal{FB}_{2,q}^{\frac{5}{2}-2\alpha})} \lesssim \|U_1\|_{\mathcal{L}^\rho([0,\infty), \mathcal{FB}_{2,q}^{\frac{5}{2}-2\alpha+\frac{2\alpha}{\rho}})} \|U_2\|_{\mathcal{L}^\infty([0,\infty), \mathcal{FB}_{2,q}^{\frac{5}{2}-2\alpha})} \\ + \|U_2\|_{\mathcal{L}^\rho([0,\infty), \mathcal{FB}_{2,q}^{\frac{5}{2}-2\alpha+\frac{2\alpha}{\rho}})} \|U_1\|_{\mathcal{L}^\infty([0,\infty), \mathcal{FB}_{2,q}^{\frac{5}{2}-2\alpha})},$$

and

$$\|B(U_1 \otimes U_2)\|_{\mathcal{L}^\rho([0,\infty), \mathcal{FB}_{2,q}^{\frac{5}{2}-2\alpha+\frac{2\alpha}{\rho}})} \lesssim \|U_1\|_{\mathcal{L}^\rho([0,\infty), \mathcal{FB}_{2,q}^{\frac{5}{2}-2\alpha+\frac{2\alpha}{\rho}})} \|U_2\|_{\mathcal{L}^\infty([0,\infty), \mathcal{FB}_{2,q}^{\frac{5}{2}-2\alpha})} \\ + \|U_2\|_{\mathcal{L}^\rho([0,\infty), \mathcal{FB}_{2,q}^{\frac{5}{2}-2\alpha+\frac{2\alpha}{\rho}})} \|U_1\|_{\mathcal{L}^\infty([0,\infty), \mathcal{FB}_{2,q}^{\frac{5}{2}-2\alpha})}.$$

Consequently,

$$\|B(U_1 \otimes U_2)\|_{\mathcal{E}} \leq C_2 \|U_1\|_{\mathcal{E}} \|U_2\|_{\mathcal{E}}. \tag{10}$$

Combining (9) and (10), we get

$$\|\Theta(U)\|_{\mathcal{E}} \leq \|G(t)U_0\|_{\mathcal{E}} + \left\| \int_0^t G(t-\tau) \tilde{\mathbb{P}} \tilde{\nabla} \cdot (U \otimes U) d\tau \right\|_{\mathcal{E}} \\ \leq \|G(t)U_0\|_{\mathcal{E}} + \|B(U \otimes U)\|_{\mathcal{E}} \\ \leq C_1 \|U_0\|_{\mathcal{FB}_{p(\cdot),q}^{4-\frac{3}{p(\cdot)}-2\alpha}} + C_2 \|U\|_{\mathcal{E}} \|U\|_{\mathcal{E}}.$$

Then, for any  $U_0 \in \mathcal{FB}_{p(\cdot),q}^{4-\frac{3}{p(\cdot)}-2\alpha}$  if  $\|U_0\|_{\mathcal{FB}_{p(\cdot),q}^{4-\frac{3}{p(\cdot)}-2\alpha}} < \frac{1}{4C_1C_2}$ , by Lemma 2.2, we conclude that the problem (1) admits a unique global mild solution  $U \in \mathcal{E}$  such that  $\|U\|_{\mathcal{E}} \leq \frac{1}{2C_2}$ .

## 5 Conclusion

In this paper, we considered the 3-D generalized micropolar fluid system which can describe many phenomena that occur in a large number of complex fluids, including animal blood and liquid crystals. By using the Littlewood-Paley decomposition theory and Fourier localization technique, we prove the global existence for the system (1) in variable exponent Fourier-Besov spaces and our result can be seen as a complement to the corresponding result of Zhu and Zhao [12].

## References

- [1] Shaolei Ru and M. Z. Abidin. Global well-posedness of the incompressible fractional Navier-Stokes equations in Fourier-Besov spaces with variable exponent. *Computers and Mathematics with Applications* **77** (4) (2019) 1082–1090.
- [2] A. Almeida and P. Hästö. Besov spaces with variable smoothness and integrability. *J. Funct. Anal.* **258** (5) (2010) 1628–1655.
- [3] M. F. de Almeida, L. C. Ferreira and L. S. M. Lima. Uniform global well-posedness of the Navier-Stokes-Coriolis system in a new critical space. *Math. Z.* **287** (3-4) (2017) 735–750.
- [4] A. Azanzal, A. Abbassi, and C. Allalou. Existence of solutions for the Debye-Hückel system with low regularity initial data in critical Fourier-Besov-Morrey spaces. *Nonlinear Dynamics and Systems Theory* **21** (4) (2021) 367–380.
- [5] Q. Chen, and C. Miao. Global well-posedness for the micropolar fluid system in critical Besov spaces. *J. Differential Equations* **252** (3) (2012) 2698–2724.
- [6] M. Cannone, and G. Karch. Smooth or singular solutions to the Navier-Stokes system. *J. Differential Equations* 197 (2004) 247-274.
- [7] L. Diening, P. Harjulehto, P. Hästö and M. Rážička. Lebesgue and Sobolev spaces with variable exponent. In: *Lecture Notes in Mathematics*, 2017. Springer, Heidelberg, 2011.
- [8] L. C. Ferreira and E. J. Villamizar-Roa. Micropolar fluid system in a space of distributions and large time behavior. *J. Math. Anal. Appl.* **332** (2) (2007) 1425–1445.
- [9] A. C. Eringen. Theory of micropolar fluids. *J. Math. Mech.* **16** (1966) 1–18.
- [10] G. P. Galdi and S. Rionero. A note on the existence and uniqueness of solutions of the micropolar fluid equations. *International Journal of Engineering Science* **15** (1977) 105–108.
- [11] J. Sun and S. Cui. Sharp well-posedness and ill-posedness in Fourier-Besov spaces for the viscous primitive equations of geophysics. *arXiv:1510.0713v1*. (2015).
- [12] W. Zhu, and J. Zhao. Existence and regularizing rate estimates of solutions to the 3-D generalized micropolar system in Fourier-Besov spaces. *Math. Methods Appl. Sci.* **41** (4) (2018) 1703–1722.
- [13] W. Zhu. Sharp well-posedness and ill-posedness for the 3-D micropolar fluid system in Fourier-Besov spaces. *Nonlinear Analysis: Real World Applications* **46** (2019) 335–351.



# The Regularization Method For Solving Sub-Riemannian Geodesic Problems

R. Saffidine<sup>1\*</sup> and N. Bensalem<sup>2</sup>

<sup>1</sup> *Fundamental and Numerical Mathematics Laboratory, Department of Basic Education  
in Technology, University of Setif, 19000 Setif, Algeria.*

<sup>2</sup> *Department of Mathematics, University of Setif, 19000 Setif, Algeria.*

Received: February 23, 2023; Revised: June 6, 2023

**Abstract:** In this paper, we used the regularization method to prove some properties of the sub-Riemannian geodesics in infinite dimension for a Hilbertian manifold. More precisely, we generalize the result obtained by S.Nikitin [14], so we prove that the sub-Riemannian distance for the Hilbert-Schmidt distribution can be approximated by the smooth sub-Riemannian geodesics.

**Keywords:** *regularization method; geodesics; sub-Riemannian geometry; control problem; Hamilton's equation.*

**Mathematics Subject Classification (2010):** 53C22, 93C10, 70H05, 49J15.

## 1 Introduction

In finite-dimension context, a sub-Riemannian distance between two fixed points is defined by the infimum length of curves connecting them and whose velocity is constrained to be tangent to sub-vector space (distribution) of the tangent space  $T_x M$  of a Riemannian manifold  $M$ , where  $x \in M$ . Such curves are called horizontal. The distance is finite if every pair of points can be connected by at least one horizontal curve and is achieved on the curves of minimal length. Finding a length minimizer is an optimal control problem, the extremals of this problem are called the sub-Riemannian geodesics. According to the Pontryagin maximum principle [6, 10, 15, 16], the optimal curves are of two types: abnormal curves and normal geodesics which are the projections of the Hamiltonian trajectories. In [14], in finite dimension, S.Nikitin presented conditions under which the sub-Riemannian distance can be measured by an infinitely smooth sub-Riemannian

---

\* Corresponding author: <mailto:rebiha.safidine@univ-setif.dz>

geodesics. This result arises from the fact that sometimes the sub-Riemannian distance is measured by abnormal extremals [10, 12, 13]. Our objective is to give a generalization of this result for an infinite dimensional manifold.

The first problem when we consider a control problem is that of controllability [1, 9, 17], which presents the first difference between the finite dimension and infinite-dimensional cases, so that the infimum could be not reached even for the Riemannian-Hilbertian manifold. The same is true in the general sub-Riemannian manifold. So the second difference is that the Pontryagin maximum principle is not available any longer. However, we still have the strong Chow-Rashevski theorem developed for the manifold modeled on Hilbert spaces and the maximum principle for certain special cases. Using them, we give analogue properties for the sub-Riemannian structure generated by a bilinear distribution of Hilbert-Schmidt.

In this work, we show that the problem of the length minimization is a control problem and we give a characterization of smooth geodesics where we use a variant of Pontryagin's maximum principle [3] and we also prove that in infinite dimension and under some conditions, we can approximate a sub-Riemannian distance by a normal sub-Riemannian geodesics. The structure of the paper is as follows. In Section 2, we introduce notations and briefly review some natural objects associated to a sub-Riemannian structure in an infinite dimensional manifold modeled on the Hilbert space. The results on the bilinear Hilbert-Schmidt distribution are given in Section 3. We characterize the sub-Riemannian geodesics in Section 4. To accomplish our objective, we replace the sub-Riemannian problem by the regularized one and we present certain conditions under which we prove, at the first step, the existence of the sub-Riemannian geodesics and, at the second step, we measure the sub-Riemannian distance by a normal geodesics. For the proof of all these results, we use some classical techniques of the functional analysis.

## 2 Preliminary Results

In this section, we will recall some basic notions of sub-Riemannian geometry in infinite dimension, for more details, we refer the reader to [1, 7].

### 2.1 Sub-Riemannian structure in infinite dimension

Let  $M$  be a connected manifold modelled on a Hilbert space  $E$ ,  $TM$  be the tangent bundle of  $M$ , then according to [7], we have the following definition.

**Definition 2.1** A sub-Riemannian structure is a triple  $(M, \mathcal{F}, \mathbf{h})$ , where

- $M$  is a Hilbert connected manifold;
- $\mathcal{F}$  is a sub-bundle of  $TM$ .
- $\mathbf{h}$  is a Riemannian metric on  $\mathcal{F}$ .

**Remark 2.1** • Given a Riemannian metric  $\bar{h}$  on  $M$ , we get a Riemannian metric on  $\mathcal{F}$  by restriction. On the other hand, there always exists a complementary  $\mathcal{V}$  of  $\mathcal{F}$  and so we can extend  $\mathbf{h}$  into the Riemannian metric  $\bar{h}$  on  $M$ , which means that  $TM = \mathcal{V} + \mathcal{F}$ .

- The requirement of the splitting is non-trivial if  $M$  is not modeled on a Hilbert space, see [7], this splitting implies that there exists a smooth projection from  $TM$  to  $\mathcal{F}$ .

**Definition 2.2** A horizontal curve is a smooth curve  $\gamma : [a, b] \rightarrow M$  such that

$$\dot{\gamma} \in \mathcal{F}_{\gamma(t)} \quad \text{for every } t \in [a, b]. \quad (1)$$

According to the previous definitions, we can also define the following.

**Definition 2.3** 1. The length of a horizontal curve is given by

$$l(\gamma) = \int_a^b \sqrt{\mathbf{h}(\dot{\gamma}(t), \dot{\gamma}(t))} dt. \quad (2)$$

2. The sub-Riemannian energy functional (Action) is given by

$$e(\gamma) = \int_a^b \mathbf{h}(\dot{\gamma}(t), \dot{\gamma}(t)) dt. \quad (3)$$

**The sub-Riemannian distance** between the distinct points is defined by

$$d_{\mathcal{F}}(x_0, x_1) = \inf \{ l(\gamma); \dot{\gamma} \in \mathcal{F}_{\gamma(t)}, \gamma(a) = x_0, \gamma(b) = x_1 \}. \quad (4)$$

The problem of the length minimization is equivalent to the problem of energy minimization, which allows us to formulate the first-order condition for length minimizer.

**Definition 2.4** (see [7]) A horizontal curve  $\gamma$  is called a **sub-Riemannian geodesics** if

$$\partial_s e(\gamma^s)|_{s=0} = 0, \quad \text{for any } \gamma^s \in \mathcal{J}_{\mathcal{F}}(\gamma), \quad (5)$$

where  $\mathcal{J}_{\mathcal{F}}(\gamma)$  is the collection of all  $\mathcal{F}$ -horizontal variations of  $\gamma$ .

Our aim is to characterize the normal sub-Riemannian geodesics for the bilinear Hilbert-Schmidt distribution on the Hilbertian manifold. We consider a manifold modeled on the Hilbert space with a strong Riemannian metric.

### 3 Bilinear Distribution

From [3–5], we recall all definitions, properties and results we shall use in this work. Let  $E$  and  $F$  be two Hilbert spaces, and let  $A \in \mathcal{L}(F; E)$  ( $u \rightarrow A_u$ ),  $B \in \mathcal{L}(F; (E; E))$  ( $u \rightarrow B_u$ ) and  $\tilde{B} \in \mathcal{L}(F \times E; E)$  be an operator associated to  $B$  and defined by

$$\forall u \in F, \forall x \in E \quad \tilde{B}(x, u) = B_u x,$$

where  $\mathcal{L}(F; E)$  is the space of linear bounded operators from  $F$  to  $E$  and  $\mathcal{L}(F; (E; E))$  is the space of the bounded operators from  $F$  to  $\mathcal{L}(E; E)$ . Denote by  $\{f_i; i \in \mathbb{N}\}$  a Hilbert basis for  $F$  and set

$$X_i(x) = A_{f_i} + B_{f_i} x.$$

We denote also by  $\mathcal{F}$  the distribution spanned by  $\{X_i, i \in \mathbb{N}\}$ .

We consider the associated system defined by

$$\dot{x} = Au + \tilde{B}(u, x). \quad (6)$$

We will say that (6) is a bilinear system of  $E$  and  $\mathcal{F}$  is a **bilinear distribution**. For a given bilinear distribution  $\mathcal{F}$  on a Hilbertian manifold, for all horizontal curves  $\gamma : [0, T] \rightarrow E$  that are tangent to  $\mathcal{F}$ , there exists a control  $u : [0, T] \rightarrow F$  such that

$$\dot{\gamma} = Au + \tilde{B}(u, \gamma). \tag{7}$$

We can assume that all horizontal curves are defined on  $[0, 1]$ , after changing the parametrization if necessary. Then for any horizontal curve, we can define its length  $l(\gamma)$  by

$$l(\gamma) = \int_0^1 \|u(t)\|_F dt, \tag{8}$$

and the energy of a horizontal curve is defined by

$$e(\gamma) = \frac{1}{2} \int_0^1 \|u(t)\|_F^2 dt, \tag{9}$$

where  $u \in L^2([0, 1], F)$  and  $\|\cdot\|_F$  denotes the Hilbertian norm on  $F$ . In this case, all requirements of the previous definitions are satisfied.

When  $A$  and  $B$  are the Hilbert-Schmidt operators, the associated distribution  $\mathcal{F}$  is called a **Hilbert-Schmidt distribution**. Then we have the following result.

**Lemma 3.1** [3] *If  $\mathcal{F}$  is a bilinear Hilbert-Schmidt distribution, then to each horizontal curve we can associate a control  $u$  and conversely.*

**Example 3.1** (see [3]) Let  $K, H$  be two separable Hilbert spaces, if we denote by  $\{k_i; i \in \mathbb{N}\}$  a Hilbert basis for  $K$  and by  $\{h_\alpha; \alpha \in \mathbb{N}\}$  a Hilbert basis for  $H$ , then the set  $\{h_\alpha \otimes k_i\}$  is a Hilbert basis for the space of Hilbert-Schmidt operators  $\mathcal{L}_{HS}(K; H)$ . On  $\mathcal{G} = \mathcal{L}_{HS}(K; H) \oplus K \oplus H$ , we define a generalized Heisenberg-Lie algebra structure by setting  $F = \mathcal{L}_{HS}(K; H) \oplus K$  and  $Z = H$  with Lie brackets defined, with respect to the basis  $Y_{\alpha i} = (h_\alpha \otimes k_i, 0)$  and  $X_i = (0, k_i)$  of  $F$ , by

$$[Y_{\alpha i}, X_i] = C_{\alpha i} Z_\alpha,$$

where  $Z_\alpha$  is the basis of  $Z$  and  $C_{\alpha i}$  are constants, the other Lie brackets are zero. Let  $G$  be a Lie group with Lie algebra  $\mathcal{G}$ .  $F$  induces on  $G$  a left invariant distribution  $\mathcal{F}$ , this distribution is a Hilbert-Schmidt distribution if  $\sum_{\alpha i} C_{\alpha i} < \infty$ .

#### 4 Optimal Control Viewpoint

Looking for the sub-Riemannian geodesics between two points means solving the smooth infinite minimization problem

$$e(\gamma) = e(u) = \frac{1}{2} \int_0^1 \|u(t)\|_F^2 dt \rightarrow \inf, \tag{10}$$

where  $u : [0, T] \rightarrow F$  with the following constraint:

$$\begin{cases} \dot{x}(t) = Au(t) + \tilde{B}(u(t), x(t)), \\ x(0) = x_0, x(1) = x_1, \end{cases} \tag{11}$$

where  $A \in \mathcal{L}(F, E)$ ,  $B \in \mathcal{L}(F, \mathcal{L}(E, E))$  and  $x_0, x_1$  are two given points of  $E$ . So we have a bilinear control problem where the spaces of a control and state have an infinite dimension.

In finite dimension, we always use the maximum principle [2, 15] to calculate the optimal trajectories. Unfortunately, in infinite dimension, we lose Pontryagin's Maximum Principle. However, in this context, we can apply a variant of the maximum principle [3, 5] which gives us a characterization of the optimal curve for a bilinear distribution on the Hilbertian manifold. In the case when the set of control is contained in a closed bounded convex subset and the operators  $A, B$  are compact, this characterization is similar to the finite dimensional case, see [6].

**Theorem 4.1** (see [4]) *Let  $u \in L^2([0, T]; K)$ , where  $K$  is a closed bounded convex subset,  $B$  and  $A$  are compact for all  $t \in [0, T]$ , there exists a control  $\bar{u}$  which minimizes the functional  $e$  and, moreover,  $\bar{u}$  satisfies the following relation for almost all  $t \in [0, T]$ :*

$$\langle A\bar{u} + \tilde{B}(\bar{u}, \bar{x}), \bar{p} \rangle + p_0 \|\bar{u}\|^2 = \min_{v \in K} \langle Av + \tilde{B}(v, x), p \rangle + p_0 \|v\|^2, \quad (12)$$

where  $\bar{x}$  is the trajectory associated to  $\bar{u}$  and where  $\bar{p}$  is a mild solution of the adjoint system

$$\frac{d}{dt} \bar{p} = -B_{\bar{u}}^* p. \quad (13)$$

$B_{\bar{u}}^*$  is the adjoint of  $B_{\bar{u}}$ .

Under these assumptions, and following the terminology introduced in [1], we can distinguish two types of the extremal.

**Definition 4.1** An extremal of minimization problem (10)-(11), i.e., a couple  $(\bar{x}, \bar{p})$ , meeting the condition of Theorem 4.1 is called the *normal bi-extremal* if  $p_0 \neq 0$  (which can be normalized to 1), and the *abnormal bi-extremal* if  $p_0 = 0$ .

In the sequel of this work, we assume that  $u(t) \in K$ , where  $K$  is a closed bounded convex subset,  $B$  and  $A$  are compact.

#### 4.1 Characterization of normal geodesics

The following proposition gives the link between the normal extremal of Theorem 4.1 and the normal geodesics.

**Proposition 4.1** *Let  $\gamma$  be a horizontal curve, then the following assertions are equivalent:*

1.  $\gamma$  is a critical point of the energy function with a fixed end point;
2. there exists a covector  $p$  such that the couple  $(\gamma, p)$  is a normal bi-extremal of maximum principle.

**Proof.** The proof of this result is an adaptation, step by step, of the proof of the corresponding result of Proposition 2 in [1].

**Remark 4.1** By the previous proposition, we deduce that the normal geodesics is a solution to the Hamiltonian system

$$\begin{cases} \dot{x} &= \frac{\partial}{\partial p} H(x, p), \\ \dot{p} &= -\frac{\partial}{\partial x} H(x, p), \\ H(x, p) &= \frac{1}{2} \|(A + B(x))^* p\|^2. \end{cases} \tag{14}$$

We recall that our objective is to generalize the result obtained by S.Nikitin in [14] to infinite dimension. We present new conditions under which the sub-Riemannian distance can be approximated by a normal sub-Riemannian geodesics. To attain this goal, we use the regularization method.

### 5 Regularization Procedure

We use the regularization method to replace a minimization problem with constraint by another one without constraint.

#### 5.1 Regularized problem

At first, we need the following hypotheses

Let  $L : E \times TE \times F \rightarrow E, \eta = (x, u) \rightarrow L(x, u) = \dot{x} - (A + B(x))u$ , and  $G : E \times F \rightarrow F, \eta = (x, u) \rightarrow u$ , where  $A \in \mathcal{L}(F, E), B \in \mathcal{L}(F, \mathcal{L}(E, E))$  and  $TE$  is the tangent space of  $E$ . We assume that  $L$  and  $G$  satisfy the following assumptions.

**Assumption 5.1** The set

$$U_L = \left\{ \begin{array}{l} (x, u) \in E \times F: \|L(x, u)\|_{L^2} = \|\dot{x} - (A + B(x))u\|_{L^2} = \\ \mu = \inf_{(x,u) \in D} \|\dot{x} - (A + B(x))u\|_{L^2}, \end{array} \right\}$$

is not empty, where  $D = E \times K$ . We define also

$$\hat{U} = \left\{ (x, u) \in E \times F: \|G(x, u)\| = \|u(t)\| = \nu_F = \inf_{(x,u) \in U_L} \|u(t)\|_{\ell^2} \right\},$$

where  $L^2([0, 1], F)$  is identified to the space  $L^2([0, 1], l^2(\mathbb{N}))$  via the Hilbertian basis  $\{f_i; i \in \mathbb{N}\}$  of  $F$  (see [3]).

**Assumption 5.2** There exists  $c > 0$  such that

$$W_C = \{(x, u) \in E \times F: \|L(x, u)\| \leq c, \|G(x, u)\| \leq c\}$$

is not empty and bounded.

The regularized problem is

$$J_\alpha(\gamma) = \frac{1}{2} \|L(x, u)\|_{\mathbb{E}} + \frac{\alpha}{2} \|G(x, u)\|_{\mathbb{F}} \rightarrow \inf, \tag{P_\alpha}$$

where  $\alpha > 0$  denotes the regularization parameter.

**Theorem 5.1** Under Assumptions 5.1 and 5.2, the problem  $(P_\alpha)$  has a solution.

*Proof.* Let  $\{\gamma_\alpha^n\}$  be a minimizing sequence

$$\gamma_\alpha^n = \{(x_\alpha^n(t), u_\alpha^n(t)); t \in [0, 1]\} \subset D \quad n = 1, 2, \dots, \quad (15)$$

such that  $m_\alpha \leq J_\alpha(\gamma^n) \leq m_\alpha + \frac{1}{n}$ ,  $n = 1, 2, \dots$ , then we have

$$\|L(x_\alpha^n, u_\alpha^n)\|_{\mathbb{E}} = \|\dot{x}_\alpha^n - (A + B(x_\alpha^n) u_\alpha^n)\| \leq (m_\alpha + 1)^{\frac{1}{2}},$$

$$\|G(x_\alpha^n, u_\alpha^n)\|_{\mathbb{F}} = \|u_\alpha^n\| \leq \left(\frac{m_\alpha + 1}{\alpha}\right)^{\frac{1}{2}}.$$

We take

$$c = \max \left\{ \left(\frac{m_\alpha + 1}{\alpha}\right)^{\frac{1}{2}}, (m_\alpha + 1)^{\frac{1}{2}} \right\}.$$

It is clear that  $\{\gamma_\alpha^n\} \subset W_c$ , as we have already noticed that the set  $W_c$  is weakly compact, then the sequence  $(\gamma_\alpha^n)$  is weakly convergent, i.e.,

$$((x_\alpha^n(t), u_\alpha^n(t))) \xrightarrow{\text{weakly}} (x_0(t), u_0(t)) \quad (\text{in } H = E \times F)$$

$$\begin{aligned} \dot{x}_\alpha^n(t) - (A + B(x_\alpha^n) u_\alpha^n(t)) &\xrightarrow{\text{weakly}} r \\ u_\alpha^n(t) &\xrightarrow{\text{weakly}} u_0(t). \end{aligned}$$

As the operators  $L, G$  are jointly weakly closed on  $D$ , then we have

$$\dot{x}_0(t) - (A + B(x_0) u_0(t)) = r.$$

It remains to prove that  $(x_0(t), u_0(t))$  is a solution of the problem  $(P_\alpha)$ .

We use the lower semi-continuity of the norm in a Hilbert space, we find that

$$m_\alpha \leq J_\alpha(\gamma^0) \leq \liminf_{n \rightarrow \infty} J_\alpha(\gamma^n) \leq \limsup_{n \rightarrow \infty} J_\alpha(\gamma^n) \leq m_\alpha,$$

then  $J_\alpha(\gamma^0) = m_\alpha$ .

Now we define a new hypothesis to show that under these conditions and Assumptions 5.1-5.2, the sub-Riemannian distance can be measured by normal minimizers.

**Assumption 5.3** The distribution  $\mathcal{F}$  satisfies the strong Chow-Rashevsky property [1], then there exists a control  $v(t)$  which steers the system

$$\dot{x} = (A + B(x))v$$

from the state  $x_0$  to the state  $x_1$ .

**Assumption 5.4** The system (6) satisfies the following condition (at points  $x_0$  and  $x_1$ ): if there exist real numbers  $\delta > 0$ ,  $P > 0$  and  $Q > 0$  such that

$$\forall 0 < \alpha \leq \delta \quad \|\sqrt{\alpha} p_\alpha(0)\|_E \leq P \Rightarrow \|p_\alpha(0)\|_E \leq Q, \quad (16)$$

$p(0)$  should be chosen so that  $x(1) = x_1$ , where  $x$  is the solution to the following Hamiltonian system:

$$\begin{cases} \dot{x} &= \frac{\partial}{\partial p} H_\alpha(x, p), \\ \dot{p} &= -\frac{\partial}{\partial x} H_\alpha(x, p), \\ x(0) &= x_0, \end{cases} \tag{17}$$

$$H_\alpha(x, p) = \frac{1}{2} \|(A + B(x))^* p\|^2 + \frac{\alpha}{2} \|p\|^2.$$

Our principal result is the following theorem.

**Theorem 5.2** *Consider the sub-Riemannian problem*

$$\int_0^1 \|u(t)\|^2 dt \rightarrow \inf,$$

where  $u$  is the unique solution of the system

$$\dot{x} = (A + B(x))u. \tag{\Sigma}$$

Suppose that Assumptions 5.1, 5.2, 5.3 and 5.4 are satisfied. Then, for all given  $x_0, x_1 \in E$ , the regularized solutions converge to the normal geodesics solution, i.e.,

$$\|x_\alpha - \tilde{x}(t)\| \rightarrow 0$$

and

$$H_\alpha \rightarrow H,$$

where  $H_\alpha, H$  are given in Assumption 5.4 and (14).

**Proof.** According to [19], the solution  $(x_\alpha(t), u_\alpha(t))$  (normal) of regularized problem  $(P_\alpha)$  necessarily satisfies the Euler-Lagrange equations

$$\frac{d}{dt} \left( \frac{\partial}{\partial \dot{x}} L_\alpha(\dot{x}, x, u) \right) - \frac{\partial}{\partial x} L_\alpha(\dot{x}, x, u) = 0, \frac{\partial}{\partial u} L_\alpha(\dot{x}, x, u) = 0,$$

where  $L_\alpha$  is the Lagrangian which is given by

$$L_\alpha(\dot{x}, x, u) = \frac{1}{2} \|L(x, u)\|_{\mathbb{E}}^2 + \frac{\alpha}{2} \|G(x, u)\|_{\mathbb{F}}^2 = \frac{1}{2} \|\dot{x} - (A + B(x))u\|_{\mathbb{E}}^2 + \frac{\alpha}{2} \|u\|_{\mathbb{F}}^2.$$

As the Lagrangian  $L_\alpha$  is hyper regular, then according to [8], we can define  $p$  as

$$p = \frac{1}{\alpha} \frac{\partial}{\partial \dot{x}} L_\alpha(\dot{x}, x, u). \tag{18}$$

Using the Euler-Lagrange equations, and according to [18], we can easily write

$$\begin{cases} \dot{x}_\alpha &= \frac{\partial}{\partial p} H_\alpha(x_\alpha, p_\alpha), \\ \dot{p}_\alpha &= -\frac{\partial}{\partial x} H_\alpha(x_\alpha, p_\alpha), \\ u_\alpha &= (A + B(x_\alpha))^* p_\alpha, \end{cases}$$

where

$$H_\alpha(x_\alpha, p_\alpha) = \frac{1}{2} \|(A + B(x_\alpha))^t p_\alpha\|^2 + \frac{\alpha}{2} \|p_\alpha\|^2.$$

By Assumption 5.3, there exists a control  $v(t)$  which steers the system

$$\dot{x} = (A + B(x))v$$

from  $x_0$  to  $x_1$ , for which we have

$$\int_0^1 \frac{1}{2} \|\dot{x}_\alpha(t) - (A + B(x_\alpha(t))u_\alpha(t))\|_E^2 dt + \frac{\alpha}{2} \|u_\alpha(t)\|_F^2 dt \leq \frac{\alpha}{2} \int_0^1 \|v(t)\|_F^2 dt.$$

Set

$$k = \frac{1}{2} \int_0^1 \|v(t)\|_F^2 dt.$$

As

$$H_\alpha = \frac{1}{\alpha} L_\alpha,$$

then

$$H_\alpha(x_\alpha, p_\alpha) \leq k \quad \forall \alpha > 0 \quad \forall t \in [0, 1],$$

it implies

$$\|\alpha p_\alpha\| \rightarrow 0 \quad \text{while} \quad \alpha \rightarrow 0.$$

According to Assumption 5.1, there exists a positive constant  $\delta$  such that

$$\|\alpha p_\alpha\| \leq \delta,$$

the function  $x_\alpha(t)$  is bounded on  $[0, 1]$ , i.e.

$$\|x_\alpha(t)\| \leq \beta,$$

and as

$$\left\| \frac{\partial}{\partial p} H_\alpha(x_\alpha, p_\alpha) \right\|$$

is bounded, we have the same for  $\dot{x}_\alpha(t)$ , i.e.,

$$\|\dot{x}_\alpha(t)\| \leq G_1,$$

where  $G_1$  is a positive constant which does not depend on  $\alpha$ ; on the other hand,

$$\frac{1}{2} \|L(x_\alpha, u_\alpha)\|_{\mathbb{E}} + \frac{\alpha}{2} \|G(x_\alpha, u_\alpha)\|_{\mathbb{F}} \leq \frac{1}{2} \|L(x, u)\|_{\mathbb{E}} + \frac{\alpha}{2} \|G(x, u)\|_{\mathbb{F}} \quad (19)$$

for all  $u \in U_L$ , then we have

$$\|G(x_\alpha, u_\alpha)\|_{\mathbb{F}} \leq \|G(x, u)\|_{\mathbb{F}}, \|L(x_\alpha, u_\alpha)\|_{\mathbb{E}} \leq \mu_L + \alpha \nu_F. \quad (20)$$

From the previous inequality, the families  $\{(x_\alpha, u_\alpha)\}$ ,  $\{G(x_\alpha, u_\alpha)\}$ ,  $\{L(x_\alpha, u_\alpha)\}$  are weakly compact, there exist weakly convergent sub-families, i.e.,

$$(x_{\alpha_j}, u_{\alpha_j}) \rightarrow (\tilde{x}, \tilde{u}),$$

$$L(x_{\alpha_j}, u_{\alpha_j}) \rightarrow r.$$

So

$$L(\tilde{x}, \tilde{u}) = r,$$

we replace  $(\tilde{x}, \tilde{u})$  in (19) and (20), we find

$$\begin{aligned} \lim_{\alpha_j \rightarrow 0} \|L(x_{\alpha_j}, u_{\alpha_j}) - L(\tilde{x}, \tilde{u})\|_{\mathbb{E}} &= 0, \\ \lim_{\alpha_j \rightarrow 0} \|G(x_{\alpha_j}, u_{\alpha_j}) - G(\tilde{x}, \tilde{u})\|_{\mathbb{F}} &= 0. \end{aligned}$$

Using the previous results and the Gronwall inequality, we prove that the solution  $x_{\alpha_j}(t)$  will converge strongly to  $\tilde{x}$ ,

$$\alpha_j \rightarrow 0 \quad \text{while} \quad j \rightarrow \infty$$

and

$$\|x_{\alpha_j}(t) - \tilde{x}(t)\| \rightarrow 0 \quad \text{while} \quad j \rightarrow \infty.$$

On the other hand, for the control  $v(t)$  which steers the system

$$\dot{x}(t) = (A + B(x(t)))v(t)$$

from  $x_0$  to  $x_1$  and for any  $\alpha > 0$ ,

$$\int_0^1 \|u_\alpha(t)\|^2 dt \leq \int_0^1 \|v(t)\|^2 dt.$$

This proves that  $\tilde{x}(t)$  is a minimizing curve which measures the sub-Riemannian distance between  $x_0$  and  $x_1$ .

The functions  $\dot{p}_\alpha$  and  $p_\alpha$  are bounded,

$$\dot{p}_\alpha = -p_\alpha^t (A + B(x)) B^t p_\alpha,$$

but

$$(A + B(x))^t p_\alpha = u_\alpha,$$

by substituting  $u_\alpha$  in the above expression, we obtain

$$\begin{aligned} \|p_\alpha(t)\| &= \left\| p_\alpha(0) + \int_0^t -u_\alpha(s) B^t p_\alpha(s) ds \right\| \\ &\leq \|p_\alpha(0)\| + \left\| \int_0^t -u_\alpha(s) B^t p_\alpha(s) ds \right\|, \end{aligned}$$

then

$$\sqrt{\alpha} \|p_\alpha(t)\| \leq \sqrt{2k} \quad \forall t \in [0, 1].$$

From Assumption 5.4, we have

$$\|p_\alpha(0)\| \leq \delta,$$

then

$$\|p_\alpha(t)\| \leq c \int_0^t \|p_\alpha(s)\| ds.$$

According to the Gronwall inequality, we get

$$\|p_\alpha(t)\| \leq G.$$

We also have

$$\left\| \frac{\partial}{\partial x} H_\alpha(x_\alpha, u_\alpha) \right\| \leq l.$$

It follows that  $\dot{p}_\alpha$  is also bounded. The proof of the convergence of  $p_\alpha$  to a continuous function  $p$  is similar to  $x_\alpha$ ; by passing to the limit in  $H_{\alpha_j}$ , we obtain

$$H_{\alpha_j} \rightarrow H.$$

## 6 Conclusion

In this paper, we studied some properties of bilinear extremals in infinite dimension, these properties have a direct application in sub-Riemannian geometry, especially in the case of a sub-Riemannian structure generated by a bilinear Hilbert-Schmidt distribution. We prove also that, under some conditions, a sub-Riemannian distance can be approximated by a normal geodesics. These results remain valid for a manifold modeled on a Hilbert space, we can also generalize these results for the Banach manifold.

## References

- [1] S. Arguillère. Sub-Riemannian Geometry and Geodesics in Banach Manifolds. *J. Geom. Ana.* **30** (3)(2020) 2897–2938.
- [2] V. Alexéev, V. Tikhomirov and S. Fomine. *Commande Optimale*. Edition Mir, Moscow, 1982.
- [3] N. Bensalem and F. Pelletier. Some geometrical properties of infinite dimensional bilinear controlled systems. *Maghreb. Math. Rev.* **10** (1) (2001) 1–16.
- [4] A. Berrabah, N. Bensalem and F. Pelletier. Optimality problem for infinite dimensional bilinear systems. *Bull. Sci. Math.* **130** (2006) 442–466.
- [5] A. Berrabah. *Obsevateurs et principe du maximum approché des systèmes bilinéaires en dimension infinie sous contrôle à paramètres distribués*. Thèse de Doctorat, Université de Savoie, 2004.
- [6] R. Brockett and L. Dai. Non holonomic kinematics and the role of elliptic functions in constructive controllability. In: *Nonholonomic Motion Planing* (1992) 1–21.
- [7] E. Grong, I. Markina and A. Vasiliev. Sub-Riemannian geometry on infinite -dimensional manifold. *The Journal of Geometric Analysis* **25** (2015) 2474—2515.
- [8] M.J. Gotay. *Presymplectic manifold, Geometric constraint theory and the Dirac-Bergman theory of constraints*. Center of theoretical physics of the university of Maryland.
- [9] M. Jidou Khayar, A. Brouri and M. Ouzaha. Exact Controllability of reaction diffusion equation under Bilinear control. *Nonlinear Dynamics and Systems Theory* **22** (5) (2022) 538–549.
- [10] W. Liu and H.J. Sussamnn. Abnormal sub-Riemannian minimizers. preprint, 1992.
- [11] V.A. Morozov. *Methods for Solving Incorrectly Posed Problems*. Springer, Verlag, 1984.
- [12] R. Montgomery. Geodesics which do not satisfy the geodesic equations. Preprint, 1991.
- [13] R. Montgomery. Abnormal minimizers. *SIAM J. Control and Optimization* **32** (1994) 1–15.
- [14] S. Nikitin. On smoothness of Sub-Riemannian minimizers. *Journal of Mathematical Systems, Estimation and Control* **7** (2)(1997) 1–12.
- [15] L. Pontryagin, V. Boltyanski, R. Gamkrelize and E. Michtchenko. *Théorie mathématique des processus optimaux*. Edition Mir, Moscow, 1974.
- [16] M. Popescu and F. Pelletier. Courbes optimales pour une distribution affine. *Bulletin des Sciences Mathématiques* **129** (9)(2005) 701–725.
- [17] A. Raheem and M. Kumar. Some Results on Controllability for a Class of Non-integer order Differential equations with impulses. *Nonlinear Dynamics and Systems Theory journal* **22** (3) (2022) 330–340.
- [18] R. Schmid. Infinite dimensional Hamiltonian systems. *Encyclopedia of Mathematical Physics* (2006) 37–44.
- [19] J.A. Vallejo. Euler-Lagrange equations for functionals defined on Fréchet manifolds. *Journal of Nonlinear Mathematical Physics* **16** (4) (2009) 443–454.